Innovative Designs in Tissue Engineering: Improvements on Scaffold Fabrication and Bioreactor Design

By

Wen Li

A thesis submitted to the Faculty of Graduate Studies of
The University of Manitoba
in partial fulfilment of the requirements for the degree of

Master of Science

Department of Mechanical and Manufacturing Engineering
Faculty of Engineering
University of Manitoba
Winnipeg, Manitoba

Abstract

This study consists of two projects related to Tissue Engineering: Engineering biomimetic scaffolds for bone regeneration and ear reconstruction, and bioreactor design for ex-vivo bioengineered scaffold.

The co-electrospinning method was used to produce composite membranes with different layers from gelatin and polycaprolactone (PCL) nanofibers, followed by paper-stacking cell seeded membranes to mimic the twisted plywood structure found in lobster cuticles. 3D laser scanner was used to capture the precise shape of a human ear model; and the negative molds were fabricated to compress scaffolds into the shape of human ear.

Design for assembly (DFA) method was used to analyze and improve the design of the current bioreactor. A new design is proposed to ease operation, save time and increase the application efficiency. The proposed solution is evaluated in a virtual environment using 3D assembly modeling and simulation.

Acknowledgments

I would like to express my deepest gratitude to my supervisors, Dr. Malcolm Xing and Dr. Qingjin Peng, for their patience, expertise, and assistance in writing this thesis. I would like to thank other members of my committee, Dr. Martin Scanlon and Dr. Tarek Elmekkawy, for taking time out from their busy schedule to attend my final oral defence.

I would also like to thank Mr. Michael Stringer for his help in tensile and compressive mechanical tests.

Finally, I would like to thank Andison Family Foundation and The Children's Hospital Foundation for their financial support on this study.

Contents

List of Tables

List of Figures

List of Copyrighted Material

Nikolov, S., Petrov, M., Lymperakis, L., Friak, M., Sachs, C., Fabritius, H. O., Neugebauer, J. (2010). Revealing the design principles of high-performance biological composites using ab initio and multiscale simulations: the example of lobster cuticle. Adv Mater, 22(4), 519-526. doi: 10.1002/adma.200902019
© Permission issued by Svetoslav Nikolov, 12/04/2011
Figure 2.1 13

Li, W., Xing, M., Peng, Q. (2011). Bioreactor Improvement Based on Design for Assembly in Virtual Environments. Proceedings of ASME 2011 International Design Engineering Technical Conferences & Computers and Information in Engineering Conference, DETC2011-47916, Washington, DC, August 28 – 31.
© Permission issued by ASME, 12/13/2011
Following sections of this thesis are based on the work of this publication (W. Li, Xing, & Peng, 2011).
Section 1.3 3
Section 2.2 17
Section 2.3 19
Section 3.3 44
Section 4.3 78
Section 5.3 89

List of Abbreviations

AHP	Analytic hierarchy process
APE	Assembly Process Engineering
CAD	Computer-aided design
DFA	Design for Assembly
GTA	Glutaraldehyde
PBS	Phosphate buffered saline
PCL	Polycaprolactone
PGA	Poly(glycolic acid)
PLA	Poly(lactic acid)
PLLA	Poly(L-lactic acid)
PLM	Product Lifecycle Management
SBF	Simulated Body Fluid
SEM	Scanning Electron Microscopy
TE	Tissue engineering
TFE	2,2,2-trifluoroethanol
VE	Virtual Environment
VR	Virtual Reality

Chapter 1

Introduction

1.1 Background

Most tissues and organs in the human body such as muscles and nerves cannot regenerate spontaneously after injury or disease. Even for tissues that can regenerate spontaneously, they may not be able to completely recover in severe cases. For example, bone loses self-healing capability once its defect reaches a critical size. Tissue engineering, a multidisciplinary science, has been developed to repair and reconstruct damaged tissues by growing cells in biodegradable porous scaffolds as implants (Langer & Vacanti, 1993). As cells grow on the scaffold to form new tissue, scaffold itself slowly degrades. Cells could migrate and grow inside the scaffold during the degradation, and eventually the scaffold will be completely degraded and newly formed tissue will take its place. This new approach has shown promising results in both research and application.

In order to fulfill their role as implants, TE scaffolds should have good degradability, cell compatibility and mechanical strength, so that they can promote cell adhesion and growth while maintaining their original shape until the new tissues are formed.

1.2 Biomimetic Scaffolds for Bone TE

Bone tissue is one of the few human tissues that is capable of self-regeneration, but only for small defects. Complete bone reunion is usually missing once bone defects exceed the critical size or the fractures are complicated. Mechanical stability is critical for the bone healing process, so defects need to be bridged in order to heal. The ideal bridging material should be osteoinductive, osteoconductive, and containing osteogenic cells (Zimmermann, Wagner, Schmeckenbecher, Wentzensen, & Moghaddam, 2009). The most popular therapeutic strategy is the use of autologous bone grafts, which incorporate all features mentioned above to induce bone repair (Janicki & Schmidmaier, 2011). However, harvesting of autologous bone grafts usually causes donor site morbidity; common risks associated include infection, hemorrhage, nerve damage, loss of function, cosmetic disability, and chronic pain (Arrington, Smith, Chambers, Bucknell, & Davino, 1996; Chou, Mann, Coughlin, McPeake, & Mizel, 2007). The use of allografts prevents these hazards, but raises other problems such as potential risk of disease transmission from donor to recipient and immune responses towards the implant. Alternatively, tissue engineered bone substitutes have the advantage of unlimited availability without limitations like donor site morbidity, disease transmission, or immunogenic reaction, making them a promising replacement for auto- and allografts (Khaled, Saleh, Hindocha, Griffin, & Khan, 2011).

Due to that no single material fulfills all the design requirements for TE scaffolds, most existing scaffolds are fabricated by mixing certain ratios of two or more materials to make up for the disadvantages of any one single material. For example, materials with

good cell compatibility like collagen are usually mixed with materials with excellent mechanical strength like Poly (lactic acid) (PLA). If the ratio of collagen is increased, the composite scaffold will have better cell compatibility but weaker mechanical strength. In other words, the composite scaffolds may not have obvious drawbacks, but the advantages of component materials are diminished at the same time. Another problem with the current scaffolds is that cell tends to grow on the surface of scaffolds instead of migrating into the scaffold, leading to slow or incomplete tissue regeneration (Szpalski, Wetterau, Barr, & Warren, 2011).

1.3 Human Ear Reconstruction

Damages to the external ear could be caused by accidents or microtia, the latter is a congenital malformation and the prevalence varies from 0.83 to 17.4/10,000/population (Suutarla et al., 2007). Since the first ear-shaped cartilage was engineered in a nude mouse model (Cao, Vacanti, Paige, Upton, & Vacanti, 1997), a lot of research has been conducted in this field with different approaches. Recently, ear-shaped cartilage was engineered in vitro from composite scaffold made of polyglycolic acid (PGA) and polylactic acid (PLA) (Y. Liu et al., 2010). Titanium wire frameworks were used in another study to support collagen made scaffold for long-term stability after implantation (Zhou et al., 2011).

Although tissue engineering is a promising method for ear cartilage reconstruction, fabrication of tissue engineered human ear is still a very challenging topic due to the fact that the shape of the ear is irregular and sophisticated. The negative molds are required to

manipulate scaffolds into the desired shape. Traditionally, negative molds were fabricated by either hand carving (Zhou, et al., 2011) or impression casting on patient's ear (Cao, et al., 1997; Isogai et al., 2004). The hand carving alternative lacks accuracy, while impression casting only works for the normal ear instead of a damaged one. CAD technology was used to transfer the shape of ear into 3D digital models, so that a precise mirror model and respective negative molds could be fabricated (Y. Liu, et al., 2010).

The goal of this study is to digitalize the human ear using a 3D laser scanner, and fabricate the negative molds using 3D printing. With this new biomimetic structure, an ear-shaped scaffold with excellent mechanical strength can be produced.

1.4 Novel Design for Bioreactor

Cardiovascular disease, the leading cause of death in the United States, kills more Americans than cancer does. More than 500,000 coronary artery bypass procedures (CABP) are performed each year (Hashi et al., 2007). Arterial and venous grafts have been used in the CABP, which are associated with high costs and risk of exposure to diseases such as AIDS and hepatitis C. Moreover, some patients do not have suitable vessels for surgical harvest (Dahl et al., 2011). Therefore, replacing autologous vascular grafts with tubular vascular scaffolds produced by tissue engineering is the best option for many patients. Due to the 3D shape, tubular scaffolds cannot be cultured in traditional petri dishes, and specially designed bioreactors are required to promote even cell distribution during cell culture.

The process of tissue production in tissue engineering relies on bioreactors to simulate the physiological environment required for cell growth, attachment, and immigration. Many types of bioreactors have been developed in the last two decades, from motionless culture flasks to rotating wall chambers (Galaction, Cascaval, & Folescu, 2007). Due to the fact that mammalian tissues are very sensitive to nutrient needs, nitrogenated waste, pH values, and shear stresses, the bioreactor design is very complex. It is still currently at early stages of development, especially for 3D tissue engineering, where many important parameters for the tissue growth have not yet been fully understood (Galaction, et al., 2007). Recently, a rotating double-chamber bioreactor designed for tubular scaffolds has been developed to properly reconstruct the world's first stem-cell-based tracheal graft (Macchiarini et al., 2008). The commercial version of this bioreactor is named as BioReactor "In Breath" TYPE 807 and launched by Harvard Apparatus GmbH (Hugo Sache, 2010).

The existing bioreactor has a number of limitations. For example, synthetic grafts with diameters less than 4mm are unreliable due to frequent thrombosis and occlusion (Hashi, et al., 2007). There have been many researches involving small-caliber vascular graft in this area. However, the scaffold holder in the existing bioreactor can only support tubular scaffolds with diameters near 10mm. A compatible scaffold holder with much smaller diameter must be developed. Other problems related to the existing bioreactor operation are as follows :

- The connection between the motor shaft and input shaft is difficult to match; operators have to manually rotate the input shaft to get a proximate matching angle, which may require many trials of angle adjustments until the perfect

matching position is obtained.

- The connection between the input shaft and scaffold holder is a flat surface, it is difficult to obtain a steady alignment required for the mixer to slide down and secure the joint.
- In addition, the rotating double-chamber bioreactor has many details that could be modified to further improve its operation performance.

As mentioned above, the BioReactor "In Breath" TYPE 807 performs poorly in manual assembly and disassembly processes, both of which are critical for reducing the unnecessary exposure time and physical contacts with growing tissues during tissue mounting and harvesting procedures. It is therefore necessary to optimize the bioreactor for manual assembly and disassembly operations to minimize the risk of contamination and possible tissue damage.

1.5 Objectives and Rationale

Current problems and challenges:

- Compromised performance in traditional composite scaffolds. It is impossible to achieve high mechanical strength and cytocompatibility at the same time with the current scaffold design.
- Precise fabrication of scaffold is difficult for tissues with sophisticated three dimensional shapes.
- Poor manual assembly performance of an existing bioreactor could lead to cell culture contamination, which not only leads to wasted money and effort, but also causes unnecessary delay on implantation.

This study aims to:

- Optimize the traditional composite nanofibrous membrane scaffolds for maximum cytocompatibility and mechanical strength using the co-electrospinning method.
- Fabricate scaffolds that mimic the twisted plywood structure found in lobster cuticles using the new composite nanofibrous membrane, so that mechanical strength could be further enhanced.
- Make a human ear-shaped scaffold using the biomimetic scaffold with the aid of CAD technology.
- Improve the manual operation performance of BioReactor “In Breath” TYPE 807 using the DFA method within a virtual environment, so that the new bioreactor can minimize tissue damage during handling.

Chapter 2

Literature Review

2.1 Tissue Engineering

Most tissues in the human body cannot regenerate spontaneously in the event of an injury or disease. Even tissues that can regenerate spontaneously, bone and skin, for example, may not be able to completely recover in large defects. Tissue engineering (TE), a multidisciplinary science, has been developed to repair, maintain, or improve tissue function (Langer & Vacanti, 1993).

The concept of TE emerged in the 1980s, and quickly became the subject of increasingly intensive research. Compared to traditional biomedical engineering, TE is involved with living cells (Viola, Lal, & Grad, 2003), and one of the most common strategies is to reconstruct tissues with cell seeded polymeric scaffolds, which are biocompatible, biodegradable, and specialized to grow tissue-specific cells (Bhatia, 2010). Scaffold-free TE strategy has also been developed to fabricate cell sheets, which could be used to reconstruct three-dimensional tissues (Elloumi-Hannachi, Yamato, & Okano, 2010). Growth factor delivery is another important aspect of TE because it plays a crit-

ical role in cell growth and differentiation (Lee, Silva, & Mooney, 2011). Electric fields have also been used to manipulate cells in TE for better control during tissue reconstruction (Markx, 2008).

TE has its roots in clinical medicine because both fields are strongly application-oriented. Tissue engineered products have been successfully used in clinical applications since 1997 (Table 2.1) and the number of commercial products are growing rapidly. Pre-clinical studies have already found many promising scaffolds and cell types for TE (Evans, 2011; Wong, Rustad, Longaker, & Gurtner, 2010), the most recent successful clinical application includes implantation of TE bladders (Atala, Bauer, Soker, Yoo, & Retik, 2006) and tracheal segment (Macchiarini, et al., 2008). Further improvements have also been done on the tracheal implants to improve its functionality (Ott, Weatherly, & Detamore, 2011). For another example, TE heart valve constructs have the potential to replace traditional mechanical valves which suffer from high risk of thrombogenesis (Apte, Paul, Prakash, & Shum-Tim, 2011).

Potential financial rewards greatly stimulates the growth of TE, by the year of 2040 a quarter of the US GDP will be related to healthcare, and more than 8% of healthcare spending will be related to organ replacement (Services, 2006). With large funding from the government, industry, and private finance, it is very likely to over-engineer the TE products and make them unpractical for clinical use (Place, Evans, & Stevens, 2009). In another word, laboratory approach should always match the clinical needs (Ott, et al., 2011).

Table 2.1 Highlights of selected commercial tissue engineering products.

Tissue	Product	Time	Description
Skin	TransCyte, Advanced Bioheal-ing	1997	Nylon mesh coated with porcine collagen, containing non-viable human fibroblasts, with upper lay-er of silicon
	PriMatrix, TEI Bi-ociences	2008	Decellularized fetal bovine skin
Bone	INFUSE Bone Draft, Medtronic	2002	Bovine type I collagen sponges soaked in rhBMP-2 in LT-CAGE Lumbar
	Bioset IC, Pioneer surgical	2008	Human demineralized bone matrix with bovine bone chips in type I collagen carrier
Carti-lage	Synvisc, Genzyme	1997	Hyaluronic acid from chicken combs
	Menaflex, Re-genbiologics	2008	Bovine type I collagen with hyalu-ronic acid and glycosaminglycans, hydrated
Bladder	Neo-bladder, Ten-gion	Phase II	Poly(lactic-co-glycolic acid) seeded with urothelial and smooth muscle cells
Blood vessel	VascuGel, Pervasis	Phase II	Gelfoam procine gelatin foam sponges seeded with endothelial cells

Tissue engineering uses biocompatible and biodegradable structures as implants; these porous structures, usually called scaffolds, are capable of mimicking extracellular matrix (ECM) to induce cell adhesion, migration, proliferation, and differentiation (Ma, 2008). Scaffolds should have enough mechanical strength to maintain their original shape during the healing process, so that a mechanical stable environment is available for new tissue formation. Scaffolds should also have the ability to deliver biofactors like cells, growth factors, and proteins, so that tissue regeneration is enhanced and the goal of tissue repair can be achieved.

2.1.1 Materials for TE scaffolds

Scaffolds can be divided into two groups based on materials: natural and synthetic. Natural scaffolds are mostly made of natural polymers like collagen (Phipps, Clem, Grunda, Clines, & Bellis, 2012), fibrin (Liang & Andreadis, 2011), chitosan (Zhao et al., 2011), silk (Y. Zhang et al., 2011), and gelatin (Hussain, Bessho, Takahashi, & Tabata, 2011). These materials have excellent cell compatibility which is enhanced by their bioactivity with related peptide sequences (Holzwarth & Ma, 2011). Synthetic scaffolds, such as poly(lactic acid) (PLA) (P. Zhang et al., 2011), poly(L-lactic acid) (PLLA) (Schofer et al., 2011), poly(glycolic acid) (PGA)(Choi, Choi, Park, Kim, & Min, 2010), and polycaprolactone (PCL) (G. H. Kim, 2008), lack bioactivity but have advantages in stability, flexibility, and mechanical strength. Since both natural and synthetic materials have their own advantages and disadvantages, composite scaffolds were developed to minimize the drawbacks of both. In this study gelatin and PCL were used to fabricate composite scaffolds for bone regeneration due to the fact that they complement each other very well. This combination of polymers was analyzed and evaluated in research with promising results (Chong et al., 2007; Jeong, Lee, Lee, & Shin, 2008; C. Y. Li et al., 2011; Xiang, Li, Zhang, Chen, & Zhou, 2011). As a denatured form of collagen, gelatin maintains excellent cell compatibility and biodegradability without causing potential immunological problems (Harrington & Von Hippel, 1961; Langer, 2009). Although tougher than collagen, its mechanical stiffness is still not high enough for bone scaffolds, so polymers with better mechanical porperties like PCL are required as a co-electrospinning polymer. PCL is also biodegradable within the human body, forming a naturally occurring chemical

called lactic acid (Khaled, et al., 2011). Compared to similar materials like PGA and PLA, PCL has the slowest degradation speed, which means it is capable of providing sufficient mechanical support for a longer period of time. The fast-degrading gelatin results in a rapid increasing in pore size, which is favorable for cell migration and differentiation, while the slow-degrading PCL makes sure that the mechanical strength of the composite scaffold is not sacrificed. It is hard for cells to attach on a pure PCL scaffold due to its hydrophobicity, and the composite scaffold has much better cell adhesion because gelatin is very hydrophilic. Another advantage of the gelatin/PCL combination is that both polymers can be fabricated into scaffolds effectively. The composite nanofibrous membrane produced in this study took only 1 hour to electrospin, which is significantly faster than polymers like chitosan and silk, and such advantage is critical for clinical translation (Place, et al., 2009).

In order to further improve the mechanical strength of the scaffold, the twisted plywood structure (Figure 2.1) was found in the cuticle of lobster *Homarus americanus*, and it greatly increases the stiffness of the cuticle while maintain a very low weight (Nikolov et al., 2010). Such structure can be mimicked by stacking layers of aligned nanofibrous membranes to create a scaffold with enhanced mechanical strength to provide a more mechanical stable environment for bone regeneration.

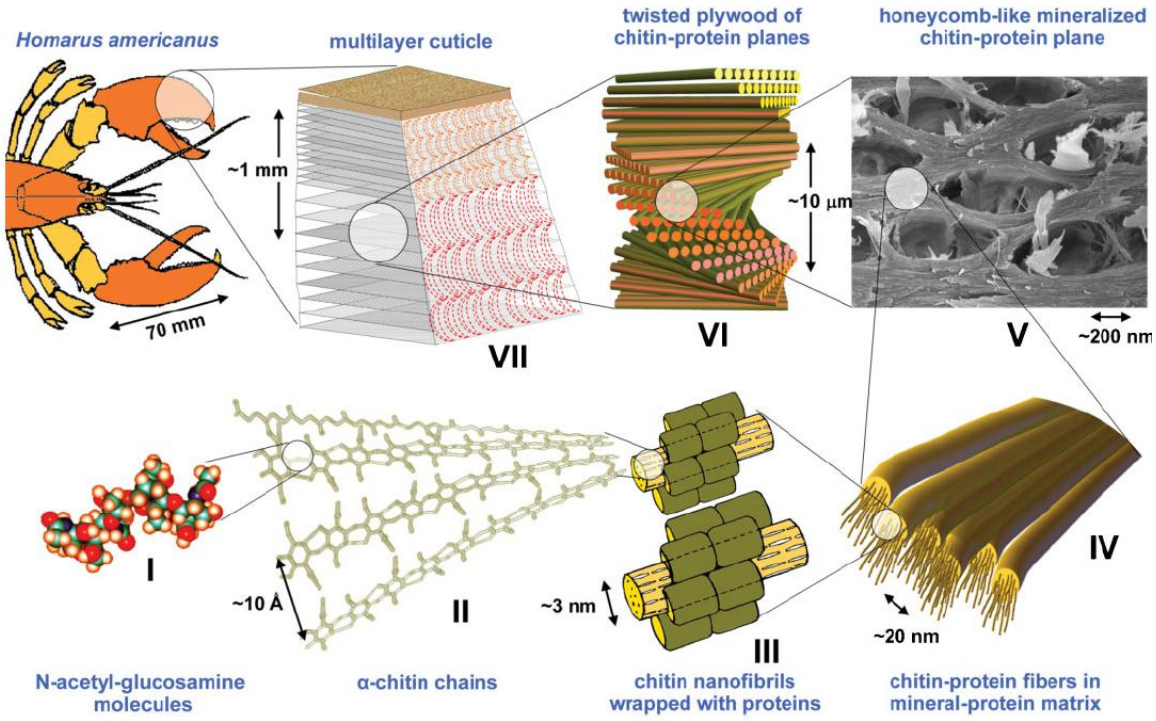

Figure 2.1 Hierarchical structure of the lobster cuticle: I) N-acetyl-glucosamine molecules, II) antiparallel chains of a-chitin, III) chitin–protein nanofibrils, IV) chitin–protein fibers in a mineral–protein matrix (not shown), V) cuticle with pore canal system (in-plane cross-section), VI) twisted plywood structure, and VII) three-layered cuticle.
Source: Nikolov, et al., 2010. Used with permission (12/04/2011), © Svetoslav Nikolov.

After electrospinning, the nanofibrous membranes need to be cross-linked to maintain the morphology of gelatin nanofibers. Genipin and Glutaraldehyde (GTA) were used as gelatin cross-linkers in previous studies and both showed promising results (Chang, Chang, Lai, & Sung, 2003; Qian, Zhang, Chen, Ke, & Mo, 2011). The method of GTA vapor cross-linking is chosen in this study due to the fact that the process is less time consuming.

Lots of bone tissue engineering related research immerse scaffolds in Simulated Body Fluid (SBF) to deposit calcium, phosphorous, and magnesium ions , which are favorable

to the bone formation (Bigi, Bracci, Cojazzi, Panzavolta, & Rubini, 2004; X. Liu, Smith, Hu, & Ma, 2009; J. Lu et al., 2011; Ren, Tsuru, Hayakawa, & Osaka, 2002), so this treatment is used to further enhance the bone repair function of our new composite scaffold. It is also possible to physically or chemically add drugs (Wei, Li, Mugishima, Teramoto, & Abe, 2011), growth factors (Du et al., 2012), enzymes (D. Lu, Cardiel, Cao, & Shen, 2010), or proteins (Zou et al., 2011) to nanofibrous scaffolds for controlled drug release or better mimicking of the cellular environment.

The main limitation of the electrospun nanofibrous membranes is its pore size, which is usually too small for cells to migrate into the scaffold so that they can only grow on the surface. With gelatin/PCL composite scaffold, larger pore size was achieved upon gelatin degradation, but the improved pore size only allows cell penetration up to 0.1 mm (Zhang, Ouyang, Lim, Ramakrishna, & Huang, 2005). In order to overcome this limitation, membranes were seeded with cells first, then stacked together to form the twisted plywood structure with cells between each layer.

2.1.2 Fabrication methods of TE scaffolds

Many scaffold fabrication methods have been developed in tissue engineering; the most common ones are cross-linking (Van Vlierberghe, Dubruel, & Schacht, 2011), self-assembly (Nowak et al., 2002), freeze-drying (Santin et al., 1996), salt-leaching (Wu, Jing, & Ding, 2006), gas-foaming (Murphy, Peters, Kohn, & Mooney, 2000), and electrospinning. Compared to other methods, electrospinning is a highly versatile technique that offers better control over scaffold composition and morphology. When it was first proposed as a viable fiber fabrication method in the early 1930s (Subbiah,

Bhat, Tock, Parameswaran, & Ramkumar, 2005), electrospinning didn't get much attention. During the past few years, due to the rapid growth in nanotechnology, lots of studies have explored the relationships between electrospinning parameters and structure features.

As shown in Figure 2.2 the basic setup of an electrospinning system consists of a high voltage power supply, a syringe mounted on a syringe pump, and a rotating drum collector. Electrostatic forces created by the high voltage difference between the syringe tip and the collector act on the polymer solution, and form a jet once the force is larger than the surface tension. As the jet travels, solvents evaporate and leave nanofibers on the collector.

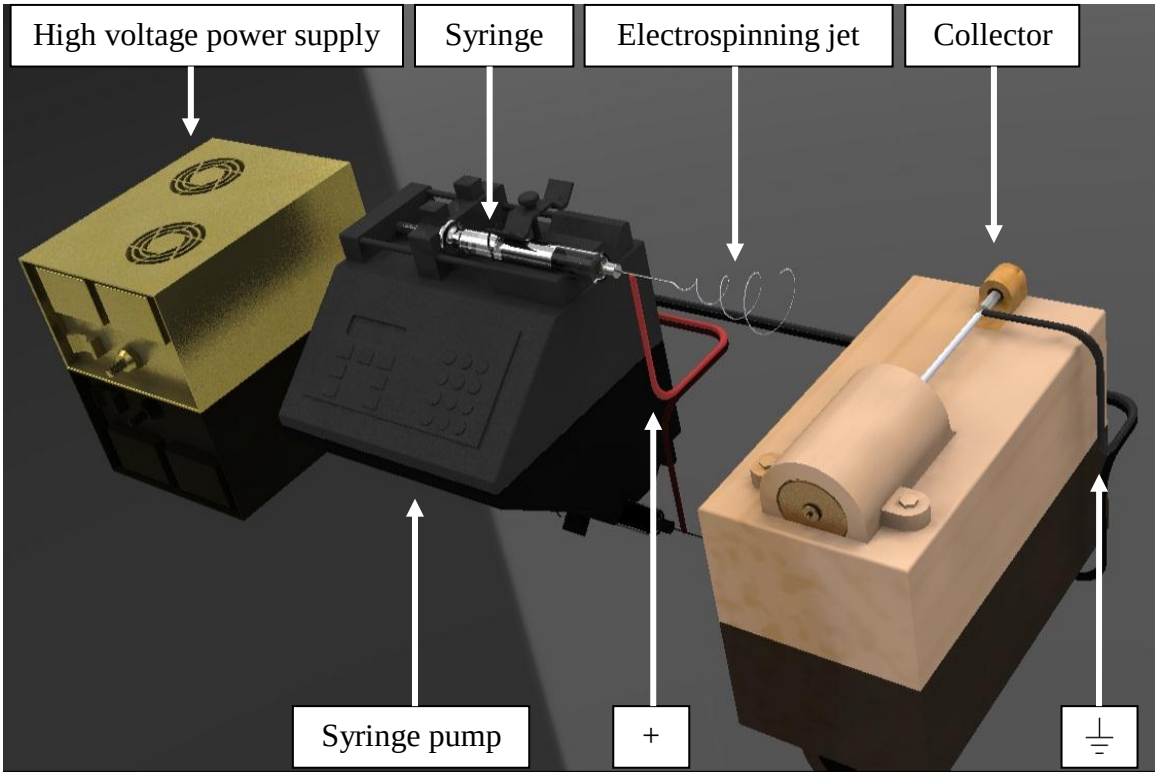

Figure 2.2 Basic setup of an electrospinning system.

Parameters of electrospinning process include solution properties, controlled variables, and ambient parameters (Doshi & Reneker, 1995). Solution viscosity has the biggest impact on fiber size and morphology among solution properties. It is very convenient to adjust viscosity by altering the polymer concentration, and higher concentration leads to larger fibers. As the driven force of electrospinning, field strength is the most important parameter among controlled variables. Higher applied voltage means higher field strength and leads to smaller fiber diameter. Ambient parameters include factors like temperature and humidity. Temperature affects the fiber size by changing the solution viscosity, and high humidity results in small circular pores on the fiber surface. Since it is relatively hard to control ambient parameters, it's more practical to adjust solvent properties and controlled variables instead.

Besides adjusting electrospinning parameters, it's also possible to modify electrospinning setup to produce fibers with unique morphologies. Aligned fibers were fabricated using a rotating drum collector, and the degree of alignment could be adjusted by changing the rotatory speed of the drum collector (Chew, Wen, Yim, & Leong, 2005). Such aligned nanofibers could be used to produce scaffolds that mimic native tissues; it could also be used to manipulate the mechanical properties of scaffolds. Hollow nanofibers were produced by using a co-axial, two capillary spinneret (Li & Xia, 2004), and they could be used for drug release.

2.2 Design for Assembly

Assembly is an important activity in product manufacturing and maintenance. Based on statistical data, assembly can take up to 50 per cent of product manufacturing cost (Mathew & Rao, 2010). Assembly-related design problems have been explored by engineers and researchers for decades. DFA evaluates product design to make it suitable for an assembly process. The published work has introduced design guidelines and heuristic rules for qualitative evaluation. Desai and Mital discussed a comprehensive design methodology for ease of assembly (Desai & Mital, 2010). Gerdemeli et al. used DFA in a redesign process of the glass block holder for an automation machine used in the glass production industry (Gerdemeli, Fetvaci, & Kayaoglu, 2011). Khan discussed DFA importance in print circuit board design, fabrication, assembly and test (Khan, 2010). Park et al. proposed an assembly strategy to satisfy basic assembly requirements of the Tokamak device. The assembly is designed based on assembly plan, available space, cost, safety, easy operation, and efficient maintenance (Park et al., 2010). Demoly et al. suggested a method of DFA for Assembly Process Engineering (APE) and Product Lifecycle Management (PLM). Assembly constraints were considered in the early product development for the need of concurrent engineering (F. Demoly, Gomes, Eynard, & Rivest, 2010). Tavares et al. considered alternatives for fasteners used in airframes to simplify the design for manufacturing and assembly process (Tavares & de Castro, 2011). Xu and Li implemented the assembly variant design for complicated task planning. They used a dimension constraint network among parts at the dimension level (Xu & Li, 2010).

In the early product design stage, it is desirable to produce a number of potential solutions to help designers fully explore possible solutions based on design for manufacture and assembly heuristics (Poppa, Stone, & Asme, 2010). Different approaches have been proposed for assembly design, process, and operations, such as assembly oriented product design and optimization; integration of assembly evaluation, assembly process planning and assembly system design; computer-aided assembly systems using assembly features supported by an agent paradigm; the decision support of parts' assembly sequences; the fuzzy DFA decision support system; and the DFA approach based on system modeling language paradigm considering an assembly oriented product structure (Frederic Demoly, Yan, Eynard, Rivest, & Gomes, 2011).

Mathematical models can be used to describe DFA heuristic rules and assembly processing for an assembly oriented design framework. They provide guidance to assembly planning and product structure (Frederic Demoly, et al., 2011). The trade-off, or solving conflict is an important process in assembly design. Trade-off parameters must be balanced to achieve design optimization. Li used an analytic hierarchy process (AHP) to aid in alternatives selection. TRIZ and AHP were integrated for the assembly design selection. TRIZ converts a complex design problem into a contradiction matrix. AHP decomposes the decision process into a hierarchical sequence to determine the relative importance of each alternative through pairwise comparisons (T. Li, 2010).

Liu used a variant design method of assembly to improve design efficiency of the product (F. Liu, Lu, & Kuang, 2011). Wang et al. used a class-diagram based assembly model in the aero-engine assembly for assembly planning, operation simulations and evaluations (Wang, Yu, & Zhang, 2010). Huang and Kong's research on product assembly consid-

ered both product and the manufacturing system applied. Uncertainties were discussed for process capability and product usability affected by users' capability (Huang & Kong, 2010).

Some ergonomic studies have found that due to improper designs, defective parts, variance in assembly system, and operating errors, failures related to operator-induced assembly defects can occur. Many researchers have discussed assembly complexity. DFA can evaluate a design based on modeling assembly difficulty, which can be measured based on component complexity and assembly complexity (Su, Liu, & Whitney, 2010).

Therefore, DFA provides useful guidelines for an optimal product design. However, its effectiveness may not be immediately tested until the product is made. VR is an ideal tool for the purpose of saving time and cost on making the actual prototype.

2.3 Virtual Reality (VR) and Applications in DFA

VR provides a sense of presence in virtual environments. It is a useful tool for simulating human-machine interactions. Using virtual assembly simulations, designers can improve DFA in virtual environments. Assembly evaluation can be performed in the early product design stage. A conceptual design can be optimized using VR simulation.

Besides offering the ability to visualize the product assembly process, complex human interactions can be analyzed in virtual simulations to identify assembly-related problems such as tools and parts accessibility, operation ability, handling ability, operation directions and angles required during assembly. VR can also provide a good training platform for users to perform assembly tasks.

As VR provides a cost-effective tool to evaluate designs without actual production, VR is widely used to support research and industrial applications. For example, Kang and Peng's application of VR in DFA analysis, used VR in product design and manufacturing simulation to address both geometric and subjective evaluations required in an assembly operation (Kang & Peng, 2010). Liu discussed the digital virtual assembly process and the assembly simulation using process modeling and simulation technology (H. Liu, Shen, & Fan, 2010). Jin et al. introduced a 3D analysis model to evaluate the different assembly schemes (Jin, Cai, Lai, & Lin, 2010). 3D CAD modeling allows the visual inspection of a design and identification of any potential problems in product assembly (Thomas, Legoy, & Amann, 2010).

Yip-Hoi analyzed product assemblies using modeling techniques and assembling mechanisms for training purposes. The simulation was applied toward both assembly modeling and collaborative assemblies (Yip-Hoi, 2010). Chen developed an assembly model in a virtual assembly system based on assembly constraints using object-oriented hierarchical structures (Chen, Wu, & Yang, 2010).

Ergonomics related design is important for product assembly, which can also be evaluated in VEs for working postures and physical workloads in assembly (Alzuheri, Luong, & Xing, 2010). Although assembly-related issues have been explored by industrial engineers and academic scholars for several decades, operator-induced assembly defects have not been fully addressed (Su, et al., 2010). VR provides an ideal interface for the evaluation of operator-induced assembly. Seth reviewed various VR applications and technologies for DFA (Seth, Vance, & Oliver, 2011).

Therefore, VR is an ideal tool for simulating tasks that require frequent and intuitive manual interaction. We propose an assembly modeling approach to meet the VR simulation by improving and integrating existing methods. A virtual environment, Eon Studio (Eon Reality, 2011), is used. The proposed method provides an optimal product design for bioreactor operators to manipulate the device accurately and efficiently.

Chapter 3

Methods

3.1 Biomimetic Scaffolds for Bone TE

3.1.1 Experiment design

The experiment is divided into two phases as shown in Figure 3.1. The first phase on the left side of the flow chart is fabrication of new composite nanofibrous membranes, and the second phase on the right side of the flow chart is fabrication of the biomimetic twisted plywood structure.

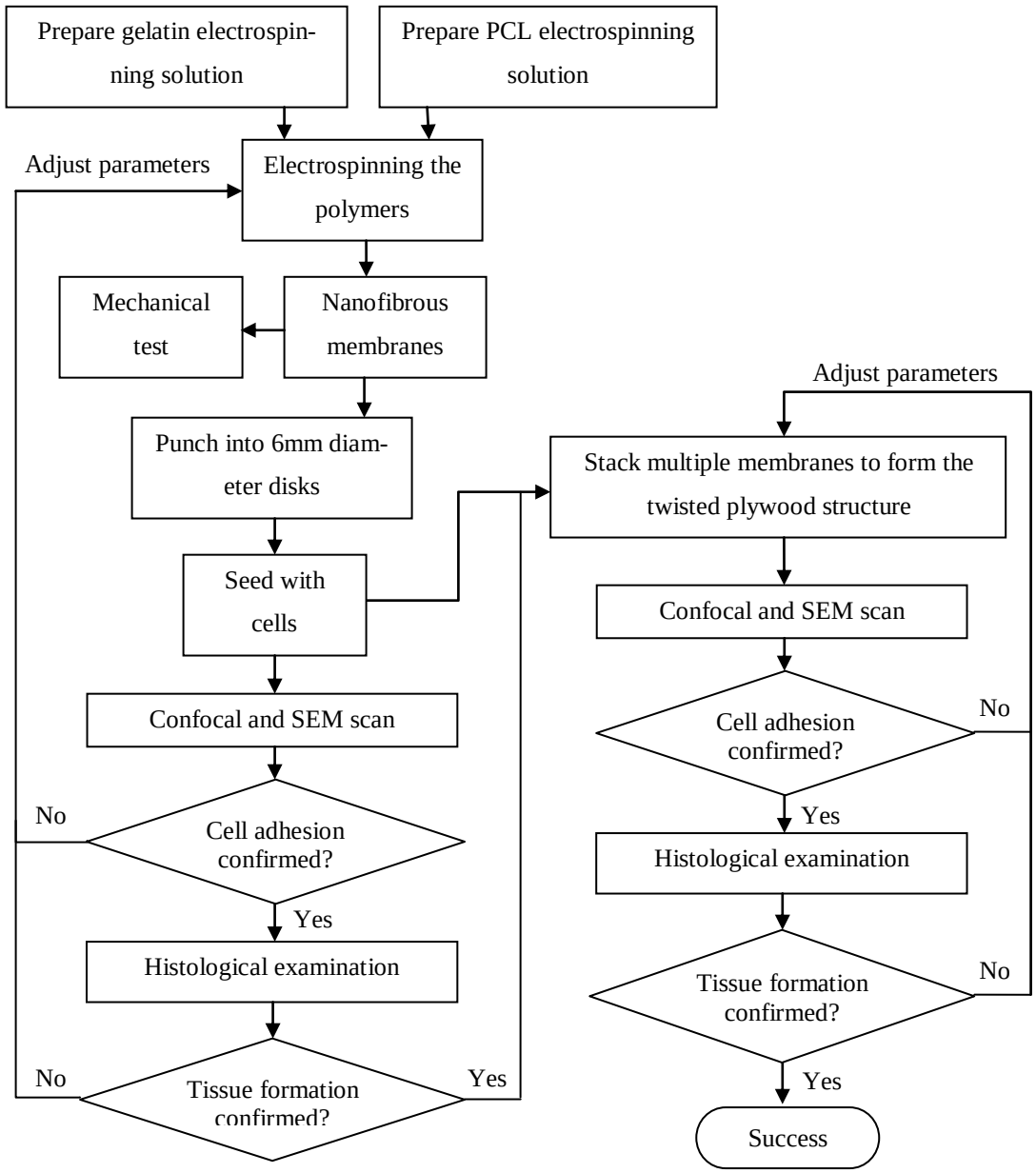

Figure 3.1 Flow chart of the experiment design for biomimetic scaffold.

3.1.2 Fabrication of aligned gelatin/PCL nanofibrous membranes with layered structure

Pre-electrospinning polymer solutions were prepared 1 day before electrospinning and stirred with magnetic bars overnight. PCL particles were added into 2,2,2-trifluoroethanol (TFE) to create 10% w/v PCL solution. Type A gelatin powder was dissolved in the water-based co-solvents containing 60% v/v acetic acid and 10% v/v ethyl acetate to produce 20% w/v gelatin solution (Song, Kim, & Kim, 2008). Syringes loaded with each pre-electrospinning polymer solution were mounted on two syringe pumps that were placed at opposite sides of the aluminum-foil-wrapped rotating drum collector (Figure 3.2). A voltage of 20 kV was applied on the two 20 gauge syringe needles to create an electrostatic force field for electrospinning, and a rotation speed of 1000 rpm was applied to the grounded drum collector to fabricate aligned nanofibrous membranes. The flow rate of gelatin and PCL solutions used for electrospinning are indicated in Table 3.1 to create membranes with layers of different compositions (Figure 3.3). The inside layer contains 70% PCL for maximum mechanical strength (M. S. Kim et al., 2010) and the outside layers contain only 10% PCL for better cell compatibility.

The fabricated membranes were removed from the drum collector with aluminum foil and dried under vacuum at room temperature overnight to fully evaporate the remaining solvent, followed by vapour crosslinking with glutaraldehyde (GTA) in a sealed chamber for 3 days, and then the membranes were vacuumed again before immersing in Simulated Body Fluid (SBF) for two days for mineral deposition. The steps of preparing SBF are shown below:

1. Add 500 ml of ion-exchanged and distilled water into a 1L bottle, and stir with a magnetic stirrer.
2. Add 7.996 g of NaCl.
3. Add 0.350 g of $NaHCO_3$.
4. Add 0.224 g of KCl.
5. Add 0.228 g of $K_2HPO_4 \cdot 3H_2O$.
6. Add 0.305 g of $MgCl_2 \cdot 6H_2O$.
7. Add 40 mL 1M-HCl.
8. Add 0.278 g of $CaCl_2$.
9. Add 0.071 g of Na_2SO_4.
10. Add 6.057 g of $(CH_2OH)_3CNH_2$.
11. Put the bottle in a water bath to adjust the temperature of the solution to 36.5℃.
12. Add 1N-HCL to adjust the pH value to 7.40.
13. Add ion-exchanged and distilled water to adjust the total volume to 1L.

The treated membranes were punched into small partial disks (Figure 3.4) for cell seeding, and the asymmetrical shape was used to indicate the orientation of the nanofibers.

By replacing the drum collector with a smaller diameter mandrel, tubular composite scaffolds with layered structure (Figure 3.5) were created. Such scaffolds were made for repairing microvessels after cell culture in BioReactor “In Breath” TYPE 807.

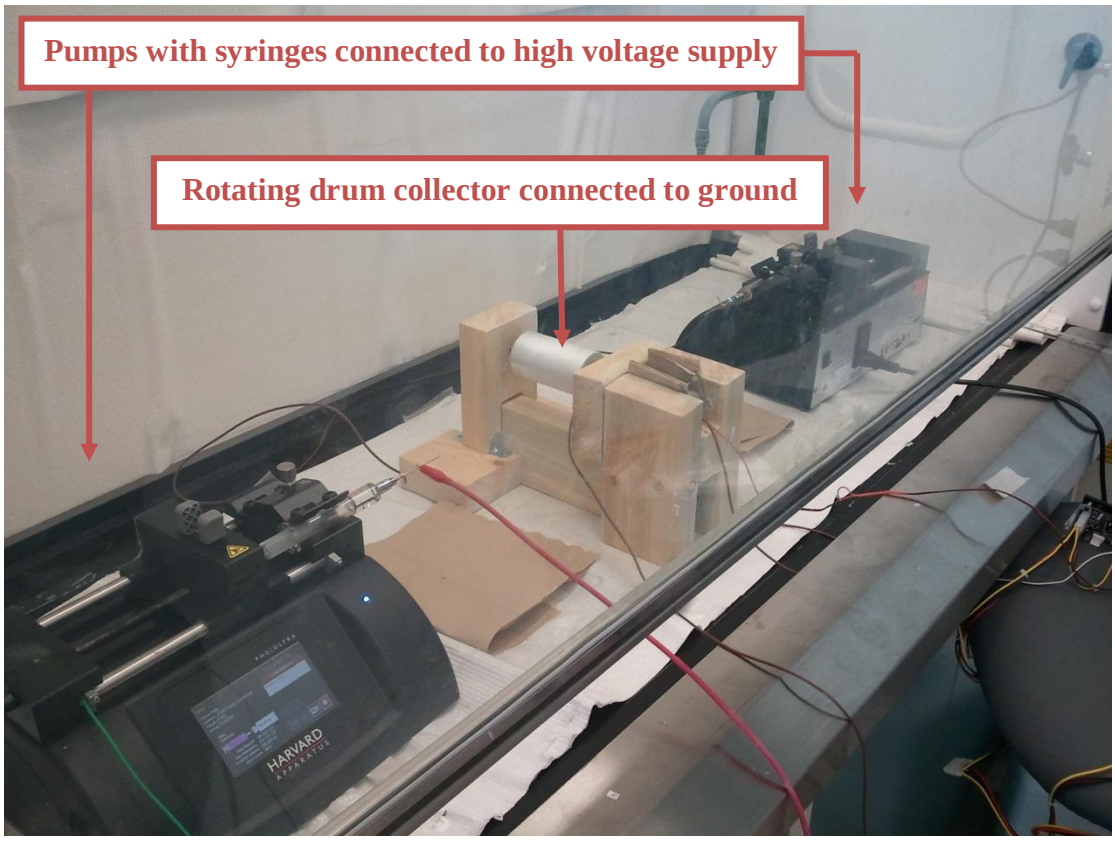

Figure 3.2 The co-electrospinning setup.

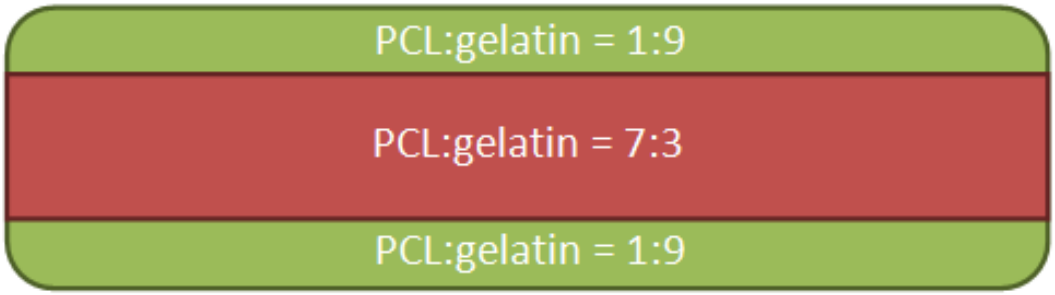

Figure 3.3 Schematic view of the cross section of gelatin/PCL composite nanofibrous membrane.

Table 3.1 Detailed feed rates used to fabricate of a new composite scaffold.

Time	0 – 20 min	20 – 100 min	100 – 120 min
PCL (10%. m/v)	0.11 ml/h	2.33 ml/h	0.11 ml/h
Gelatin (20%, m/v)	0.5 ml/h	0.5 ml/h	0.5 ml/h

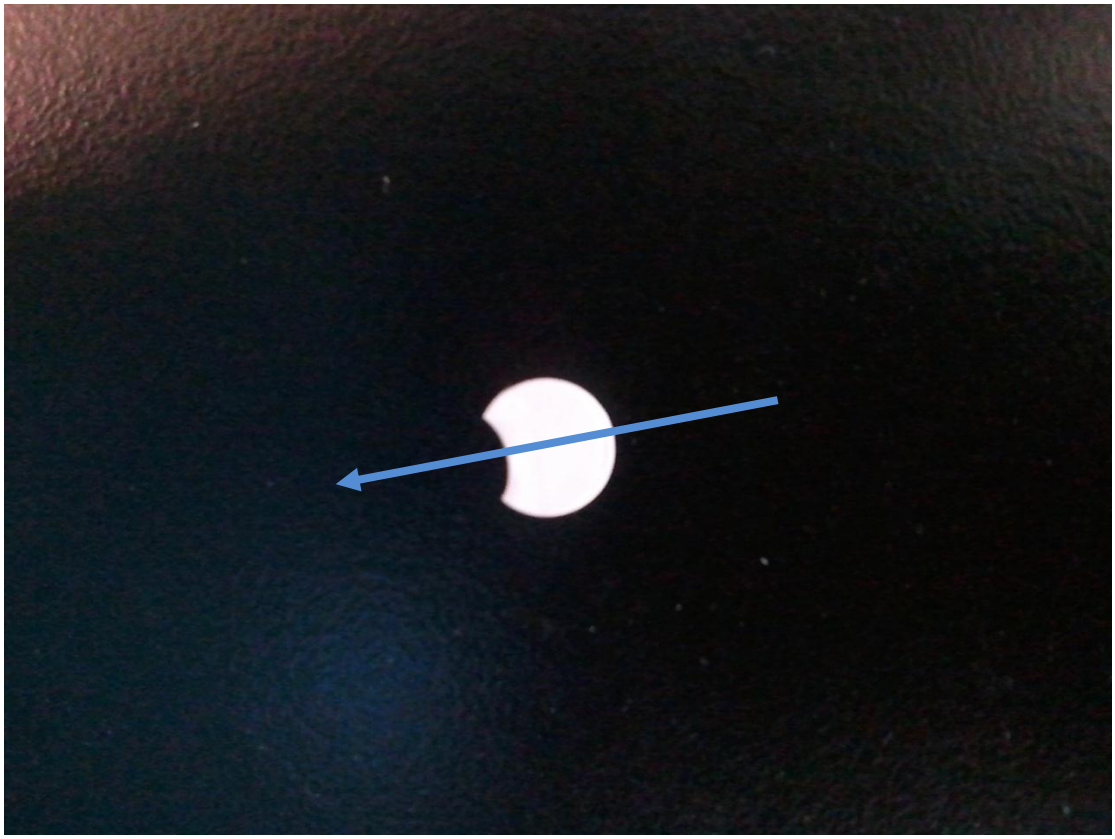

Figure 3.4 Partially punched membrane disk for indication of alignment direction.

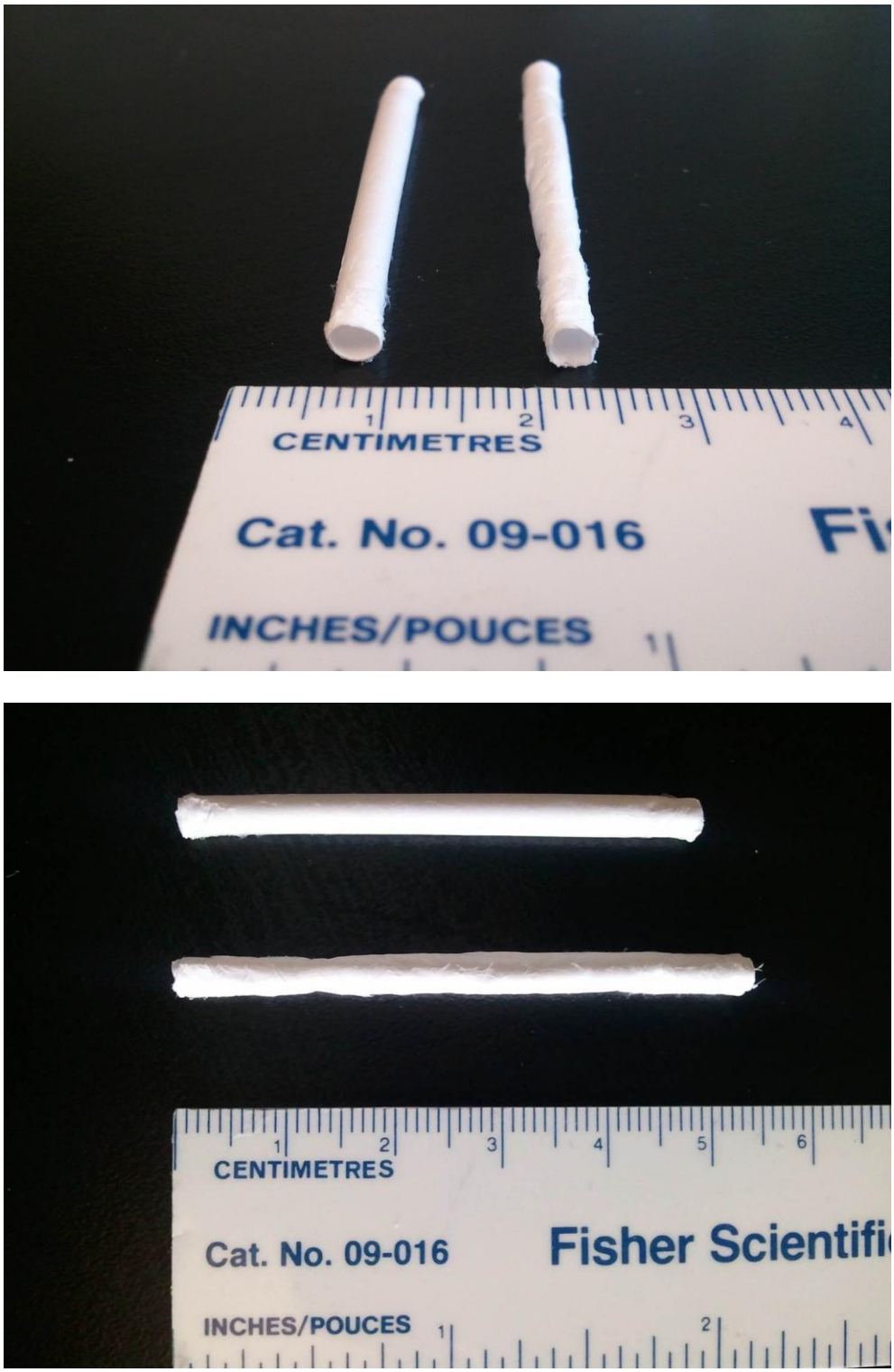

Figure 3.5 Tubular scaffolds for small-caliber vascular graft.

3.1.3 Cell culture

Preosteoblasts were purchased from American Type Culture Collection (ATCC) and cultured with Alpha Modification of Minimum Essential Medium supplemented with 10% fetal bovine serum and 1% penicillin, at 37 ℃ and 5% CO_2. Cells were harvested by adding 0.25% Trypsin in Balanced Salt Solution followed by quenching with medium to re-suspend the cells. Nanofibrous membranes were pre-treated for seeding by incubating with Phosphate-buffered Saline (PBS) overnight and dried on filter paper immediately prior to cell seeding. Cell suspension was centrifuged at 3000 rpm for 8 minutes, then the cellular concentration was adjusted to 5×10^6 cells mL^{-1}. Each nanofibrous membrane was incubated for 3 hours after cell seeding with 20 μL of cell suspension to allow cell attachment, then culture medium was added and changed every 2 days (ATCC, 2011).

3.1.4 Fabrication of paper-stacked biomimetic scaffold with twisted plywood structure

The twisted plywood structure (Figure 3.6) is obtained by stacking multiple aligned PCL/gelatin nanofibrous membranes with a clockwise twist in alignment direction of 15 degrees after one week of cell seeding. In order to track the alignment direction after cell seeding, membranes were punched into partial disks (Figure 3.4) as mentioned in section 3.1.2. Each twisted plywood scaffold was made of five layers of membranes, and they were cultured in multi-layer scaffold holder as shown in Figure 3.7, such holder makes sure the scaffolds maintain their twisted wood structure during cell culturing by sandwiching them between autoclavable stainless steel meshes.

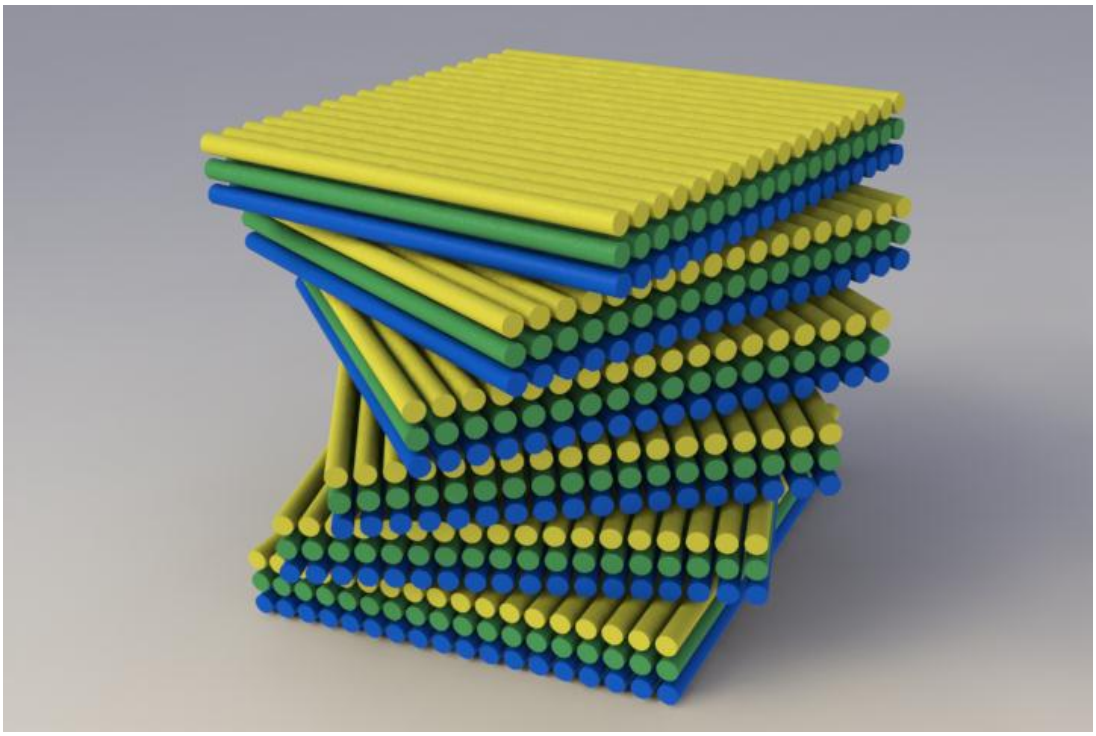

Figure 3.6 The twisted plywood structure.

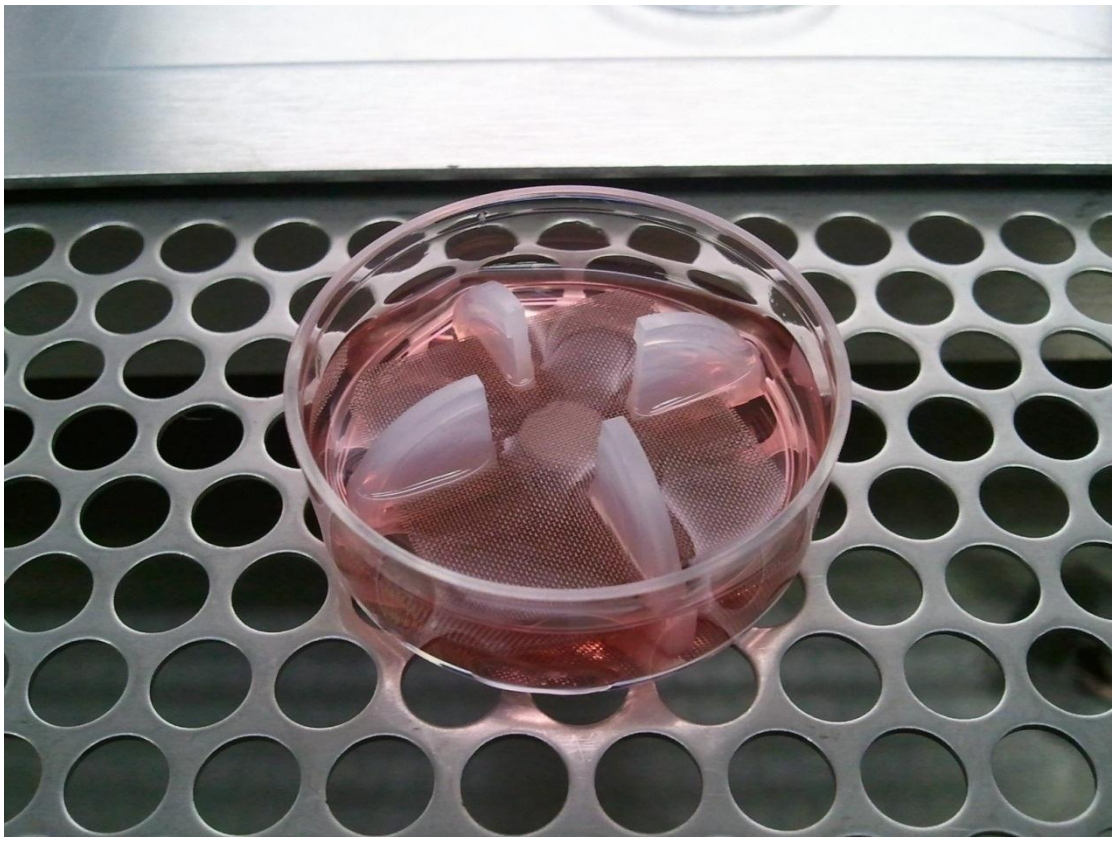

Figure 3.7 The multi-layer scaffold holder during cell culture.

The downside of the scaffold holder in Figure 3.7 is that precise insertion is required during assembly and contacts with gloves are unavoidable, causing high risk of contamination. The new design of the scaffold holder (Figure 3.8) is made of only two pieces of stainless steel meshes that automatically clamp together when the top piece is pushed down, and this operation could be done using autoclaved tweezers to prevent contamination.

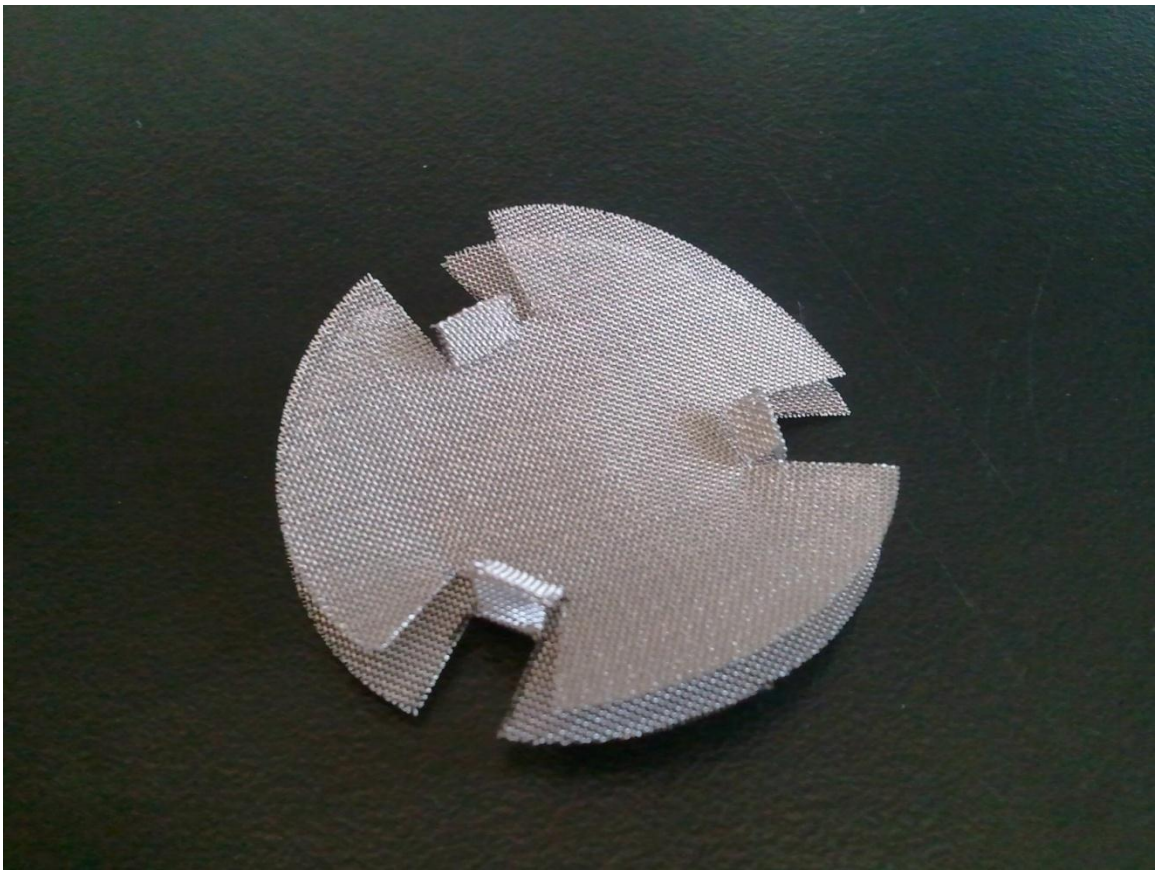

Figure 3.8 The new design of multi-layer scaffold holder.

3.1.5 Mechanical testing

Tensile tests on biomimetic scaffolds, pure PCL scaffolds, and pure gelatin scaffolds were performed on a Zwick Z005 testing machine. In order to eliminate failure caused by griping force, nanofibrous membranes were cut into dog-bone-shaped specimens, which are 70mm × 20mm overall in size and 40mm × 10mm in the gauge area (Figure 3.9). For the biomimetic scaffolds, samples were made of 6 layers with a twist angle of 30 degree and a total thickness of 0.5mm. For the nonwoven pure PCL and gelatin scaffolds, the same thickness of 0.5mm was used. A stretching rate of 4mm per minute was applied until the load drop below 60% of the maximum load.

Figure 3.9 Dog-bone-shaped specimen for tensile tests.

Compressive tests were performed on the same testing machine Zwick Z005 with a compression rate of 2mm per minute. Samples were punched into small discs with diameter of 6mm and thickness of 1mm. Cyclic compression tests were performed first to bring the samples to a stable condition for the large loading tests. During cyclic compression tests, samples were compressed until 15N of resistance was achieved, then the testing machine removed all the loading before next compression cycle. 3 cycles were performed before the samples were compressed to a maximum strain of 0.9 for the large loading tests.

3.1.6 Scanning Electron Microscopy (SEM)

After 1 week of cell culturing, sample scaffolds were fixed with 4% paraformaldehyde for 24 hours then dehydrated in graded concentrations of ethanol (10 min each in 30, 50, 70, 90, and 100%, followed by two more times in 100% ethanol). The dehydrated scaffolds were gold coated and observed under the SEM under an accelerating voltage of 20 kV.

3.1.7 Confocal Laser Scanning Microscopy

After 1 week of cell culture, scaffold samples were stained in the following steps for confocal laser scanning microscopy:

1. Wash with PBS for 3 times to remove cells from the culture medium.
2. Add 4% paraformaldehyde to fix the cells for 10 min.
3. Wash with PBS once.
4. Add bovine serum albumin and immerse for 10 min
5. Add Triton X-100 and immerse for 5 min.
6. Wash with PBS once.
7. Add phallacidin to stain cytoskeleton for 20 min.
8. Wash with PBS twice.
9. Add TO-PRO-3 to stain cell nuclear for 20 min.
10. Wash scaffolds with PSB twice to remove excessive stains.
11. Wait for stained scaffolds to dry then fix them between microscope slides and top slips for observation under confocal laser scanning microscopy.

In order to view the cross section of paper-stacked scaffold under confocal microscopy, cryosection was performed after performing the staining procedures mentioned above. The stained samples were transferred into embedding molds filled with tissue freezing medium then froze at -80 ℃ overnight. Slices with thickness of 10 micrometers were cut using the cryostat LEICA CM3050S for observation under confocal laser scanning microscopy.

3.1.8 Von Kossa Stain

Sample scaffolds were treated in the following steps to verify calcification:

1. Incubated with 1% silver nitrate solution in a clear glass coplin jar placed under UV light for 20 minutes.
2. Wash with distilled water twice.
3. Add 5% sodium thiosulfate to remove un-reacted silver for 5 minutes.
4. Wash with distilled water once.
5. Counterstain with nuclear fast red for 5 minutes.
6. Wash with distilled water once.
7. Dehydrate through graded alcohol and clear in xylene.
8. Wait for stained scaffolds to dry then fix them between microscope slides and top slips for observation under optical microscopy.

3.2 Reconstruction of Human Ear

3.2.1 Experiment design

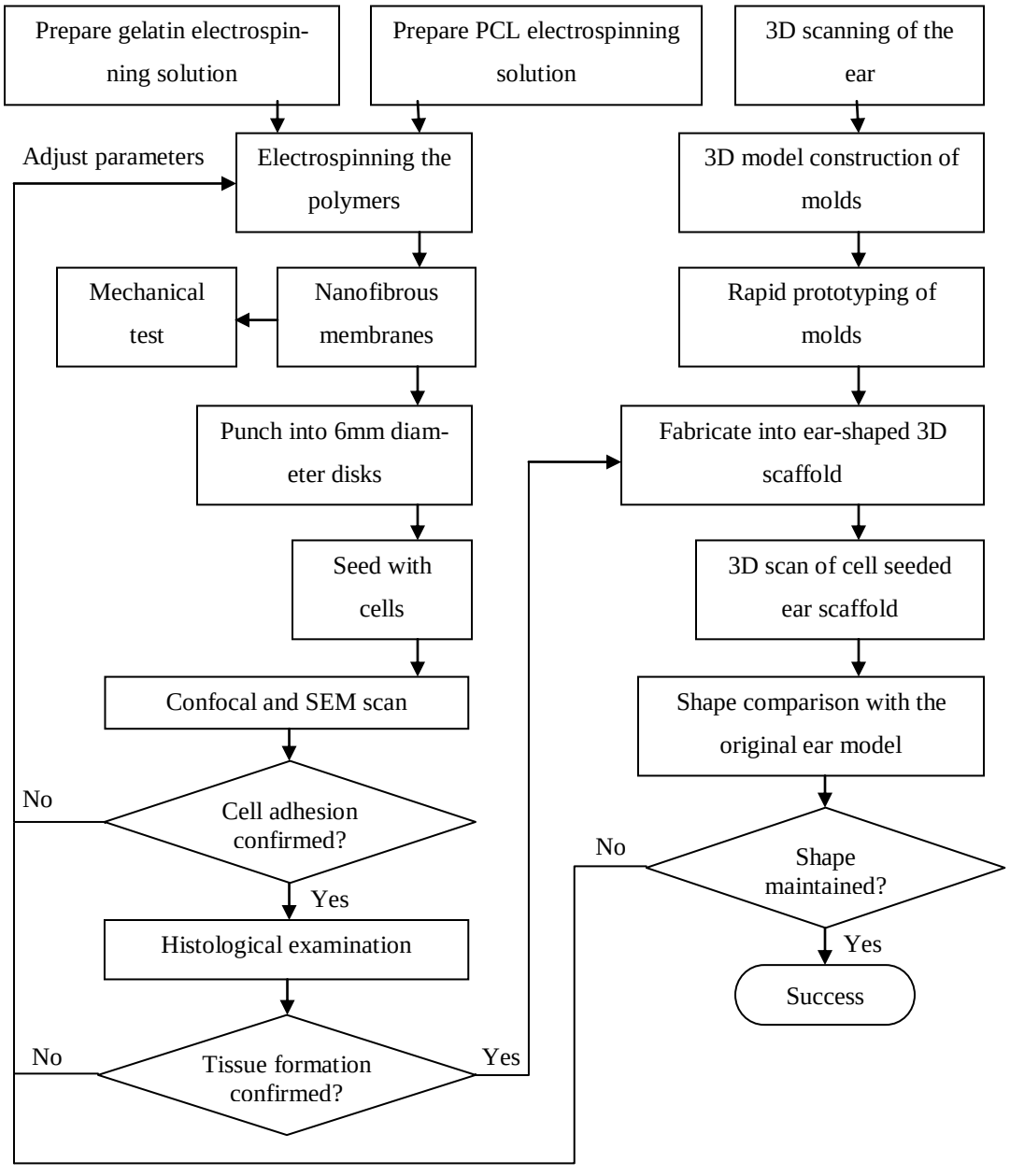

Figure 3.10 Flow chart of the experiment design for human ear reconstruction.

The experiment design is shown in Figure 3.10. Due to the fact that fabrication process of the biomimetic scaffold has already been discussed in the previous section, this section will focus on VR technology and mold fabrication. A human ear model was used for this study to provide consistent measurement (Figure 3.11).

Figure 3.11 The ear model used for this study.

3.2.2 Laser scanning of the human ear model

ShapeGrabber 3D laser scanner (Figure 3.12) was used in this study to capture the geometric data of the human ear model. The scan resolution was set to 0.05mm to match the maximum resolution of the 3D printing system used later on.

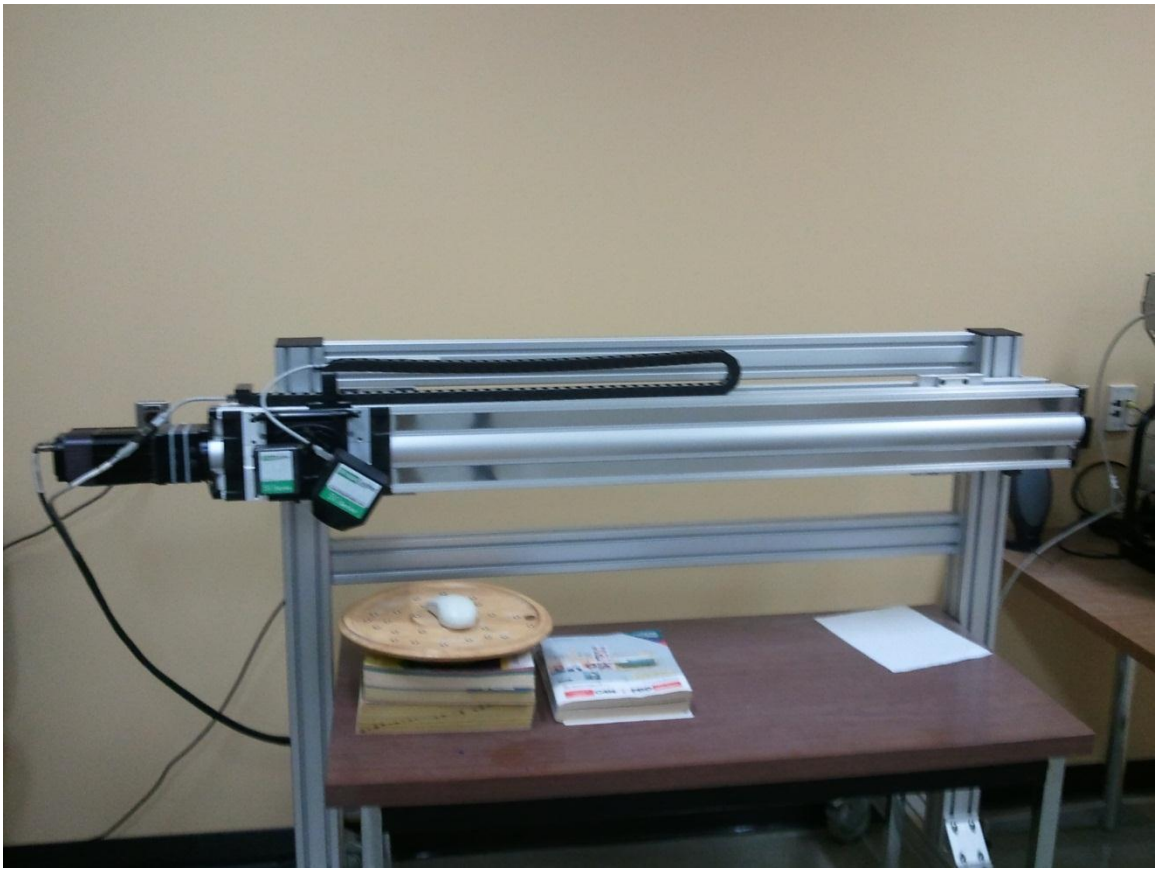

Figure 3.12 The 3D laser scanner.

A single scan can only digitize part of the ear model from one angle as shown in Figure 3.14.a. In order to construct a complete 3D CAD model, a total of 9 scans of the ear model were captured from different angles using the 3D laser scanner.

3.2.3 Construction of CAD models

The work flow used in this study is shown in Figure 3.13. All data gathered by the 3D laser scanner are in point phase, and need to be combined (Figure 3.14.c) in Geomagic Studio to create a rough 3D model. The rough model is then transformed into polygon data for further optimization. After repairing holes and smoothing the surfaces of the initial polygon model, the completed 3D positive human ear model is obtained (Figure 3.14.d).

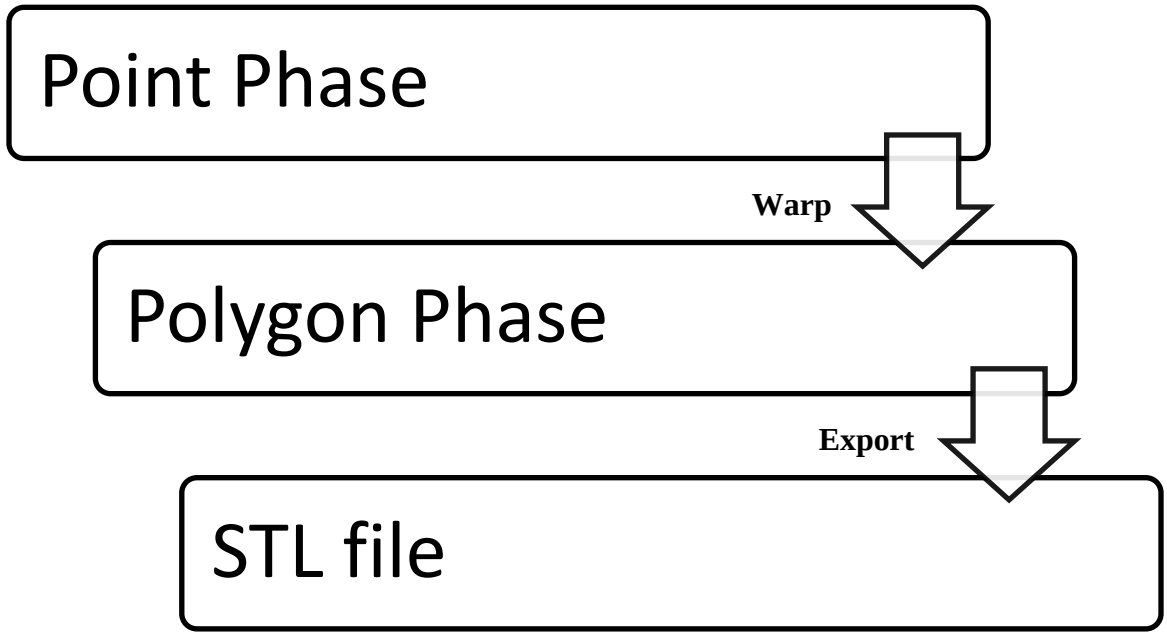

Figure 3.13 The basic workflow of Geomagic Studio.

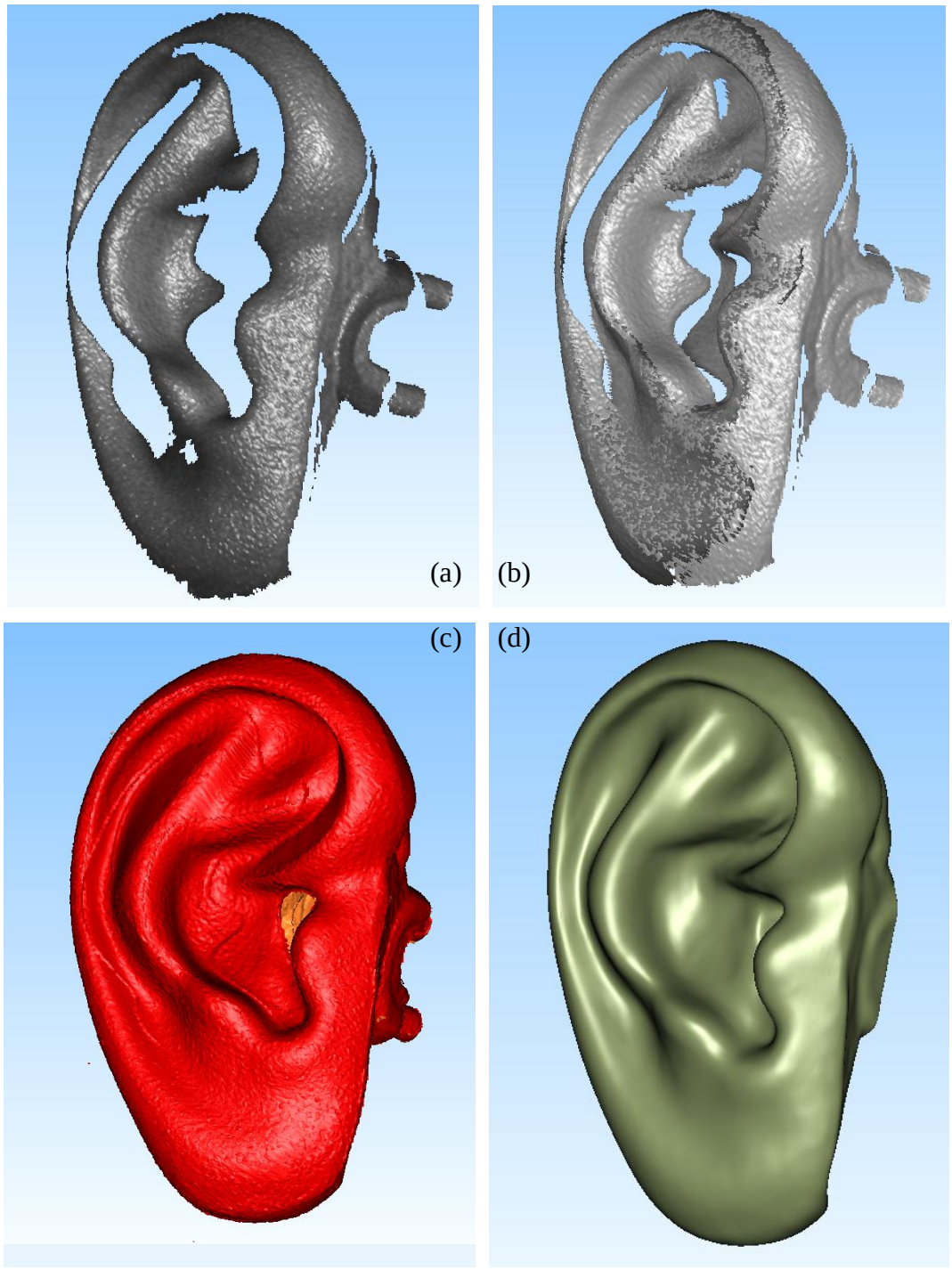

Figure 3.14 Construction of the 3D positive ear model. (a) a single scan; (b) two scans combined; (c) nine scans merged together to form the 3D model; (d) the final 3D positive ear model after optimization.

After the 3D CAD model of the ear was finished, 3D CAD models of the negative molds were constructed by subtracting the positive model from cuboid shaped bases. As shown in Figure 3.15, the base before subtraction is represented in blue, the base after subtraction is represented in black, and the ear model is represented in gray. The geometric feature of three regions was lost after subtraction as indicated by yellow arrows. This is caused by the incomplete contact between base and ear models when the front half of the ear model is immersed.

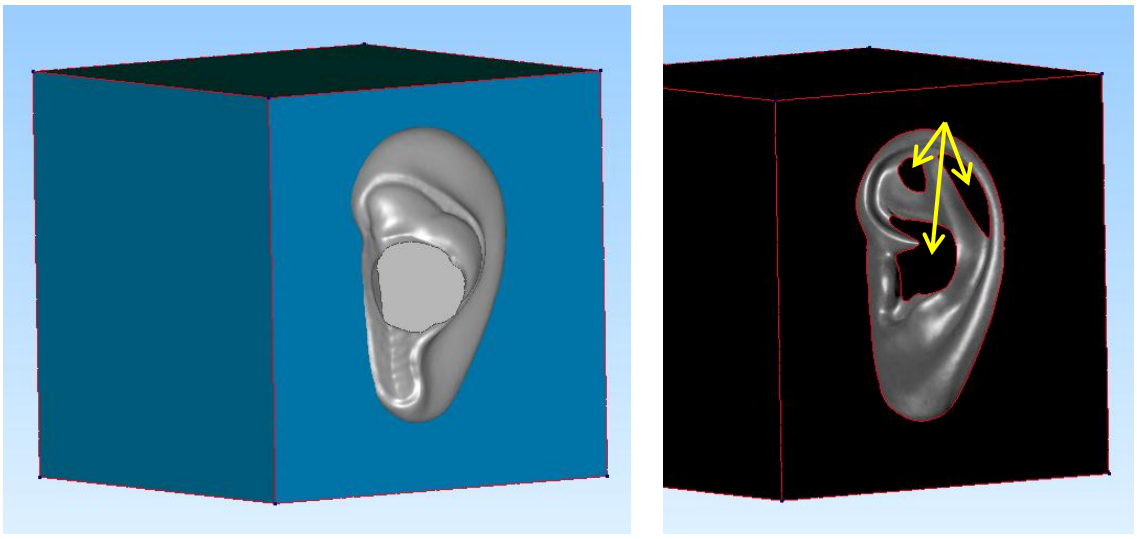

Figure 3.15 Missing features caused by subtracting the ear model from a cube.

In order to solve this problem, modifications on the contact surface of the base are necessary. By adding an extension that covers all the region of feature loss (Figure 3.16), complete contact between base and ear models was achieved to eliminate any feature loss after the subtraction operation. The final 3D CAD model is shown in Figure 3.17.

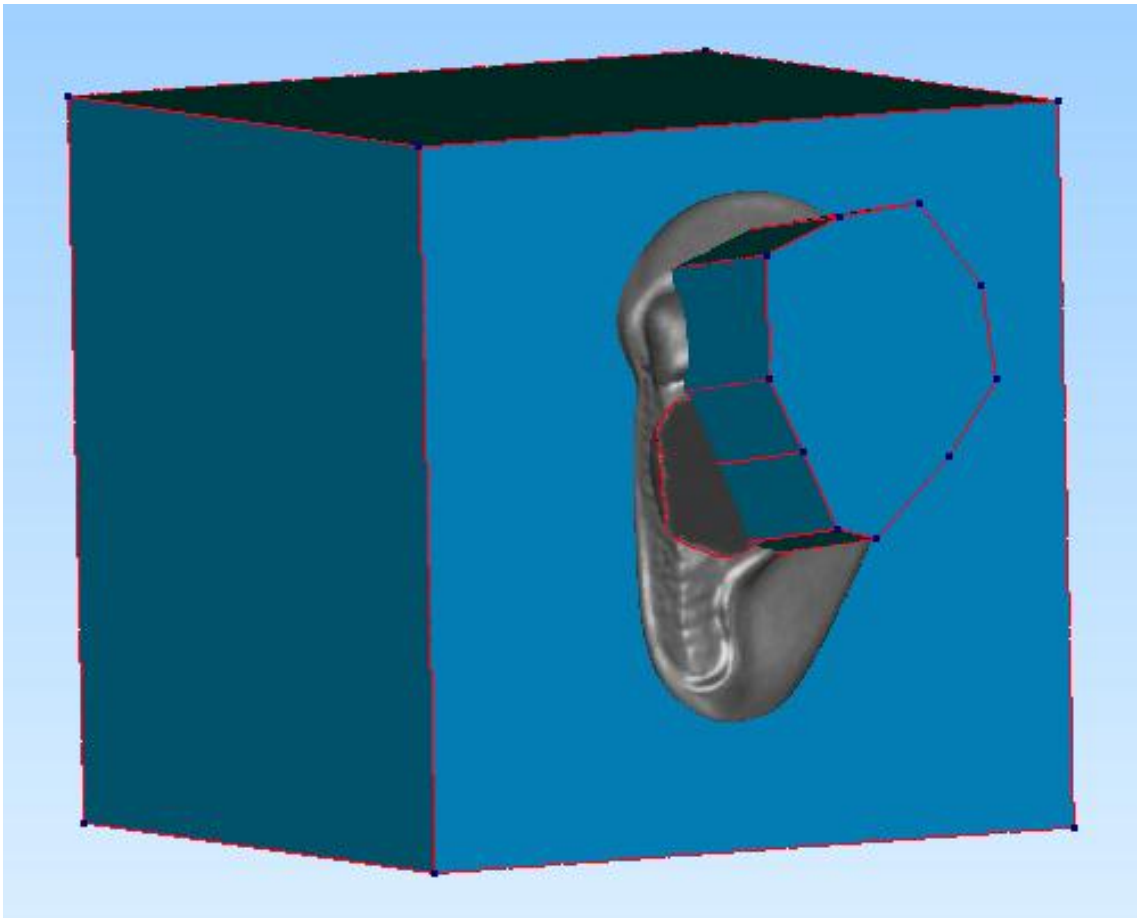

Figure 3.16 The modified base with half-immersed ear model before subtraction.

Figure 3.17 The final negative mold after subtraction.

3.2.4 Rapid prototyping of negative molds

The negative molds were exported into binary STL files for rapid prototyping using a SLA 3500 solid imaging system. Molds were fabricated in layers of 0.05mm for maximum 3D printing resolution.

The SLA 3500 is loaded with 3D Systems Accura® SI 10 resin, which has the following typical Post-Cured Material Properties (U of M, 2011):

• Tensile strength of 62-76 MPa (9010-10940 PSI)

• Flexural strength of 89-115 MPa (12900-16600 PSI)

• Hardness 86 shore D

• Elongation at break of 4-5%

3.3 Novel Design for Bioreactor

Assembly modeling is an extension of geometric modeling that facilitates construction, modification and analysis of complex assemblies. In assembly modeling, a product model is created to represent a product with several smaller components. Parts and components are added to an assembly by specifying mating conditions or constraints. Therefore, an assembly model includes not only components, but also relationships among them. To describe a product, the elementary components and their relationships should be defined. A component that cannot be further divided into smaller components is called a single part. A group of components merged together is called a sub-assembly. The installation of sub-assembly and components forms the final product.

3.3.1 Product representation

The liaison graph and assembly matrix are commonly used in assembly modeling to indicate a product structure. For a multi-level assembly process, a product can be described by components and their connections. An example is shown in Figure 3.18. An assembly model represented by a typical liaison graph is shown in Figure 3.19, where lines represent connections between components denoted as 1 to 7. Based on graph theory, the relationship in a graph can be mapped one-to-one into an adjacency matrix R, as shown in Figure 3.20. It is a 7x7 sized matrix. In the matrix, $R_{ij} = 1$ indicates a connection between components i and j; $R_{ij} = 0$ means no connection between parts i and j.

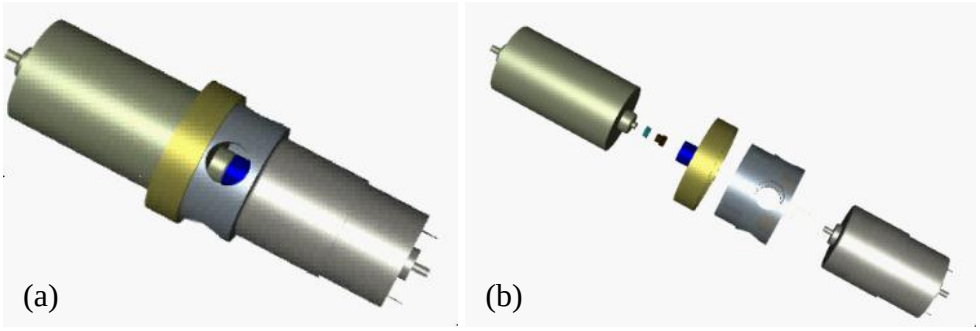

Figure 3.18 (a) Assembly and (b) components view of the sample product.

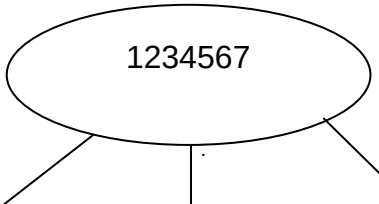

R =

	1	*2*	*3*	*4*	*5*	*6*	*7*
1	0	1	0	0	0	0	0
2	1	0	1	0	0	0	0
3	0	1	0	1	0	0	0
4	0	0	1	0	1	0	0
5	0	0	0	1	0	1	1
6	0	0	0	0	1	0	1
7	0	0	0	0	1	1	0

Figure 3.20 Adjacency matrix of the liaison graph.

3.3.2 Product complexity and DFA evaluation

Product assembly complexity is the degree of individual parts or subassemblies that have geometrical attributes to cause difficulties or problems during assembly processes. Prod-

uct complexity directly affects the performance of DFA. Identification and measurement of assembly complexity will support DFA to guide designers toward creating a product with low assembly difficulty.

An analytic DFA model is the description of assembly relationships between assembly components with constraints such as assembly features, component types and their sequences, engineering constraints such as assembly operations and assembly tools. Based on the method developed by Boothroyd et al. (Boothroyd, Dewhurst, & Knight, 2002), DFA provides a guideline for product design with the easy assembly. Dimensions of the DFA evaluation shown in Figure 3.21 include processing setup time, part insertion difficulty, fastening operation, positioning difficulty, handling difficulty, labor skills required, and assembly tools required. Evaluation criteria of the bioreactor product assembly complexity can be identified based on these dimensions.

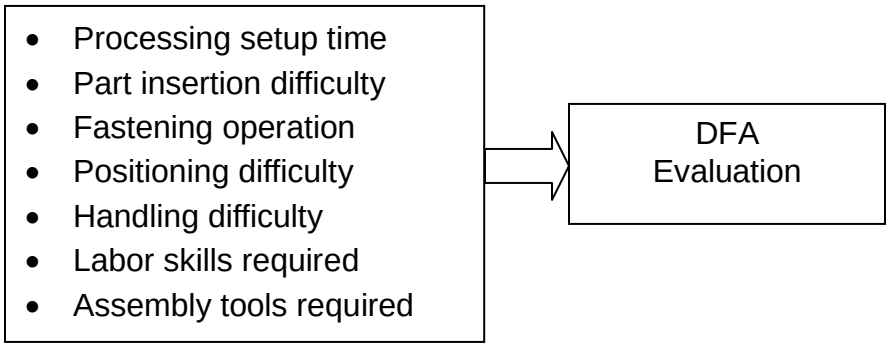

Figure 3.21 Design for assembly evaluation dimensions.

Table 3.2 Criteria of product assembly complexity.

Criterion	Complex level
Part geometry	Part size: (1) Easy to handle - 1 (2) Too small - 4 Alignment for assembly: (1) Easy – natural resting - 1 (2) Locator reference required - 3 (3) peg insertion - 5 Part symmetry: (1) symmetric - 1 (2) semi-symmetric - 2 (3) Non-symmetric - 4 Handling difficulty: (1) one hand - 1 (2) two hands - 2 (3) fixture or tool required - 4 Features may cause jam and tangle (1) yes – 3 (2) no - 0
Process complexity	Fastening type: (1) Integrated with assembly (snaps etc.)- 1 (2) Rivets, staples and adhesive - 3 (3) Screws and nails - 5 (4) Multi-pieces (nuts and bolts) - 5 Parts' connection ways (1) shaft-hole-fit - 2 (2) plane-oriented-fit - 1 (3) screw-joint - 5 (4) key-slot-joint - 4 Chamfers to reduce resistance of a part insertion (1) yes - 0 (2) no - 3 Enough space for assembly operations (1) yes – 0 (2) no – 3 Interference with other parts (1) yes – 3 (2) no - 0

DFA guides a design for simplifying of parts and operations in the assembly process. It requires investigating design details for assembly operations, such as any hand or fixture

required to hold parts, parts assembly order, tools required, accessibility of parts, tools or hands, visibility of mating surfaces, and part position for alignment and rotation.

The assembly complexity consists of design-based complexity and process-based complexity (Su, et al., 2010). We set difficulty levels based on time required for handling the part and in operations of the assembly. Different connection structure needs different time to complete an assembly. Commonly used methods in bioreactor operation and difficulty levels are collected in Table 3.2.

Based on DFA analysis, the shape of parts greatly affects the operator's ability to grasp, orient, insert and fasten in assembly operations, reducing an individual part's complexity will result in simplifying product assembly. The assembly complex is classified into two groups: the part complex based on product design, and the process complex based on assembly operations. In Table 3.2, average difficulty levels are listed using empirical data. The total difficulty or complexity of an assembly is the sum of all the parts' complexity levels. For example, the adjacency matrix in Figure 3.20 can be extended into a complex matrix based on data in Table 3.2, as shown in Figure 3.22.

$$\text{Complex} = \begin{vmatrix} 0 & 10 & 0 & 0 & 0 & 0 & 0 \\ 10 & 0 & 10 & 0 & 0 & 0 & 0 \\ 0 & 10 & 0 & 10 & 0 & 0 & 0 \\ 0 & 0 & 10 & 0 & 10 & 0 & 0 \\ 0 & 0 & 0 & 10 & 0 & 7 & 7 \\ 0 & 0 & 0 & 0 & 7 & 0 & 7 \\ 0 & 0 & 0 & 0 & 7 & 7 & 0 \end{vmatrix}$$

Figure 3.22 Complex matrix of the sample product.

Therefore, DFA analysis is converted into a process to reduce the sum of the complex or difficulty level of a product based on the complex matrix. DFA evaluation and improvement are described in the flow chart in Figure 3.23. The process starts based on the model structure of a product. A liaison graph is formed based on the product design. The adjacency matrix is developed from the liaison graph. The product geometric complexity and process complexity are added into the matrix for complexity calculation. The product is then evaluated based on product complexity to arrive at the product difficulty level, which will be used as a reference for product improvement. The DFA improvement looks at the component with the higher difficulty level in three aspects: possibilities of component combination, part redesign, and alternative assembly methods. The possible search is constrained by part types, functions, manufacturing methods and cost. A threshold is set based on product feature and manufacturer capacity. Related data and knowledge are stored in a database. A user interface is provided for users to interact with the system to finalize the feasible solution.

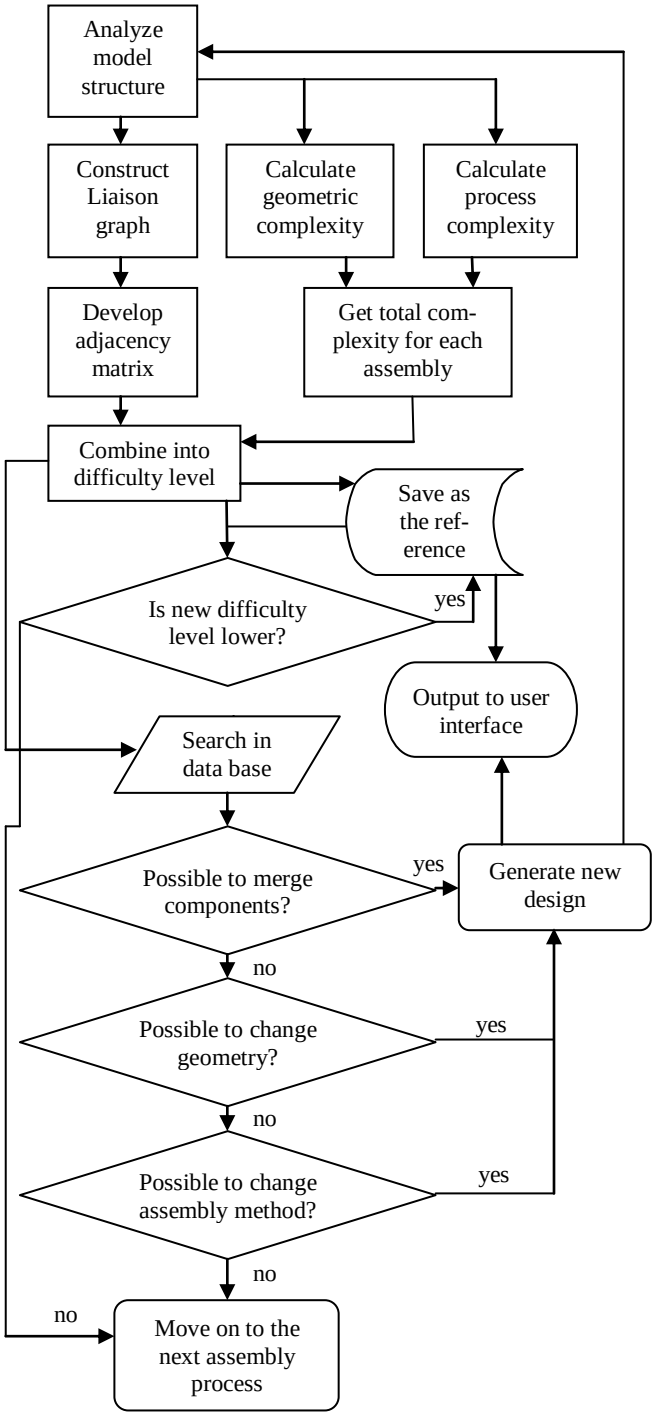

Figure 3.23 Flow chart of the design process based on DFA.

3.3.3 DFA analysis of the current bioreactor product

The bioreactor analyzed in this study is commercially available from Harvard Apparatus GmbH and its product name is BioReactor "In Breath" TYPE 807. Components of this rotating double-chamber bioreactor are shown in Figure 3.24. The detailed functions of major components are listed in Table 3.3.

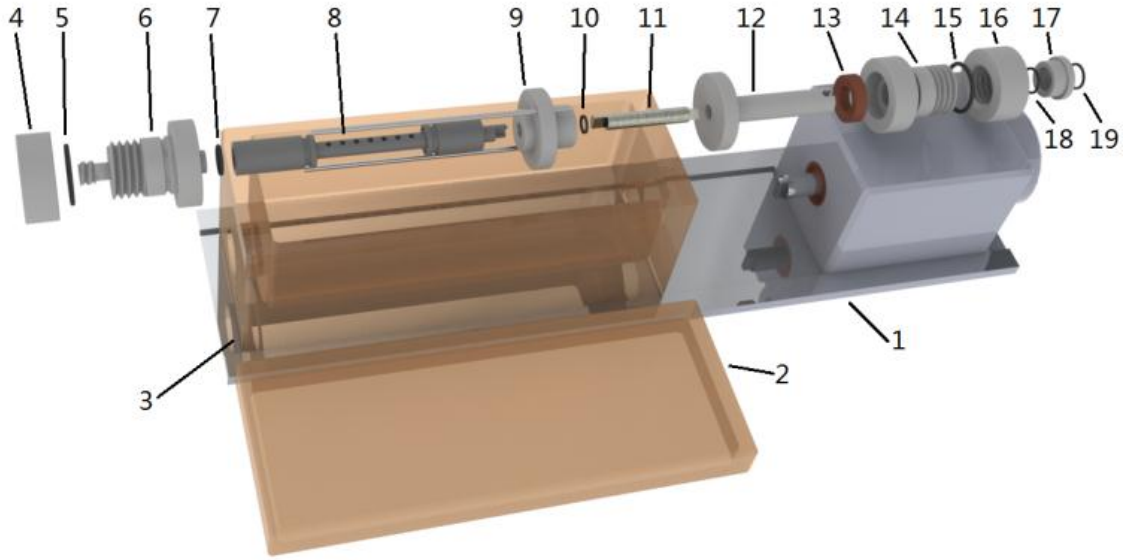

Figure 3.24 Components of the BioReactor "In Breath" TYPE 807.

Table 3.3 Bioreactor's components and functions.

No.	Name	Function
1	Motor and Base	Provide rotatory motion, and secure the culture chamber in place
2	Cover	Protective cover for the culture chamber
3	Culture chamber	External chamber of the bioreactor to culture cells on the outside surface of a tubular shaped scaffold
4	Cap	Screw cap for component 6
5,7,10, 15,18,19	O rings	Increase friction of insertions to hold parts together, and prevent leakage of culture medium.
6	Inlet/outlet	For the inner chamber connecting to the scaffold holder
8	Scaffold holder	For positioning scaffold, it rotates with the input shaft. There is a hollow inside as the inner chamber with holes connecting the inner chamber to the lumen of scaffold to transfer oxygen and nutrition
9	Mixer	On the input shaft being slid to secure/unsecure the scaffold holder. It rotates with the input shaft to provide a turbulence environment in culturing medium and preventing cell attachment to the surface of outer chamber
11,12	Input shaft	Connect the motor shaft and scaffold holder
13	Seal	Preventing the leakage of culture medium
14	Holder	For the dynamic seal and also providing a passage for the input shaft to penetrate the base
16	Cap	Screw cap for component 14
17	Input shaft ring	Secure the input shaft, attached to the input shaft using the friction force

Assumptions used in the bioreactor DFA analysis are as follows:

- The parts will be assembled one by one, there is no parallel operation considered.
- Manual operations are applied. There is no automatic device or robot used in the assembly.
- Product functions cannot be affected when any design change is made.

The product can be built by a set of components that are linked together by a set of detachable fasteners. The product must be assembled in the final step of production. It is

necessary to have an optional structure for the product to be assembled easily with minimal time and operations.

The DFA objective is to minimize the number of products assembled, or improve the part design to make the assembly easy, and to minimize the time required in the assembly. For the bioreactor, the parameters shown in Table 3.2 are used to evaluate the assembly complexity following the flow chart shown in Figure 3.23.

Liaison graph of an existing product is formed in Figure 3.25. Its complex matrix of assembly shown in

Figure 3.26 has a size of 19 by 19. Following the process described in Figure 3.23, a new design is proposed based on the data in Table 3.2 to reduce the difficulty levels of the components in structure and operations.

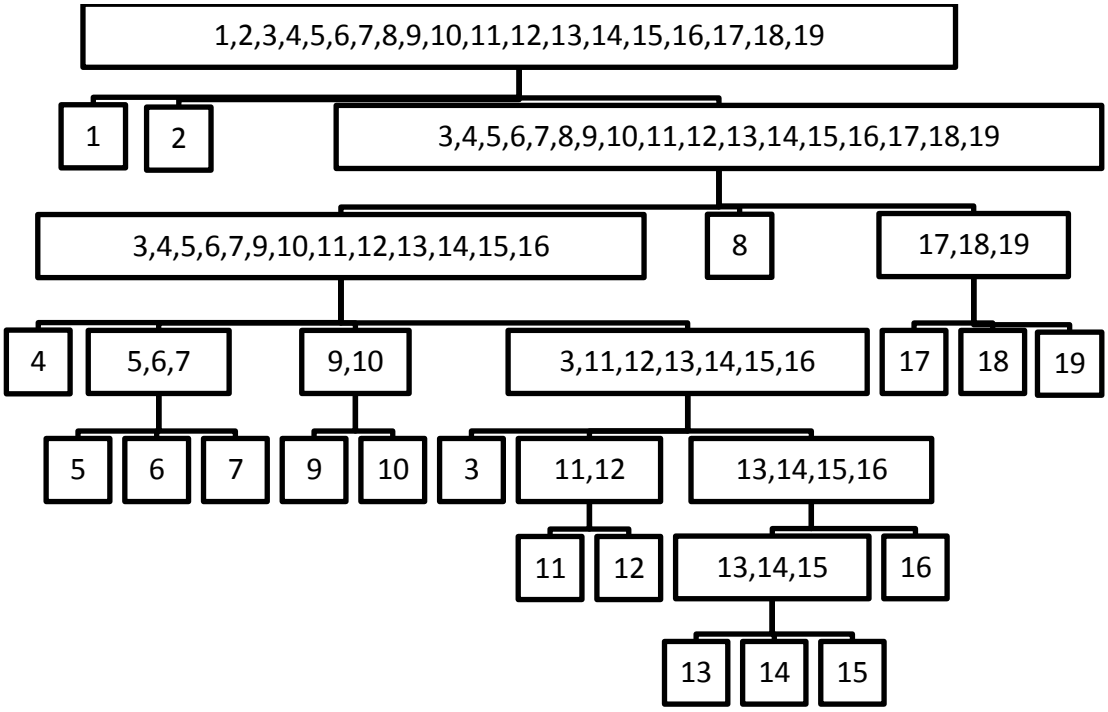

Figure 3.25 Liaison graph of the BioReactor "In Breath" TYPE 807.

$$C_{old} = \begin{vmatrix}
0 & 0 & 12 & 0 & 0 & 0 & 0 & 0 & 0 & 0 & 0 & 0 & 0 & 0 & 0 & 0 & 0 & 0 & 0 \\
0 & 0 & 7 & 0 & 0 & 0 & 0 & 0 & 0 & 0 & 0 & 0 & 0 & 0 & 0 & 0 & 0 & 0 & 0 \\
12 & 7 & 0 & 0 & 0 & 8 & 0 & 8 & 0 & 0 & 0 & 0 & 0 & 8 & 0 & 0 & 8 & 0 & 0 \\
0 & 0 & 0 & 0 & 12 & 0 & 0 & 0 & 0 & 0 & 0 & 0 & 0 & 0 & 0 & 0 & 0 & 0 & 0 \\
0 & 0 & 0 & 12 & 0 & 11 & 0 & 0 & 0 & 0 & 0 & 0 & 0 & 0 & 0 & 0 & 0 & 0 & 0 \\
0 & 0 & 1 & 0 & 11 & 0 & 8 & 0 & 0 & 0 & 0 & 0 & 0 & 0 & 0 & 0 & 0 & 0 & 0 \\
0 & 0 & 0 & 0 & 0 & 8 & 0 & 0 & 0 & 0 & 0 & 0 & 0 & 0 & 0 & 0 & 0 & 0 & 0 \\
0 & 0 & 1 & 0 & 0 & 0 & 0 & 0 & 10 & 0 & 13 & 0 & 0 & 0 & 0 & 0 & 0 & 0 & 0 \\
0 & 0 & 0 & 0 & 0 & 0 & 0 & 10 & 0 & 11 & 8 & 0 & 0 & 0 & 0 & 0 & 0 & 0 & 0 \\
0 & 0 & 0 & 0 & 0 & 0 & 0 & 0 & 11 & 0 & 0 & 0 & 0 & 0 & 0 & 0 & 0 & 0 & 0 \\
0 & 0 & 0 & 0 & 0 & 0 & 0 & 13 & 8 & 0 & 0 & 10 & 0 & 0 & 0 & 0 & 0 & 0 & 0 \\
0 & 0 & 0 & 0 & 0 & 0 & 0 & 0 & 0 & 0 & 10 & 0 & 8 & 0 & 0 & 0 & 8 & 0 & 0 \\
0 & 0 & 0 & 0 & 0 & 0 & 0 & 0 & 0 & 0 & 0 & 8 & 0 & 8 & 0 & 0 & 0 & 0 & 0 \\
0 & 0 & 8 & 0 & 0 & 0 & 0 & 0 & 0 & 0 & 0 & 0 & 8 & 0 & 11 & 12 & 0 & 0 & 0 \\
0 & 0 & 0 & 0 & 0 & 0 & 0 & 0 & 0 & 0 & 0 & 0 & 0 & 11 & 0 & 0 & 0 & 0 & 0 \\
0 & 0 & 0 & 0 & 0 & 0 & 0 & 0 & 0 & 0 & 0 & 0 & 0 & 12 & 0 & 0 & 0 & 0 & 0 \\
0 & 0 & 8 & 0 & 0 & 0 & 0 & 0 & 0 & 0 & 0 & 8 & 0 & 0 & 0 & 0 & 0 & 11 & 11 \\
0 & 0 & 0 & 0 & 0 & 0 & 0 & 0 & 0 & 0 & 0 & 0 & 0 & 0 & 0 & 0 & 11 & 0 & 0 \\
0 & 0 & 0 & 0 & 0 & 0 & 0 & 0 & 0 & 0 & 0 & 0 & 0 & 0 & 0 & 0 & 11 & 0 & 0
\end{vmatrix}$$

Figure 3.26 Complex matrix of the BioReactor “In Breath” TYPE 807.

3.3.4 Design verification using VR

The new designs were verified in a VR system, Eon Studio. The processing is shown in Figure 3.27. Simulation models were built based on both existing and improved bioreactors, and the software used was SolidWorks 2010. All CAD models were assembled in SolidWorks first before exporting into STL files, so that all parts were perfectly positioned after importing into Eon Studio. During importing STL files, a size ratio of 0.1 was used to ensure proper display of bioreactor models.

Eon prototype “TextBoxButton”, a clickable text box, is used to develop the user interface that provides interaction between operators and models. Eon prototype “ObjectNav”, a navigation tool, is used to let operators freely drag, rotate, or zoom in/out to review the model. A close-up view is also developed using the “resetting view camera” function of ObjectNav. Eon node “Place”, a movement controller, is used to simulate the disassembly and assembly processes. Eon prototype “SmoothOperator”, an opacity controller, was used to gradually change the opacity of some components of the model for better demonstration of joints and connections.

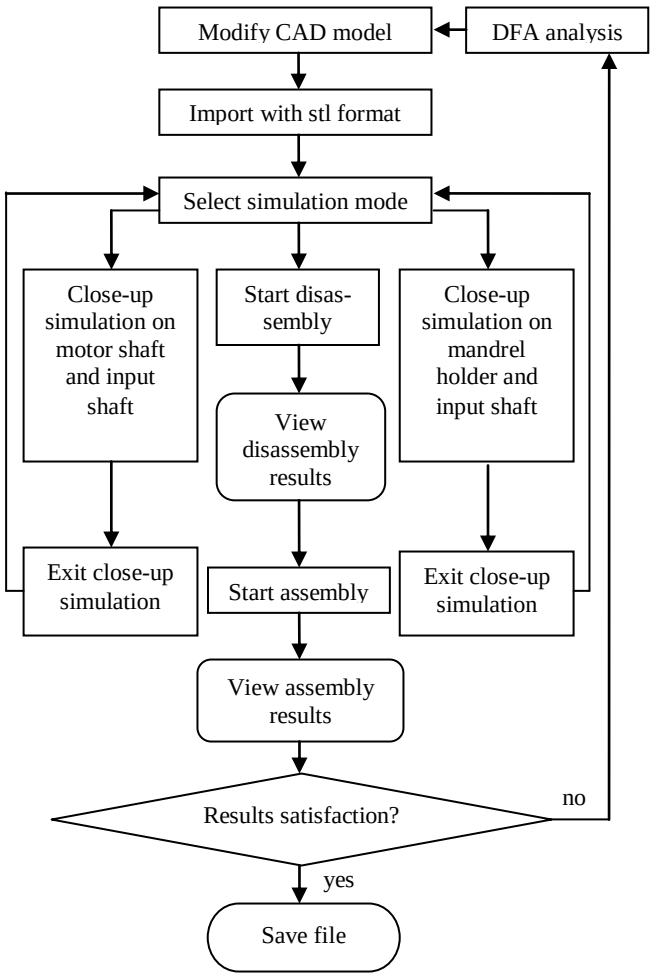

Figure 3.27 Flow chart of the VR simulation.

The simulation route shows the detailed relations of the product components and operations. As shown in Figure 3.28, two textboxes are used to initiate the disassembly and assembly process of the existing product and the new conceptual design. The movements are controlled by Place nodes, and the simulation results are displayed using textboxes. Figure 3.29 demonstrates routes for close-up simulations, which is also initiated by textboxes. During the close-up simulation, the camera position and angle are reset, and the opacity of related components is reduced.

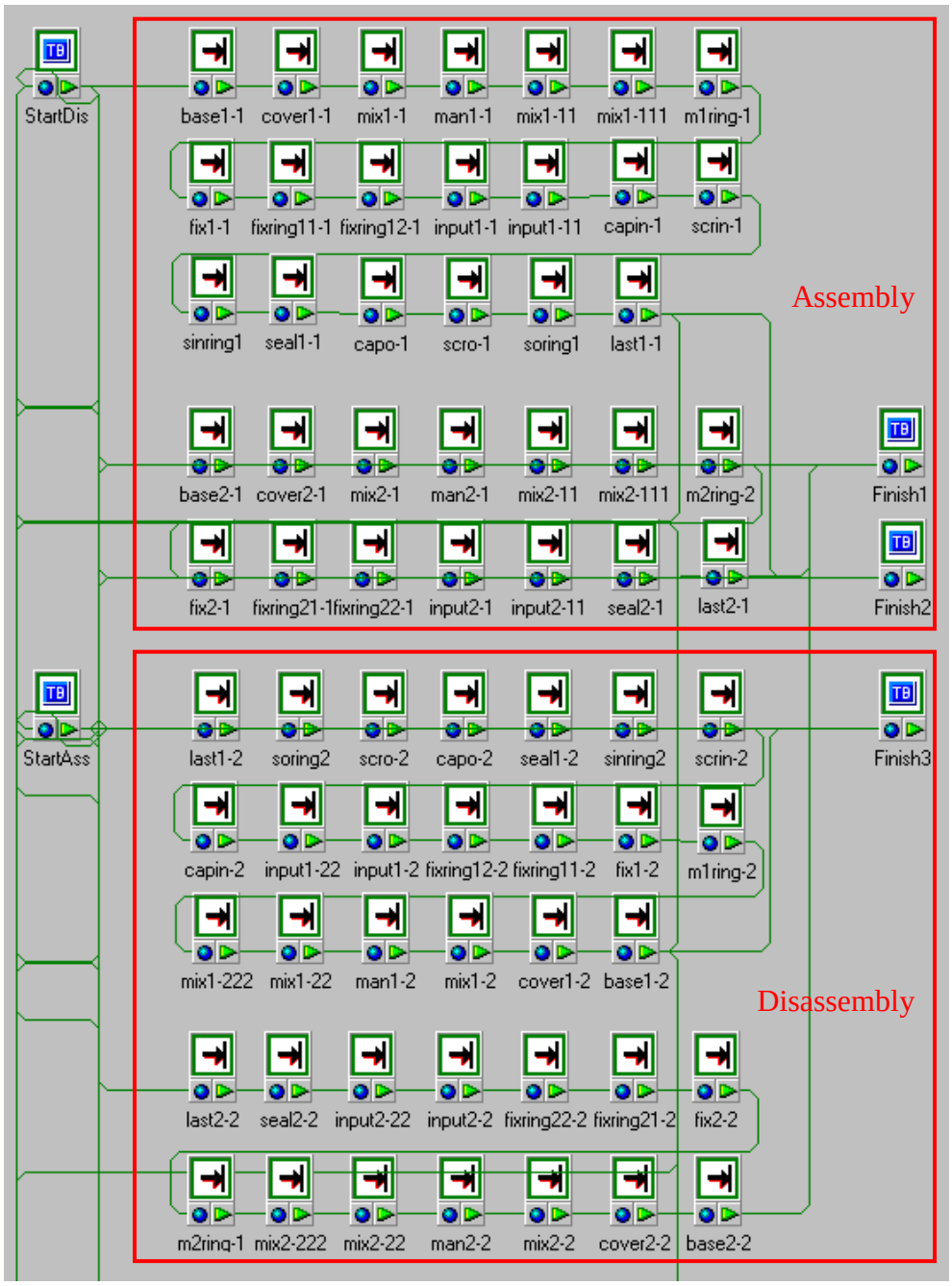

Figure 3.28 Simulation routes for assembly and disassembly processes.

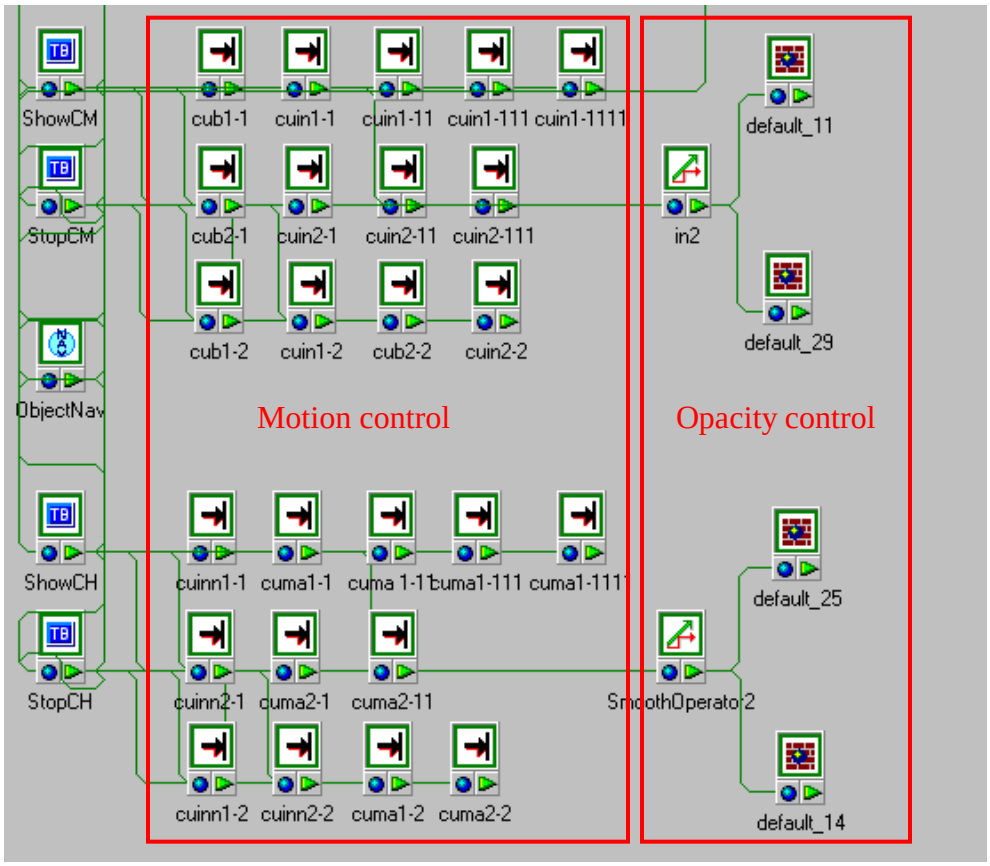

Figure 3.29 Simulation routes for close-up simulations.

Chapter 4

Results

4.1 Biomimetic Scaffolds for Bone TE

4.1.1 Mechanical testing

Bone is a porous composite material mainly made of calcium hydroxylapatite and Type I collagen nanofibers. The goal of using composite scaffold is to mimic collagen nanofibers to allow cell growth then induce calcification, and the calcium hydroxylapatite produced can significantly increase scaffold stiffness. Mechanical strength is important in clinical applications because it not only provides a mechanical stable environment for tissue repair, but also makes handling and suturing easier.

Figure 4.1 shows loading curves of pure PCL, pure gelatin, and biomimetic scaffolds under tension. PCL scaffolds have higher breaking strength and elasticity than gelatin scaffolds. Biomimetic scaffolds have the highest breaking strength, and its stiffness is significantly higher than PCL scaffolds.

Figure 4.2 shows loading curves under cyclic compressions. All samples are able to maintain their mechanical strength under repeating pressure of 530 kPa. PCL and biomimetic scaffolds have very similar performance while gelatin scaffolds have a slower response, indicating higher compressive stiffness in PCL and biomimetic scaffolds.

Figure 4.3 shows loading curves of compressive testing samples under large loadings, and the compressive moduli of the biomimetic scaffolds are between 6 and 8 MPa, which are higher than 1 – 3 MPa found in traditional chitosan based bone TE scaffold (Tanner, 2010). Biomimetic scaffolds have higher resistance than PCL and gelatin scaffolds under the same strain, but the difference is not significant compared to their tensile strength. This behaviour can be explained by the fact that nanofibrous membranes were vertically positioned for tensile tests and horizontally positioned for compressive tests, so that the angle between the direction of fiber alignment and the direction of loading is different. Theoretically, maximum mechanical strength occurs when the angle is 0° and minimum mechanical strength occurs when the angle is 90° . During compressive tests, this angle is always 90° , which means the advantage of aligned structure was not fully revealed.

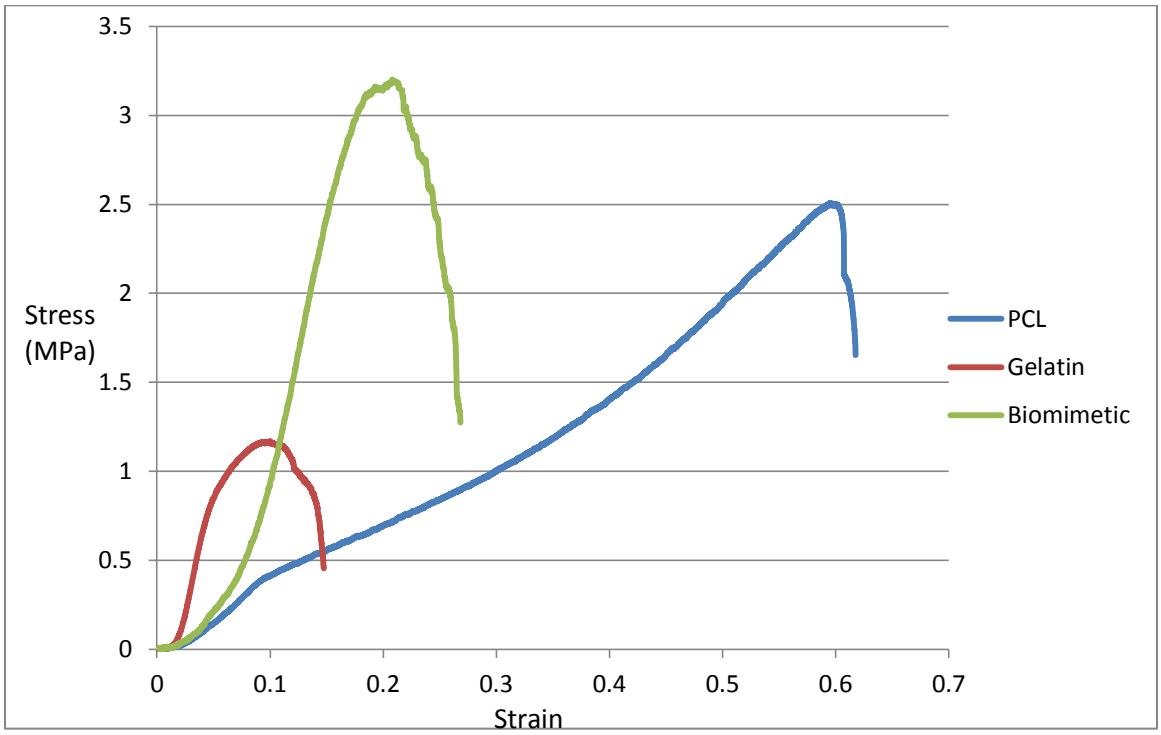

Figure 4.1 True stress-true strain curve of different scaffolds under tension.

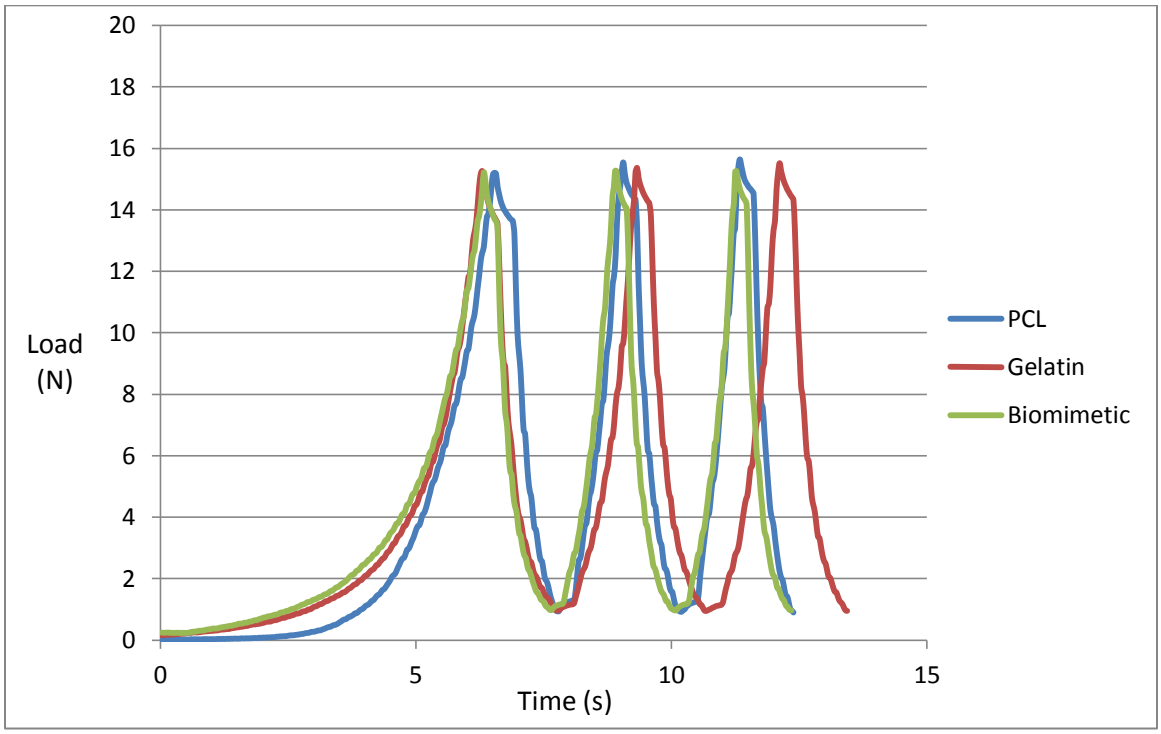

Figure 4.2 Cyclic compression results of different scaffolds.

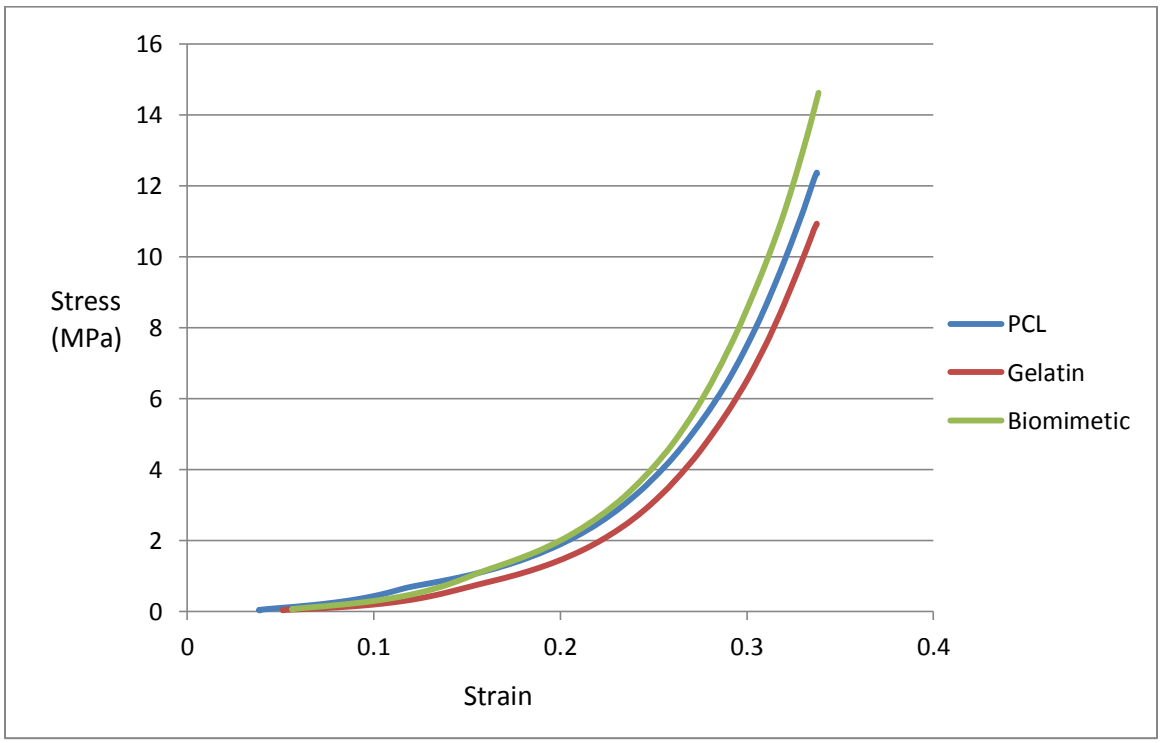

Figure 4.3 True stress-true strain curve of different scaffolds under compression.

4.1.2 SEM images

The alignment of nanofibers was observed in all samples, and the degree of alignment was enough to guide cell growth while maintaining appropriate pore size. Figure 4.4 shows that gelatin nanofibers can maintain their morphology in culture medium after vapour crosslinking. Figure 4.5 shows nanoparticles depositing on the composite membrane after immersion in SBF for 2 days, such nanoparticles contain calcium, phosphorous, and magnesium ions (J. Lu, et al., 2011), which can increase mechanical strength of scaffolds and mimic environment for bone growth to enhance osteogenic differentiation (X. Liu, et al., 2009). Figure 4.6 and Figure 4.7 show cells attached on the nanofibrous samples.

Fiber diameters observed before cell seeding vary from 500 nm to 800 nm, some of the fibers remain the same diameter after cell seeding, and the rest has increased diameters up to 5000 nm. The increase in fiber diameter is caused by swelling of gelatin fibers after exposure to culture medium, and such behaviour is beneficial to cell migration due to the fact that pore size is increased at the same time.

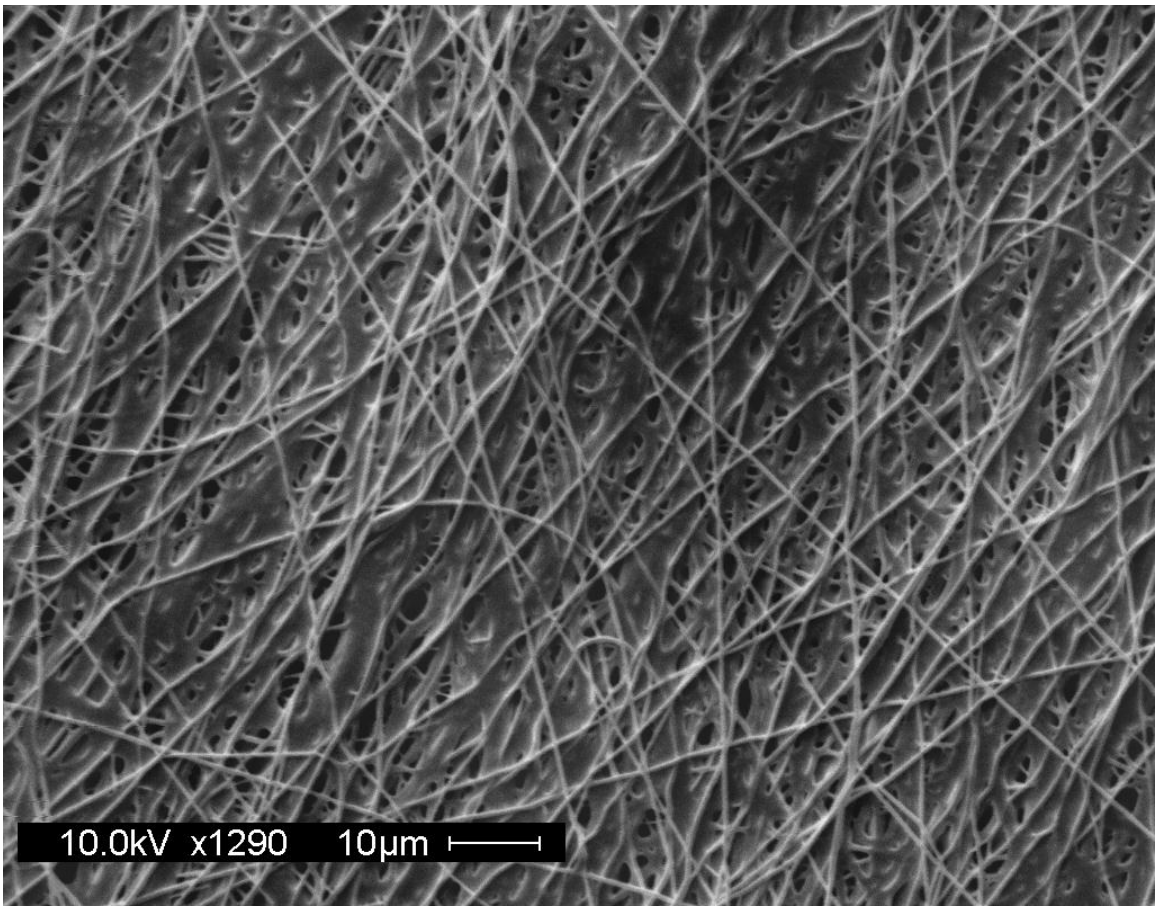

Figure 4.4 SEM image of vapour crosslinked gelatin/PCL composite scaffold.

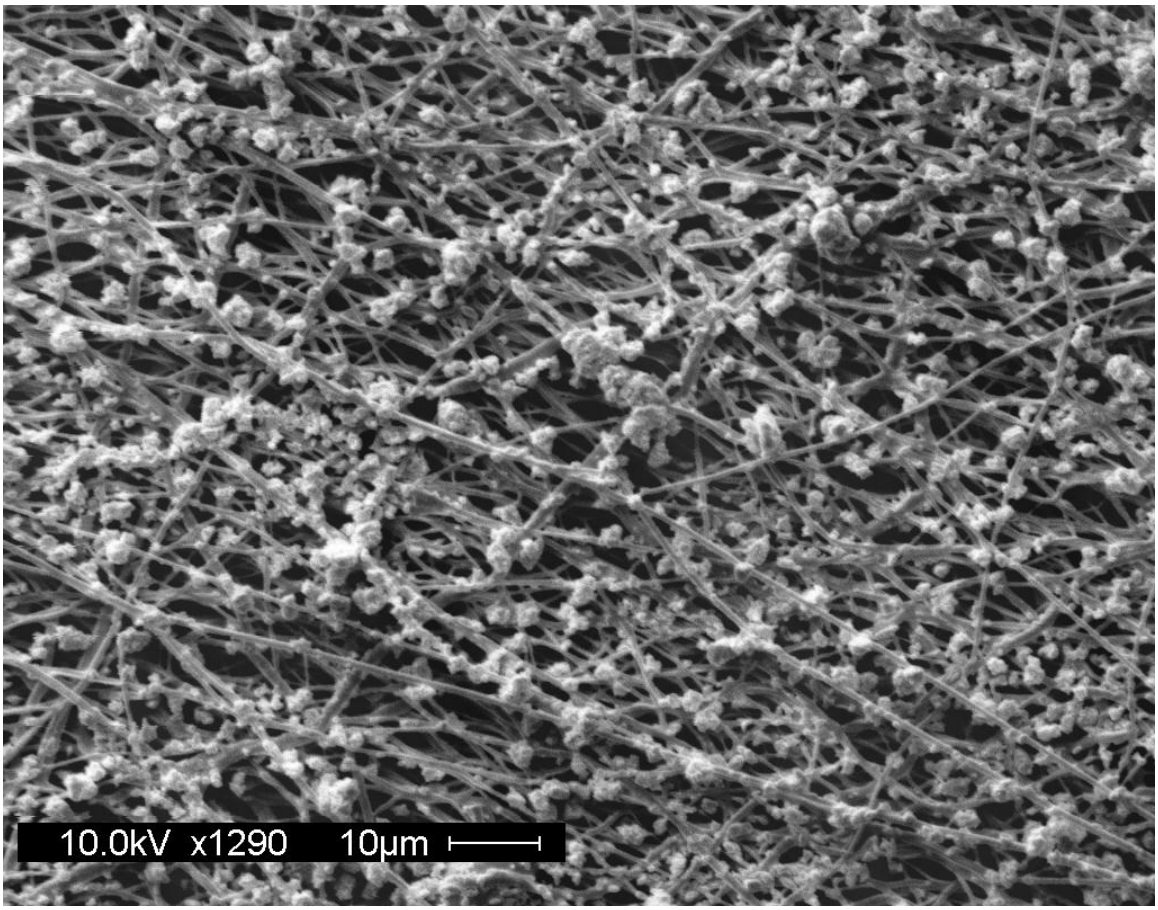

Figure 4.5 SEM image of SBF deposited gelatin/PCL composite scaffold.

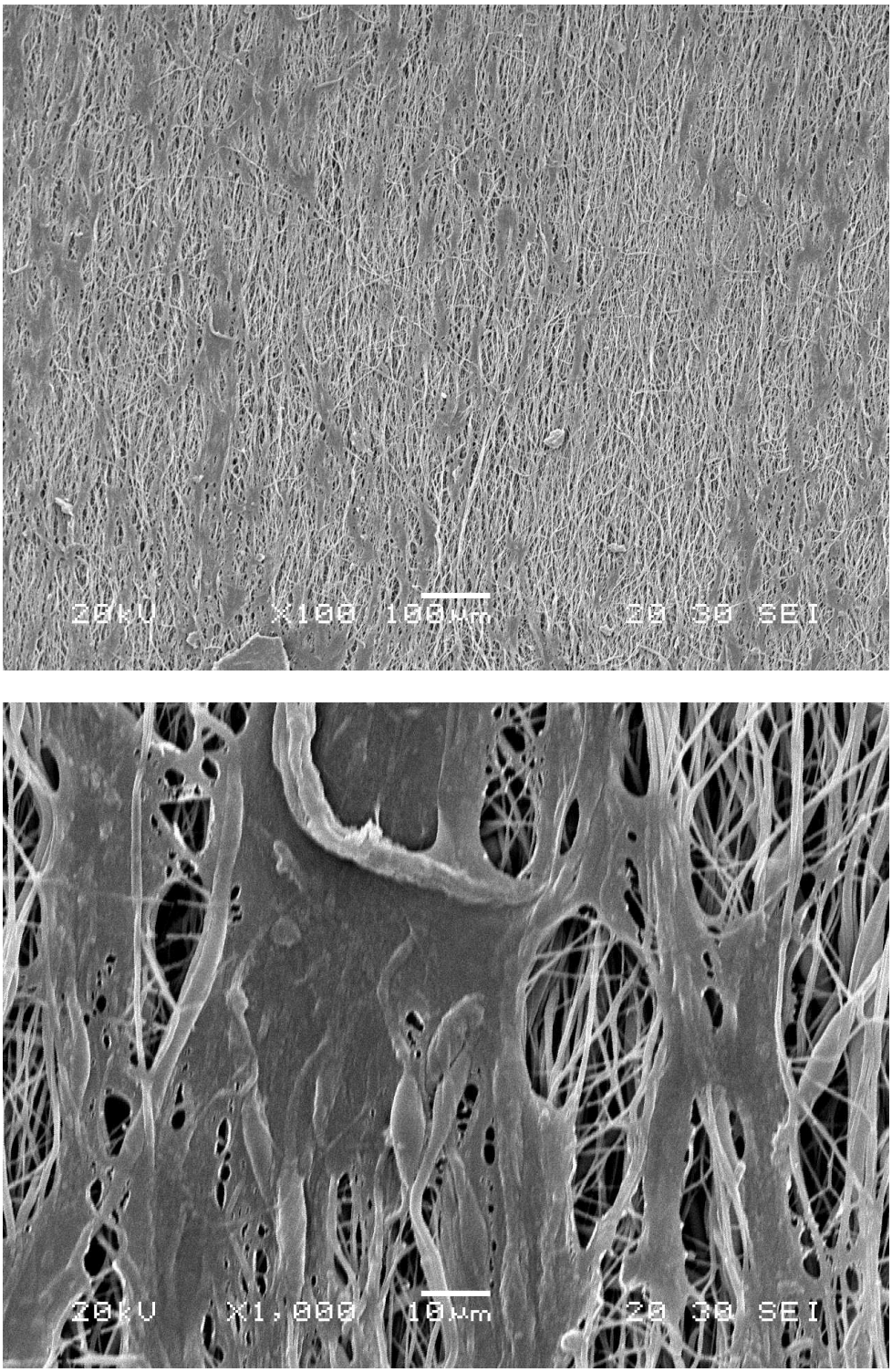

Figure 4.6 SEM images with different magnifications of preosteoblasts seeded traditional gelatin/PCL scaffold after 1 week of cell seeding.

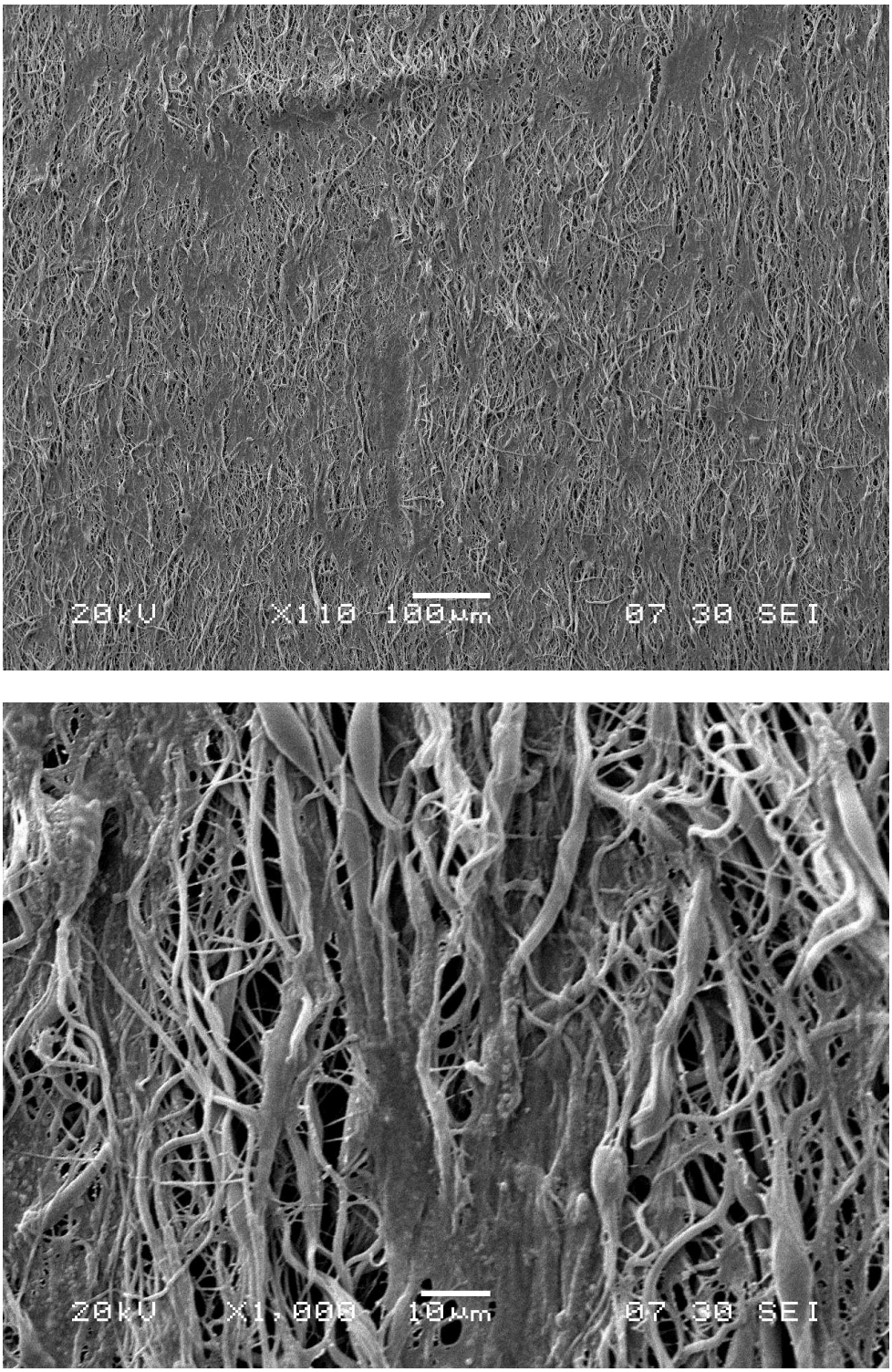

Figure 4.7 SEM images with different magnifications of preosteoblasts seeded new gelatin/PCL composite scaffold after 1 week of cell seeding.

4.1.3 Confocal Laser Scanning Microscopy images

The green color was stained by phallacidin, which is a fluorescent dye for actin cytoskeleton (Barak, Yocum, Nothnagel, & Webb, 1980). The red color was stained by TO-PRO-3, which is a fluorescent dye for nuclear counterstaining (Ploeger, Dullens, Huisman, & van Diest, 2008).

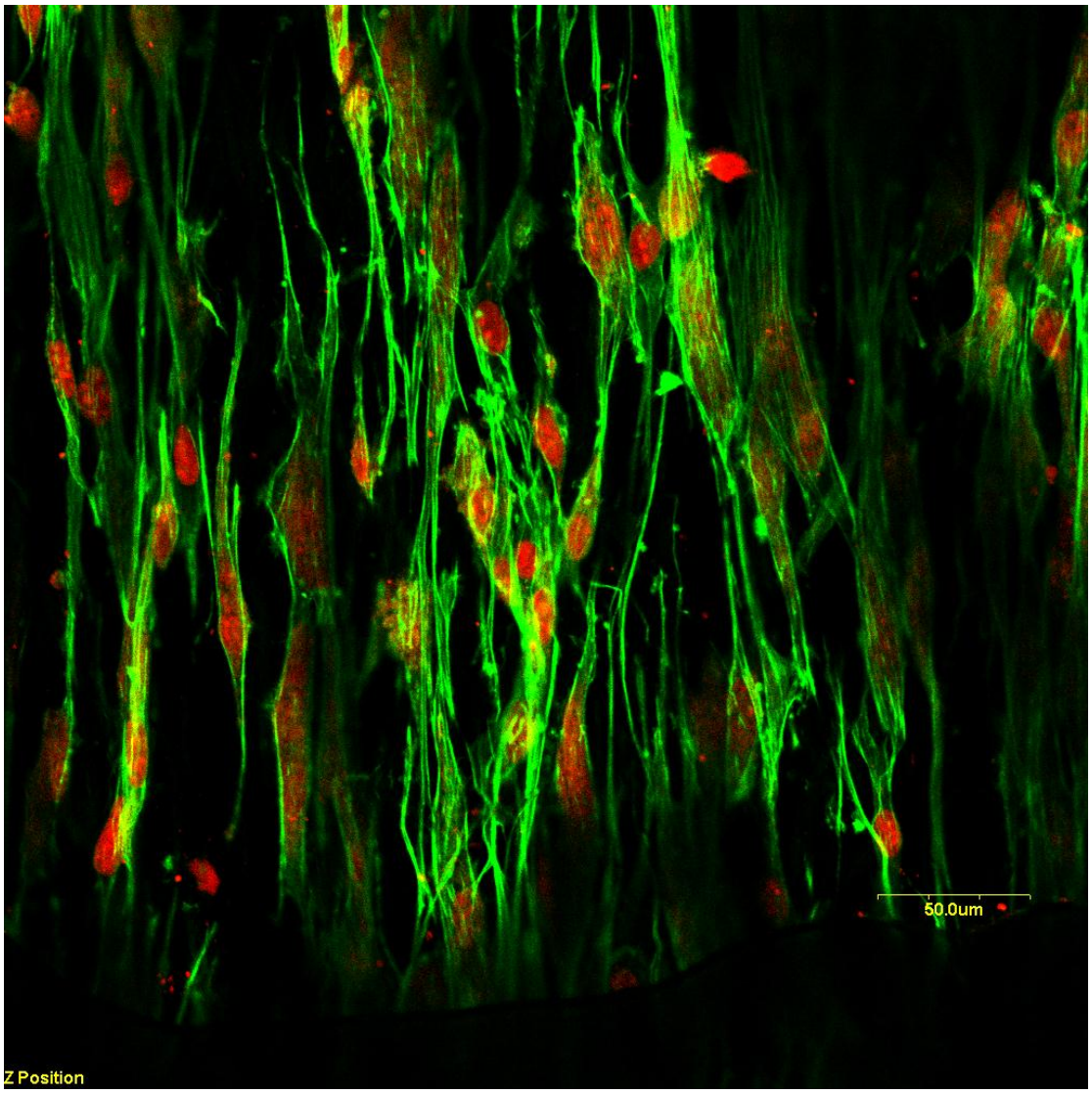

Figure 4.8 Confocal microscopy image of preosteoblasts on traditional gelatin/PCL scaffold 1 week after cell seeding.

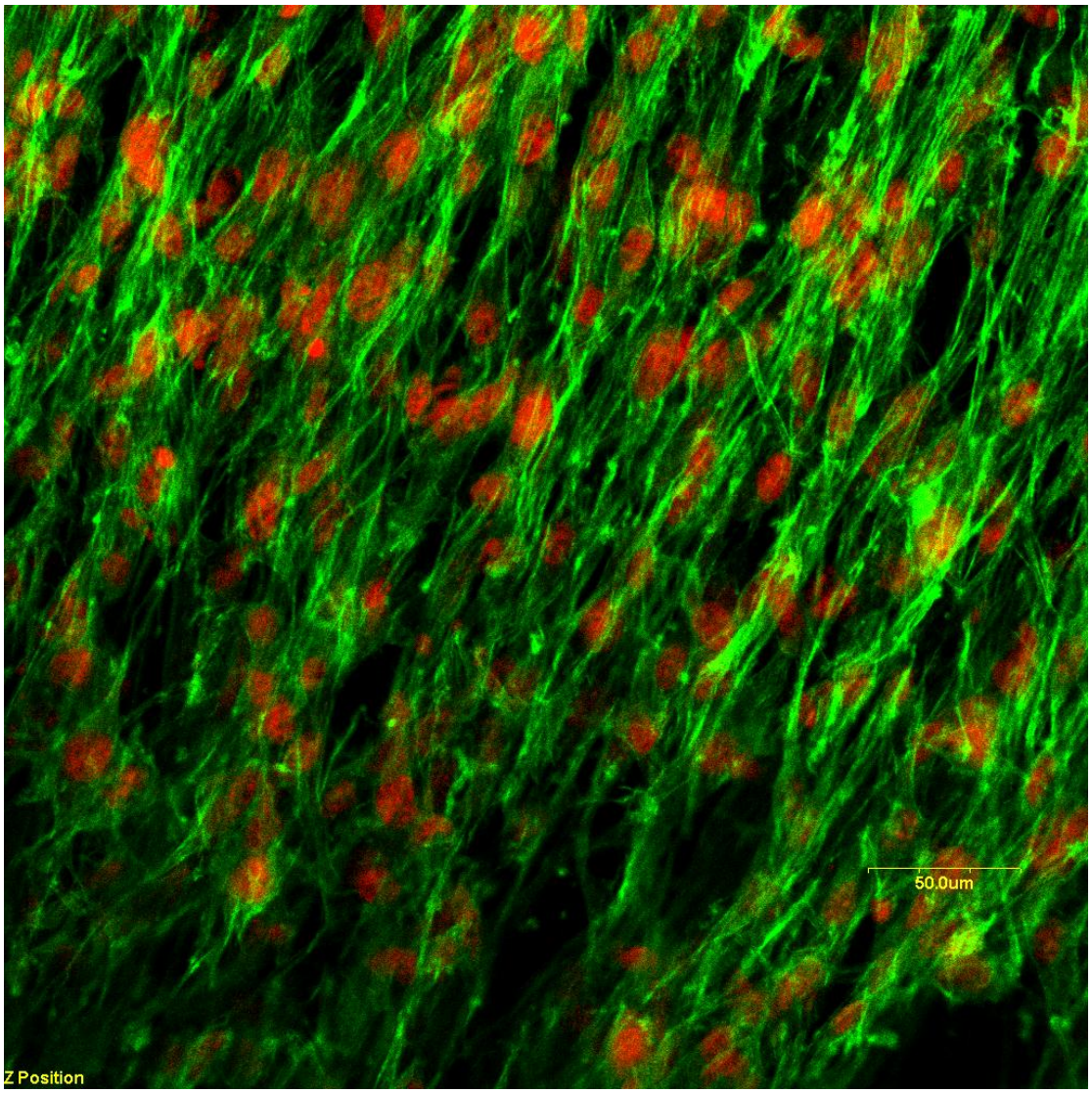

Figure 4.9 Confocal microscopy image of preosteablasts on new gelatin/PCL composite scaffold 1 week after cell seeding.

For all scaffold samples, cells were observed to be growing in the same direction under confocal microscopy, which confirms the fact that aligned nanofibrous membranes fabricated by electrospinning can effectively guide the direction of cell growth. More cells were observed on the new gelatin/PCL composite scaffolds, thus we could conclude that the composite scaffolds have better cytocompatibility compared to traditional scaffolds.

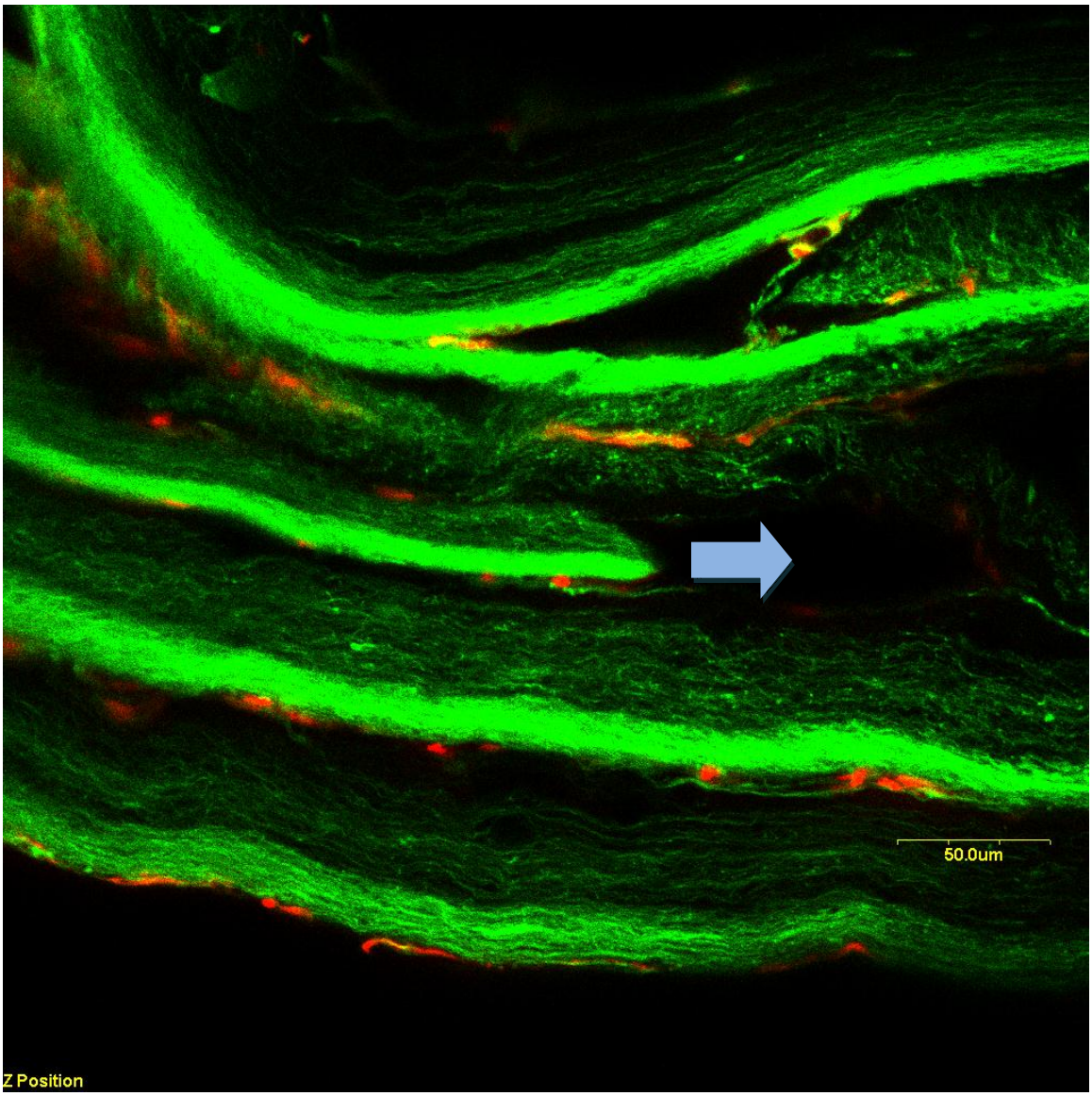

Figure 4.10 Confocal microscopy image of the paper-stacked biomimetic scaffold 2 week after cell seeding, a cross-section view.

In Figure 4.10, nanofibrous membranes are shown in green color due to the residual stain on scaffolds, and cells are shown in red color due to the cell nuclear stain. Cells are observed between the layers of membranes, and the empty space marked by the blue arrow is caused by the small piece been cut from the circular disk for keeping track of alignment direction (Figure 3.4).

4.1.4 Von Kossa Stain images

The black color indicates calcium salts, the purple color indicates cell nuclei, and the pink color indicates cytoplasm in Figure 4.11 and Figure 4.12.

The majority of bone is made of the bone matrix, which consists of Type I collagen based organic part and carbonated hydroxyapatite based inorganic part. Hydroxyapatite is a mineral form of calcium apatite, and osteoblasts are cells that specialize in calcification of the bone matrix. Von Kossa stain can quantify calcification in scaffolds to confirm bone formation.

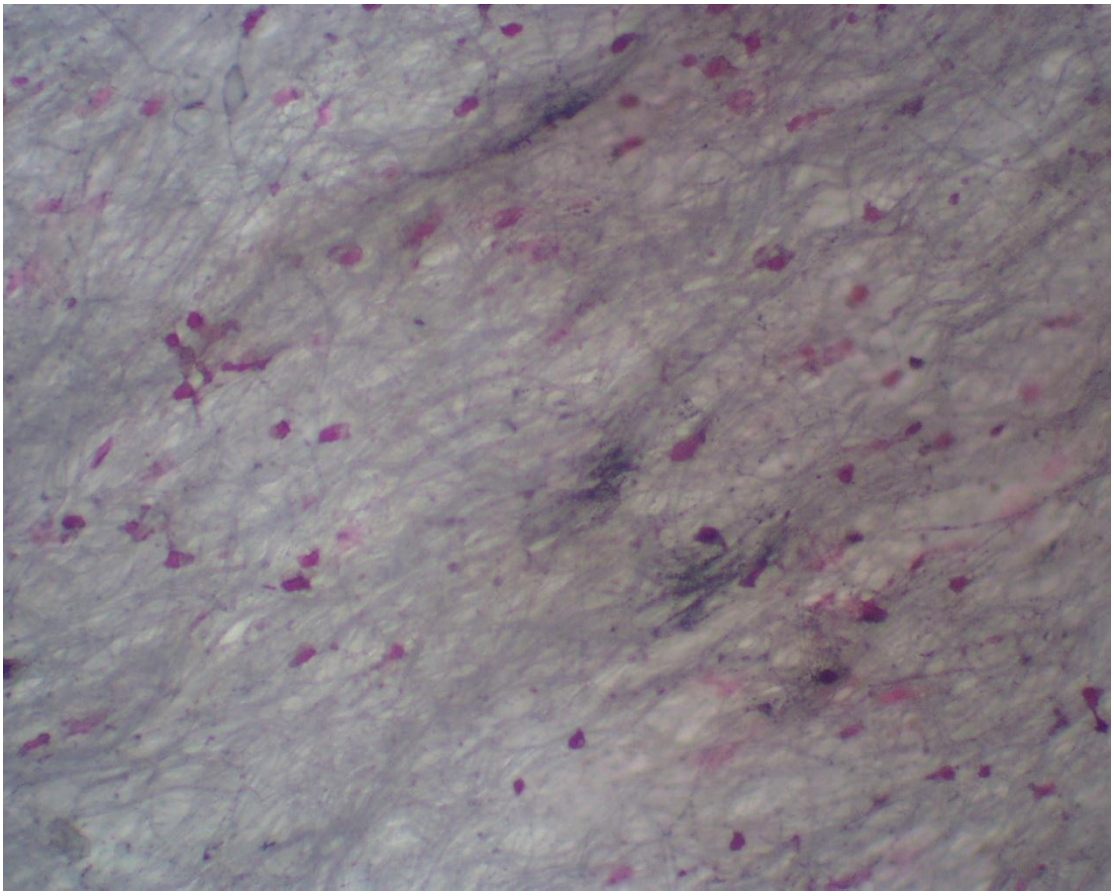

Figure 4.11 Von Kossa stain result on preosteoblasts seeded traditional gelatin/PCL scaffold after 1 week of cell seeding

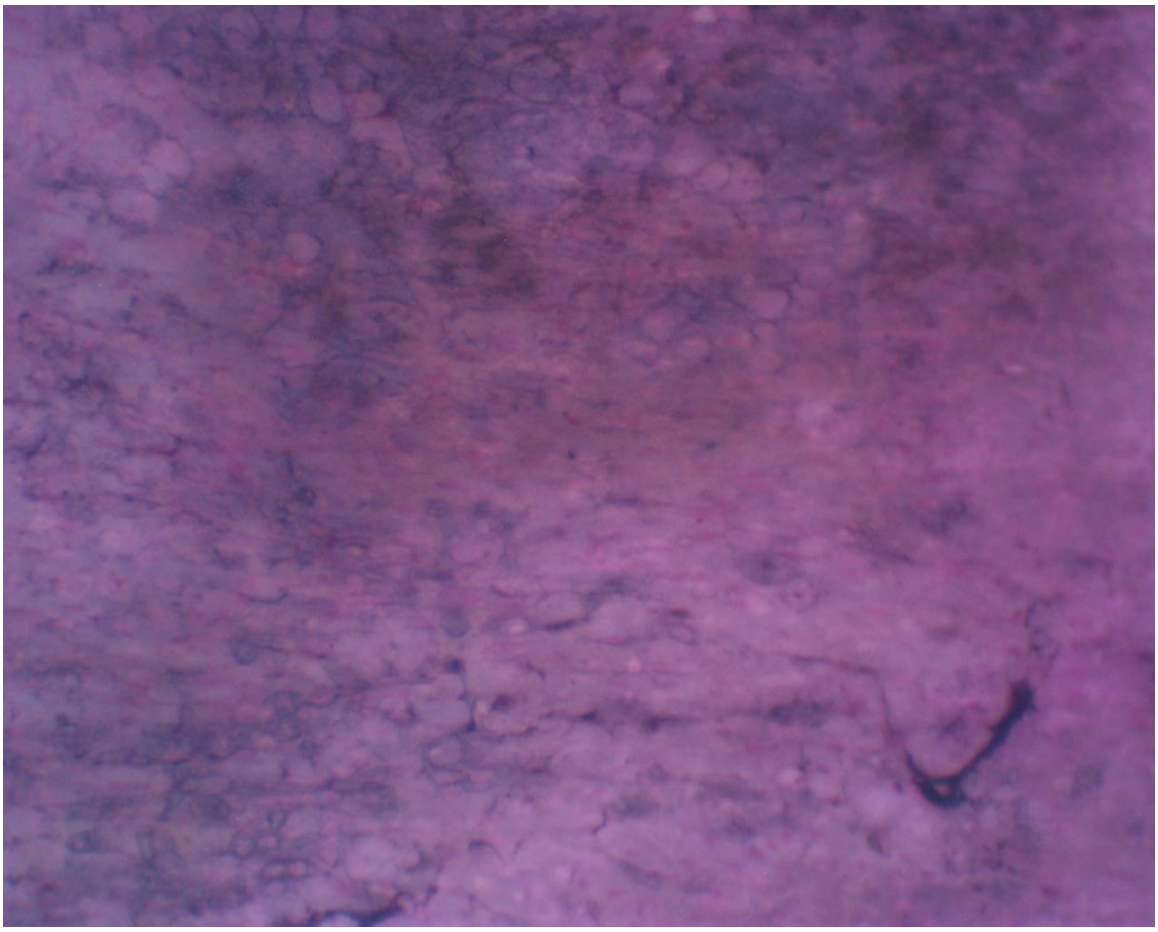

Figure 4.12 Von Kossa stain result on preosteoblasts seeded new gelatin/PCL composite scaffold after 1 week of cell seeding

For all scaffold samples, sign of calcification was shown, and cells were observed to be growing in the same direction under optical microscopy, which confirms the fact that aligned nanofibrous membranes fabricated by electrospinning can effectively guide the direction of cell growth. More pink color was observed on the new gelatin/PCL composite scaffolds, thus we could conclude that the composite scaffolds have better cytocompatibility compared to the traditional ones.

4.2 Reconstruction of Human Ear

4.2.1 Fabricated negative molds

Negative molds (Figure 4.13) are fabricated by the SLA 3500 solid imaging system with a resolution of 0.05 mm. The original ear mold fits tightly with the negative mold, which confirms the accuracy of the fabrication method used in this study.

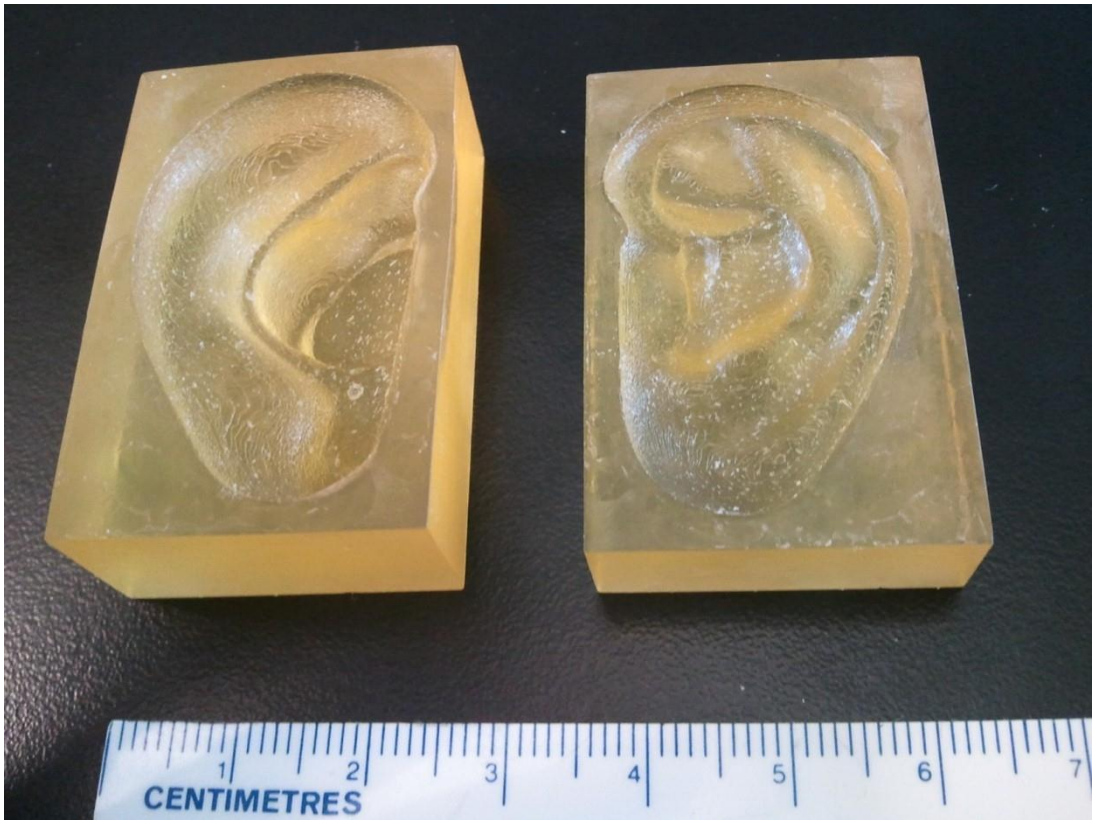

Figure 4.13 Negative molds fabricated by the SLA 3500 solid imaging system.

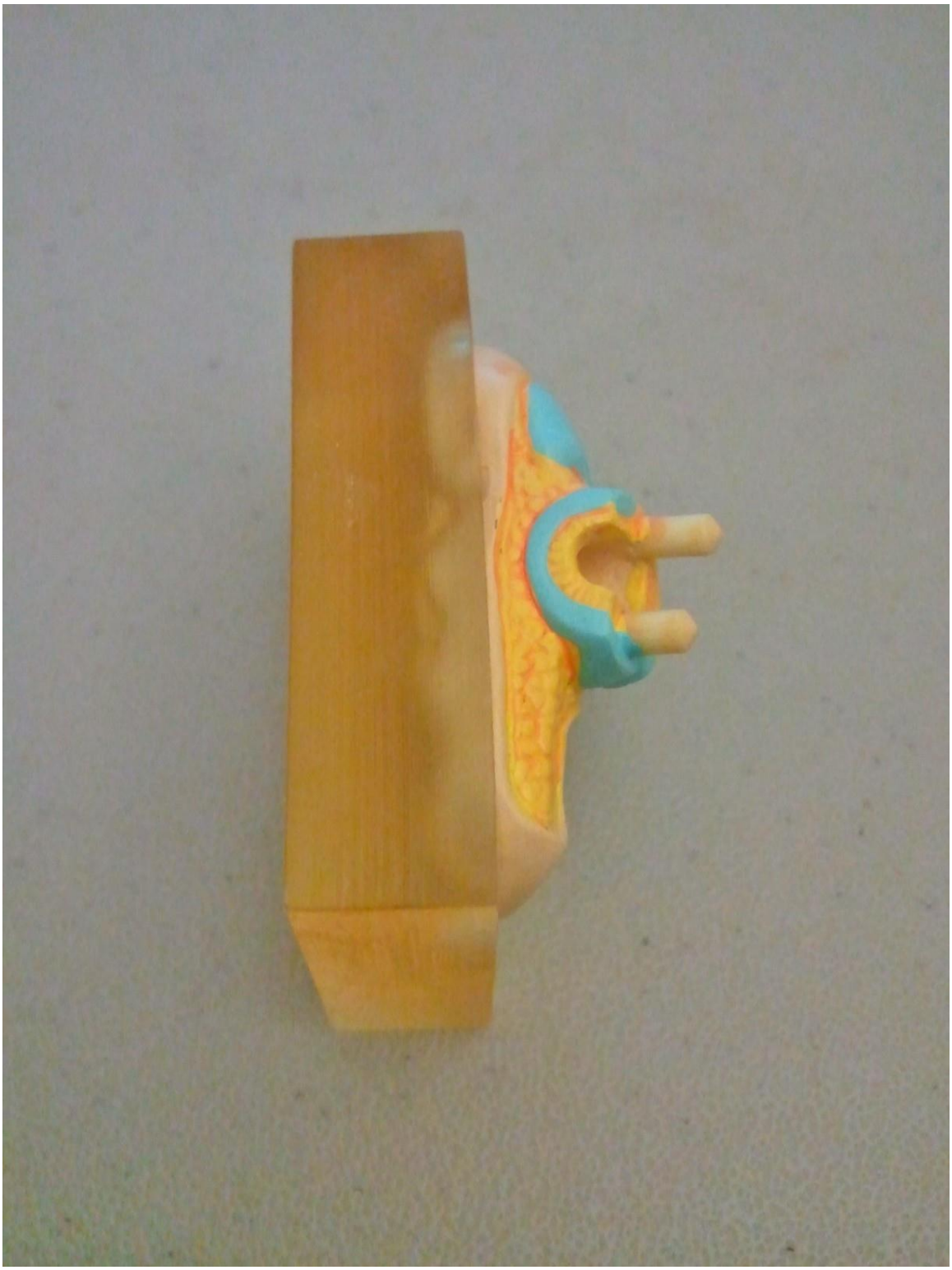

Figure 4.14 The ear model fits tightly with the negative mold.

4.2.2 Nanofibrous scaffold in the shape of human ear

The ear-shaped nanofibrous scaffold (Figure 4.15) is obtained using the negative molds to compress the biomimetic scaffold. This scaffold maintains its shape after removing the negative molds.

Figure 4.15 Human ear shaped nanofibrous scaffold.

4.3 Novel Design for Bioreactor

4.3.1 The final design of bioreactor

Following the process described in Section 3.3, a new design is proposed based on the data in Table 3.2 to reduce the difficulty levels of the components in structure and operations. The number of components is reduced from 19 to 12 as shown in Figure 4.16.

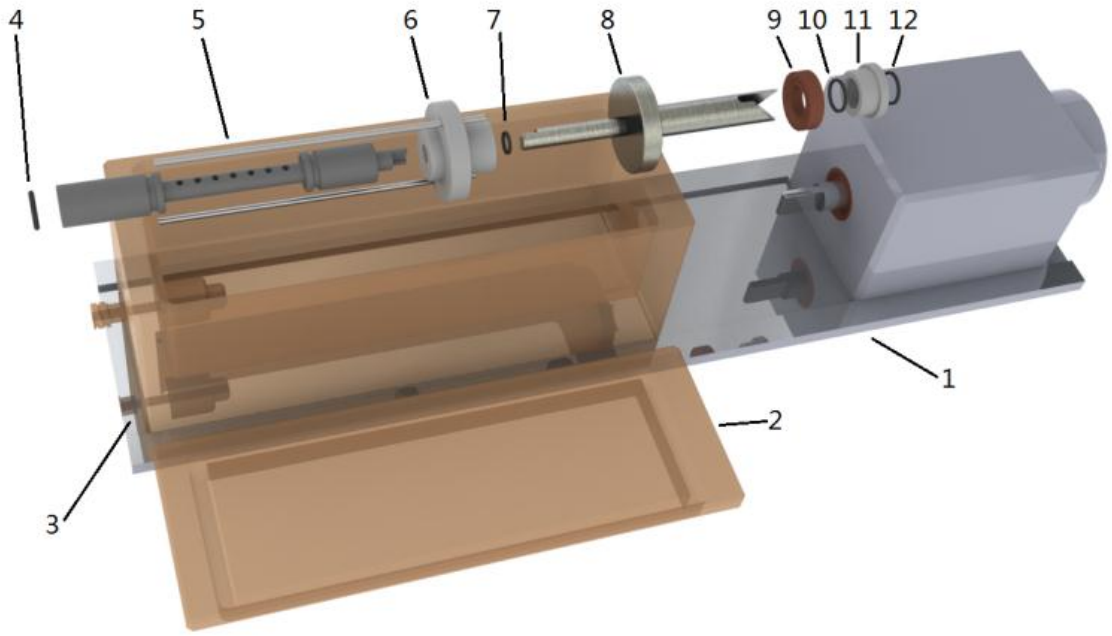

Figure 4.16 Final design of the bioreactor.

The mandrel holder has also been redesigned for the vascular scaffolds with small diameters (3-5 mm). With the addition of a slidable mount, the new scaffold holder fits scaffolds with variable lengths (30-90 mm), as shown in Figure 4.17.

Figure 4.17 Scaffold holder designed for microvessels.

4.3.2 Evaluation with DFA

The Liaison graph (Figure 4.18) and Complex matrix (Figure 4.19) are evaluated for the new design. Comparing to the existing design, the total difficulty level is reduced from 196 to 115, which is a 41% improvement.

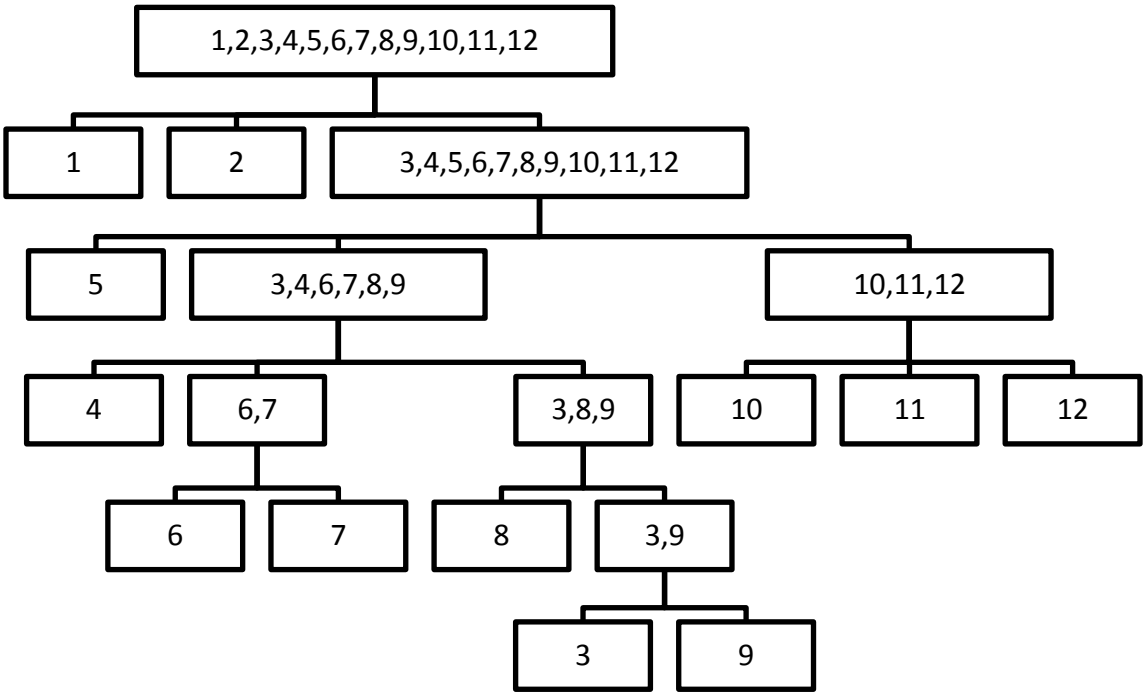

Figure 4.18 Liaison graph of proposed product.

$$C_{new} = \begin{vmatrix} 0 & 0 & 8 & 0 & 0 & 0 & 0 & 0 & 0 & 0 & 0 & 0 \\ 0 & 0 & 7 & 0 & 0 & 0 & 0 & 0 & 0 & 0 & 0 & 0 \\ 8 & 7 & 0 & 8 & 8 & 0 & 0 & 0 & 8 & 0 & 0 & 0 \\ 0 & 0 & 8 & 0 & 0 & 0 & 0 & 0 & 0 & 0 & 0 & 0 \\ 0 & 0 & 8 & 0 & 0 & 10 & 0 & 9 & 0 & 0 & 0 & 0 \\ 0 & 0 & 0 & 0 & 10 & 0 & 11 & 8 & 0 & 0 & 0 & 0 \\ 0 & 0 & 0 & 0 & 0 & 11 & 0 & 0 & 0 & 0 & 0 & 0 \\ 0 & 0 & 0 & 0 & 9 & 8 & 0 & 0 & 8 & 0 & 8 & 0 \\ 0 & 0 & 8 & 0 & 0 & 0 & 0 & 8 & 0 & 0 & 0 & 0 \\ 0 & 0 & 0 & 0 & 0 & 0 & 0 & 0 & 0 & 0 & 11 & 0 \\ 0 & 0 & 0 & 0 & 0 & 0 & 0 & 8 & 0 & 11 & 0 & 11 \\ 0 & 0 & 0 & 0 & 0 & 0 & 0 & 0 & 0 & 0 & 11 & 0 \end{vmatrix}$$

Figure 4.19 Complex matrix of the proposed product.

4.3.3 Evaluation with VR

From the main menu of Eon simulation, users can choose to start the disassembly operation or one of the two close-up simulations, assembly or disassembly simulation. The starting view is shown in Figure 4.20. The disassembled view is shown in Figure 4.21.

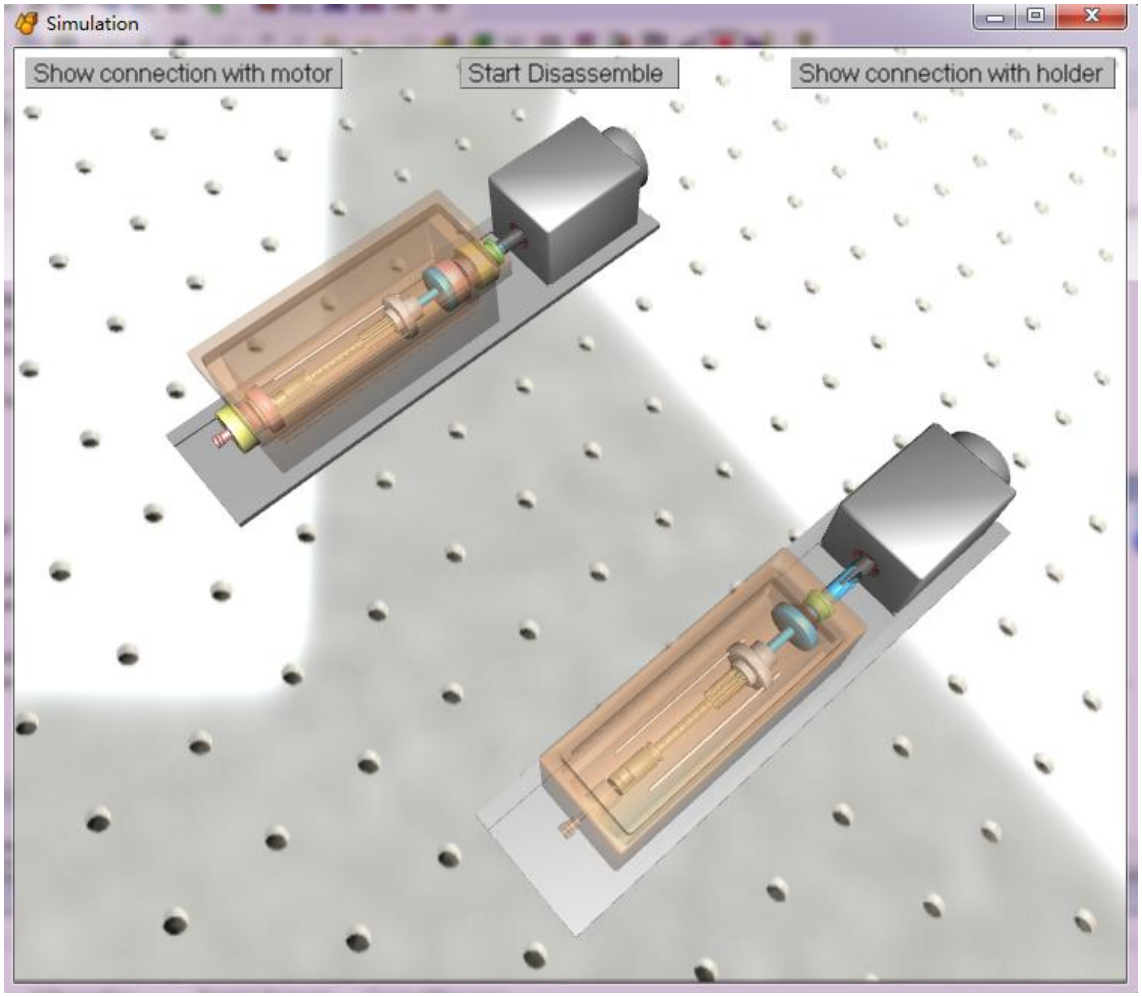

Figure 4.20 Operation interface of the evaluation simulation, both bioreactors were fully assembled at the beginning of the simulation.

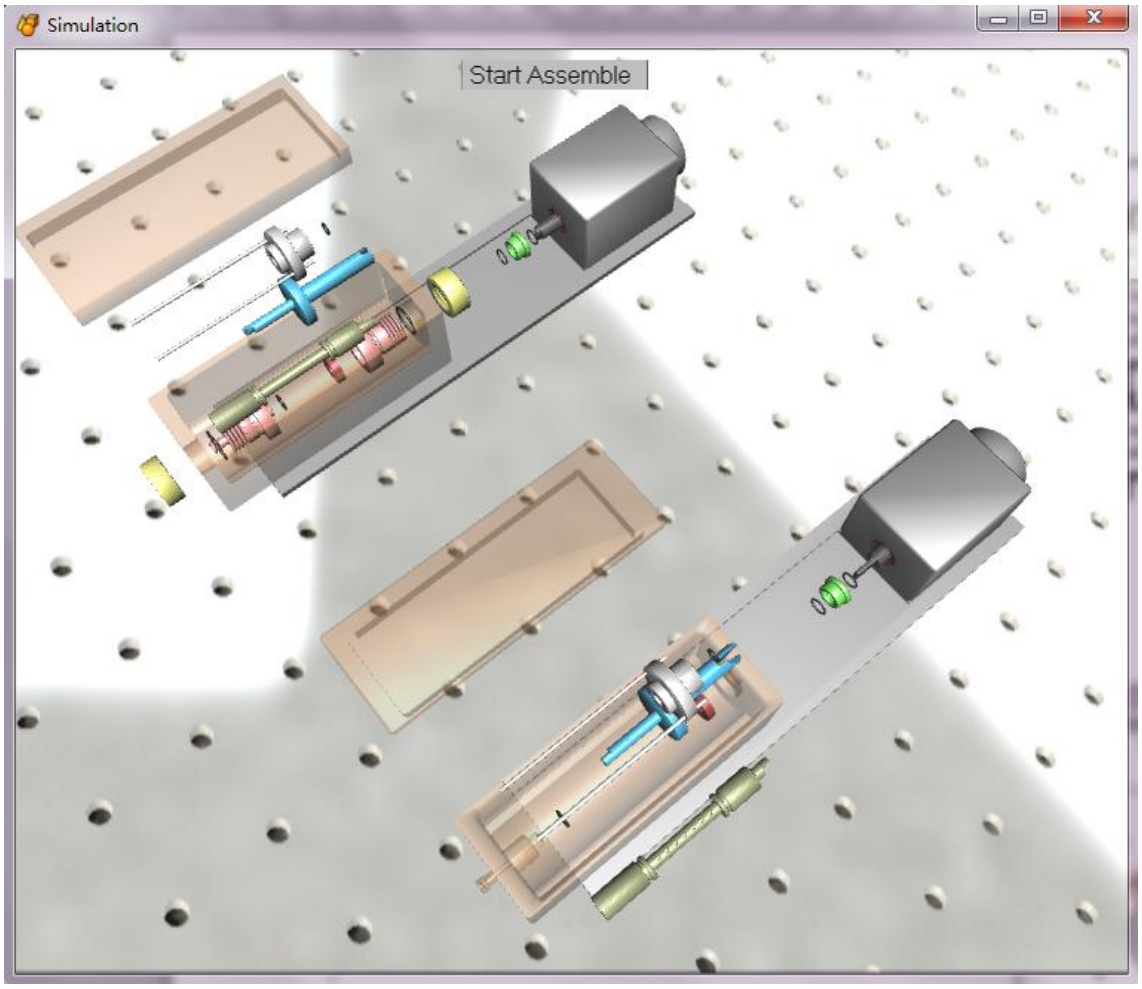

Figure 4.21 The disassembled view of both bioreactors.

Using the close-up simulation, users can have a detailed view of the point of interests to compare the performance between the two designs. Figure 4.22 shows the connection between the motor shaft and input shaft, where the input shaft has been modified to auto-match with the motor shaft. Figure 4.23 shows the connection between the input shaft and scaffold holder, where both components have been modified to auto-locate the alignment and prevent slip.

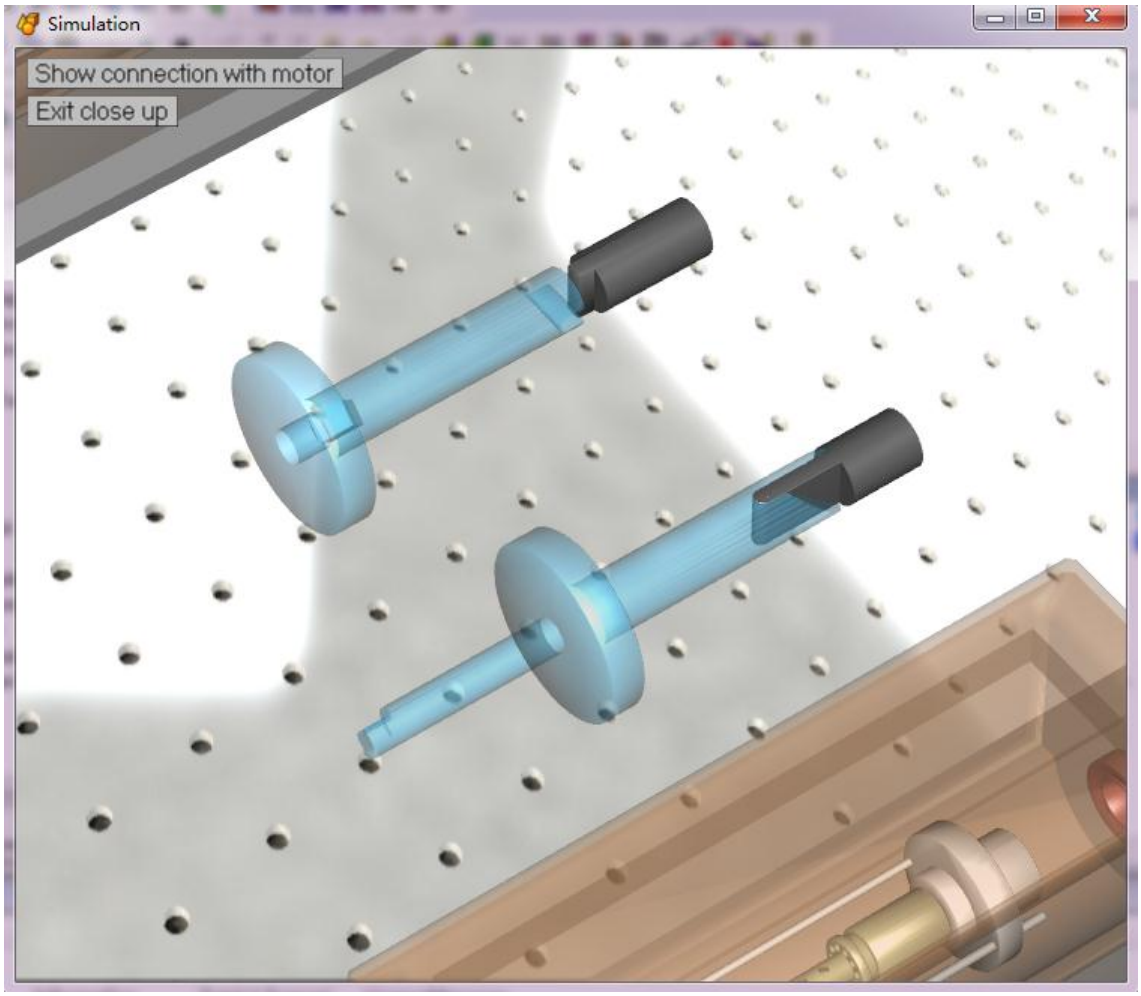

Figure 4.22 Close-up simulation of the connection between motor shaft and input shaft.

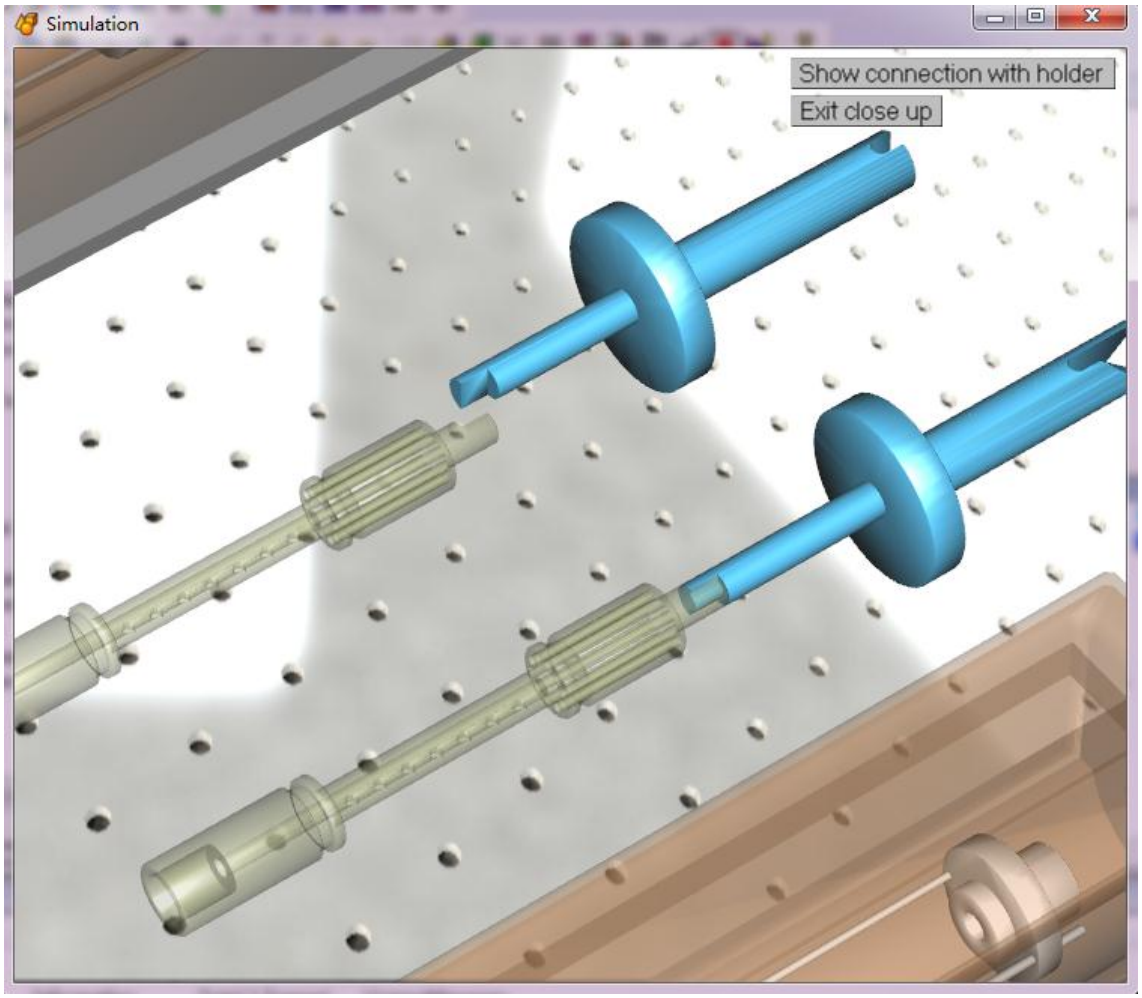

Figure 4.23 Close-up simulations of the connection between input shaft and scaffold holder.

Chapter 5

Discussion

5.1 Biomimetic Scaffold for Bone TE

Although the traditional composite scaffolds have no apparent shortcomings, they lack excellent properties, since all performances are averaged between different polymers. For example, the traditional gelatin/PCL composite scaffold with a fixed composition always has lower cell compatibility than pure gelatin scaffolds and lower mechanical strength than pure PCL scaffolds, and improvement of one of the properties always results in compromise of the other. In order to overcome such constraints we designed a new composite scaffold with layers that contain different ratio of materials (Figure 3.3). With higher gelatin percentage on the surfaces and higher PCL percentage in between, the new composite scaffold has better cell compatibility and mechanical strength than the traditional one.

In order to fabricate such a scaffold, electrospinning method was used due to its ability to construct nanofibrous membrane in a layer-by-layer fashion. Other fabrication methods like freeze-drying, salt-leaching, and gas-foaming all lack the ability to produce layers

with different compositions. The electrospinning method is also highly flexible, thus random or aligned nanofibrous membrane could be obtained with different rotary speed of the rotating drum collector; membranes with different thickness could be created with different electrospinning duration; nanofibers with different diameter could be electrospun with different voltages; and the ratio of gelatin and PCL could be modified with different flow rate of the polymer solutions. For this study a rotary speed of 1200 rpm was used to fabricate nanofibrous membranes with an appropriate degree of alignment to be able to guide cell growth but not to promote significant reductions in pore size and inhibit cell migration.

Depending on the pattern of collagen fibers, bone can be divided into two groups: woven or lamellar. Woven bone contains randomly organized collagen fibers and it is mostly created after fractures in adults. Lamellar bone contains layers of aligned collagen fibers and its mechanical strength is higher than woven bone. Since gelatin is biologically similar to collagen and the aligned nanofibrous structure is observed in lamellar bone, the new composite scaffold should be able to recreate an ideal environment for bone repair. SEM, confocal microscopy, and Von Kossa stain results all demonstrated the fact that the alignment of nanofibers can guide the direction of cell growth. Such mechanism should further improve the scaffold because aligned cells are found to increase mechanical strength in its direction of alignment. For example, smooth muscle cells in blood vessels are aligned in the circumferential direction to withstand circumferential pulsatile stretch caused by blood flow (Hashi, et al., 2007).

Both confocal microscopy and Von Kossa stain has shown more cells on the new gelatin/PCL nanofibrous membranes compared to the traditional ones, indicating better cell

compatibility of the new composite scaffold. The SEM images also exhibited positive results on vapour crosslinking with GTA and SBF immersing. All evidence indicates that the newly designed composite scaffolds with layered structure are superior to the traditional mono-ratio ones.

The paper-stacking approach ensures that cells are inside of the scaffold at the very beginning of cell culture, so that cell migration is no longer a problem for electrospun scaffolds. However, it is important to ensure that each membrane is thin enough to allow nutrition transportation to occur between the sandwiched layers.

5.2 Reconstruction of Human Ear

The shape of the human ear is complicated, and traditional fabrication methods of negative molds have their drawbacks. Hand carved molds are very experience dependent and clearly lack accuracy; impression casted molds can only been used to duplicate the shape of the normal ear which is a mirror image of the damaged ear. With the introduction of CAD technology, the shape of ear can be quickly captured using a 3D laser scanner. Once the 3D CAD models are constructed, the precise creation of mirror images and negative molds is made convenient.

The main source of error is the process of assembling the 9 individual scans into a complete 3D body. Multi-point registration is used in Geomagic Studio for maximum accuracy, but picking identical points on different scans is a manual process that can result in erroneous execution. In addition, the process of constructing the 3D ear model and nega-

tive molds is very accurate and computerized, and the same approach can be used for other tissues with irregular shapes.

Due to the financial constraints, the ear-shaped scaffold is not cell seeded for biological evaluations and further research is required.

5.3 Novel Design for Bioreactor

The existing design of the bioreactor is not optimized for manual assembly, causing excessive operation time while mounting and harvesting scaffold from the bioreactor. Although gloves are spread with 70% ethanol for disinfection in the cell culture lab, there are still risks that touching the bioreactor can contaminate the scaffold. Unlike sterilization, disinfection does not eliminate all microorganisms. Contamination bears severe consequences – it is not only a waste of money, time, and effort, but can also lead to contamination of the entire incubator and damages of others' cell culture work.

By applying the DFA method, every assembly process was analyzed based on part geometry and process complexity. After decreasing the component number and modifying the part geometry for more stable connection between parts, the new bioreactor designed achieved 41% reduction in difficulty level.

When importing 3D models from SolidWorks to Eon Studio, it is recommended to assemble the parts in SolidWorks because the same process is more time-consuming in Eon Studio. It is also important to set the proper size ratio during importing FTL files so that all components are visible in the simulation window. The actual value depends on the size of the model, so it is a trial and error process.

VR provides an easier tool to compare the performance of a new design with the existing product. VR-based simulation can guide and verify the design step-by-step in the process of design improvement with less time and cost compared to the traditional prototyping approach.

Chapter 6

Conclusions

6.1 Conclusion Remarks

This study optimizes aligned composite gelatin/PCL nanofibrous membrane by altering the composition ratio to form a sandwiched structure. Compared to traditional composite membranes, the new membranes demonstrate performances in both cell compatibility and mechanical strength. In order to further improve mechanical strength, the new composite membranes were paper-stacked to bio mimic the twisted plywood structure observed in lobster cuticles. The paper-stacking method ensures that cells are presented inside the bi-omimetic scaffold to overcome the poor cell migration performance of traditional electro-spun scaffolds. Due to the fact that the fabrication method with electrospinning is highly flexible, nanofibrous membranes with different thicknesses, composition, and layers can be produced simply by altering the respective electrospinning parameters.

The newly designed biomimetic scaffold was then used to reconstruct the human ear. With the aid of CAD technology, precise negative molds were fabricated using a 3D laser

scanner and 3D printer. The final scaffold produced is capable of sustaining its original shape after removing the negative molds.

In order to minimize tissue damage during handling, DFA methods and VR simulation has been successfully integrated to improve the BioReactor “In Breath” TYPE 807. The new design optimizes the manual assembly and disassembly to ensure the quality of tissue growth, and the VR evaluation shows significant improvements in operation difficulty level.

6.2 Contributions

All test results suggested that the optimized composite nanofibrous membrane combined with the paper stacked biomimetic scaffold not only enhances cytocompatibility and mechanical strength, but also solves the problem that the pore size of electrospun scaffolds is too small for cell migration. In conclusion, this study has developed a promising approach to fabricate a new generation of scaffolds for a wide range of tissue engineering applications.

This study also demonstrated how to precisely construct human ear-shaped scaffolds, and this approach can be used in any application that is related to the reconstruction of human tissues with a complex and irregular shape.

As for the bioreactor project, this study combined DFA and VR for systematic improvement of the existing bioreactor and fast evaluation of the new design. This is a promising approach to extend functions and applications of other bio-medical related products.

6.3 Future Work

Future work should focus on evaluating the biomimetic scaffold for gene expression to confirm osteogenesis. If the rate of cell growth is too low between the inner layers of the paper-stacked scaffold, a specially designed bioreactor should be developed to enhance nutrition transportation by applying constant culture medium flow through the scaffold. Live/dead assay should also be performed to check cell viability.

Mechanical tests should be performed after cell culture to explore the effects of cell growth on the scaffold's mechanical strength. For the human ear-shaped scaffold, it is recommended to evaluate its shape after cell culture by 3D scanning and compare with the original model. Proper skin TE products could be also used to fully reconstruct human ears.

Finally, a prototype of the new bioreactor should be constructed to verify the DFA/VR solution proposed in this research.

Bibliography

Alzuheri, A., Luong, L., & Xing, K. (2010). *Ergonomics design measures in manual assembly work*. Paper presented at the The 2nd International Conference on Engineering System Management and Applications

Apte, S. S., Paul, A., Prakash, S., & Shum-Tim, D. (2011). Current developments in the tissue engineering of autologous heart valves: moving towards clinical use. *Future Cardiol, 7*(1), 77-97. doi: 10.2217/fca.10.120

Arrington, E. D., Smith, W. J., Chambers, H. G., Bucknell, A. L., & Davino, N. A. (1996). Complications of iliac crest bone graft harvesting. *Clin Orthop Relat Res*(329), 300-309.

Atala, A., Bauer, S. B., Soker, S., Yoo, J. J., & Retik, A. B. (2006). Tissue-engineered autologous bladders for patients needing cystoplasty. *Lancet, 367*(9518), 1241-1246. doi: S0140-6736(06)68438-9 [pii]
10.1016/S0140-6736(06)68438-9

ATCC. (2011). Manufacturer's protocol, 2011, from http://www.atcc.org/

Barak, L. S., Yocum, R. R., Nothnagel, E. A., & Webb, W. W. (1980). Fluorescence staining of the actin cytoskeleton in living cells with 7-nitrobenz-2-oxa-1,3-diazole-phallacidin. *Proc Natl Acad Sci U S A, 77*(2), 980-984.

Bhatia, S. K. (2010). Tissue engineering for clinical applications. *Biotechnol J, 5*(12), 1309-1323. doi: 10.1002/biot.201000230

Bigi, A., Bracci, B., Cojazzi, G., Panzavolta, S., & Rubini, K. (2004). In vitro mineralization of gelatin-polyacrylic acid complex matrices. *J Biomater Sci Polym Ed, 15*(3), 243-254.

Boothroyd, G., Dewhurst, P., & Knight, W. A. (2002). *Product design for manufacture and assembly*: New York: Marcel Dekker.

Cao, Y., Vacanti, J. P., Paige, K. T., Upton, J., & Vacanti, C. A. (1997). Transplantation of chondrocytes utilizing a polymer-cell construct to produce tissue-engineered cartilage in the shape of a human ear. *Plast Reconstr Surg, 100*(2), 297-302; discussion 303-294.

Chang, W. H., Chang, Y., Lai, P. H., & Sung, H. W. (2003). A genipin-crosslinked gelatin membrane as wound-dressing material: in vitro and in vivo studies. *J Biomater Sci Polym Ed, 14*(5), 481-495.

Chen, C.-j., Wu, Y.-f., & Yang, Y. (2010). A Modeling and Representation Method for Virtual Assembly System. In H. H. Tan (Ed.), *Applied Mechanics and Mechanical Engineering, Pts 1-3* (Vol. 29-32, pp. 1057-1062).

Choi, K. H., Choi, B. H., Park, S. R., Kim, B. J., & Min, B. H. (2010). The chondrogenic differentiation of mesenchymal stem cells on an extracellular matrix scaffold derived from porcine chondrocytes. *Biomaterials, 31*(20), 5355-5365. doi: S0142-9612(10)00424-2 [pii]
10.1016/j.biomaterials.2010.03.053

Chong, E. J., Phan, T. T., Lim, I. J., Zhang, Y. Z., Bay, B. H., Ramakrishna, S., & Lim, C. T. (2007). Evaluation of electrospun PCL/gelatin nanofibrous scaffold for wound healing and layered dermal reconstitution. *Acta Biomater, 3*(3), 321-330. doi: S1742-7061(07)00015-3 [pii]
10.1016/j.actbio.2007.01.002

Chou, L. B., Mann, R. A., Coughlin, M. J., McPeake, W. T., 3rd, & Mizel, M. S. (2007). Stress fracture as a complication of autogenous bone graft harvest from the distal tibia. *Foot Ankle Int, 28*(2), 199-201. doi: 10.3113/fai.2007.0199

Dahl, S. L., Kypson, A. P., Lawson, J. H., Blum, J. L., Strader, J. T., Li, Y., . . . Niklason, L. E. (2011). Readily available tissue-engineered vascular grafts. *Sci Transl Med, 3*(68), 68ra69. doi: 3/68/68ra9 [pii]
10.1126/scitranslmed.3001426

Demoly, F., Gomes, S., Eynard, B., & Rivest, L. (2010). PLM-based approach for Assembly Process Engineering. *International Journal of Manufacturing Research, 5*(4), 413-428.

Demoly, F., Yan, X.-T., Eynard, B., Rivest, L., & Gomes, S. (2011). An assembly oriented design framework for product structure engineering and assembly sequence planning. *Robotics and Computer-Integrated Manufacturing, 27*(1), 33-46. doi: 10.1016/j.rcim.2010.05.010

Desai, A., & Mital, A. (2010). Facilitating Design for Assembly Through the Adoption of A Comprehensive Design Methodology. *International Journal of Industrial Engineering-Theory Applications and Practice, 17*(2), 92-102.

Doshi, J., & Reneker, D. H. (1995). Electrospinning process and applications of electrospun fibers. *Journal of Electrostatics, 35*(2-3), 151-160. doi: 10.1016/0304-3886(95)00041-8

Du, F., Wang, H., Zhao, W., Li, D., Kong, D., Yang, J., & Zhang, Y. (2012). Gradient nanofibrous chitosan/poly varepsilon-caprolactone scaffolds as extracellular microenvironments for vascular tissue engineering. *Biomaterials, 33*(3), 762-770. doi: S0142-9612(11)01241-5 [pii]
10.1016/j.biomaterials.2011.10.037

Elloumi-Hannachi, I., Yamato, M., & Okano, T. (2010). Cell sheet engineering: a unique nanotechnology for scaffold-free tissue reconstruction with clinical applications in regenerative medicine. *J Intern Med, 267*(1), 54-70. doi: JIM2185 [pii]
10.1111/j.1365-2796.2009.02185.x

Eon Reality. (2011), from www.eonreality.com

Evans, C. (2011). Barriers to the clinical translation of orthopaedic tissue engineering. *Tissue Eng Part B Rev*. doi: 10.1089/ten.TEB.2011.0228

Galaction, A., Cascaval, D., & Folescu, E. (2007). Bioreactors for 3D tissue engineering. *Romanian Biotechnilogical Letters, 12*, 1-8.

Gerdemeli, I., Fetvaci, C., & Kayaoglu, E. (2011). Design For Assembly In Concurrent Engineering A Case Study On Its Application: Glass Block Holder and Glass Mold. In D. Z. Z. Q. B. Z. S. F. Su (Ed.), *Advanced Design and Manufacture Iii* (Vol. 450, pp. 141-144).

Harrington, W. F., & Von Hippel, P. H. (1961). The structure of collagen and gelatin. *Adv Protein Chem, 16*, 1-138.

Hashi, C. K., Zhu, Y., Yang, G. Y., Young, W. L., Hsiao, B. S., Wang, K., . . . Li, S. (2007). Antithrombogenic property of bone marrow mesenchymal stem cells in nanofibrous vascular grafts. *Proc Natl Acad Sci U S A, 104*(29), 11915-11920. doi: 0704581104 [pii]

10.1073/pnas.0704581104

Holzwarth, J. M., & Ma, P. X. (2011). Biomimetic nanofibrous scaffolds for bone tissue engineering. *Biomaterials, 32*(36), 9622-9629. doi: S0142-9612(11)01050-7 [pii]

10.1016/j.biomaterials.2011.09.009

Huang, W., & Kong, Z. (2010). Process Capability Sensitivity Analysis for Design Evaluation of Multistage Assembly Processes. *Ieee Transactions on Automation Science and Engineering, 7*(4), 736-745. doi: 10.1109/tase.2009.2034633

Hugo Sache, E. (2010). Operating Instructions. *Harvad Apparatus GmbH*.

Hussain, A., Bessho, K., Takahashi, K., & Tabata, Y. (2011). Magnesium calcium phosphate as a novel component enhances mechanical/physical properties of gelatin scaffold and osteogenic differentiation of bone marrow mesechymal stem cells. *Tissue Eng Part A*. doi: 10.1089/ten.TEA.2011.0310

Isogai, N., Asamura, S., Higashi, T., Ikada, Y., Morita, S., Hillyer, J., . . . Landis, W. J. (2004). Tissue engineering of an auricular cartilage model utilizing cultured chondrocyte-poly(L-lactide-epsilon-caprolactone) scaffolds. *Tissue Eng, 10*(5-6), 673-687. doi: 10.1089/1076327041348527

Janicki, P., & Schmidmaier, G. (2011). What should be the characteristics of the ideal bone graft substitute? Combining scaffolds with growth factors and/or stem cells. *Injury, 42 Suppl 2*, S77-81. doi: S0020-1383(11)00251-8 [pii]

10.1016/j.injury.2011.06.014

Jeong, S. I., Lee, A. Y., Lee, Y. M., & Shin, H. (2008). Electrospun gelatin/poly(L-lactide-co-epsilon-caprolactone) nanofibers for mechanically functional tissue-engineering scaffolds. *J Biomater Sci Polym Ed, 19*(3), 339-357. doi: 10.1163/156856208783721029

Jin, S., Cai, W., Lai, X., & Lin, Z. (2010). Design automation and optimization of assembly sequences for complex mechanical systems. *International Journal of Advanced Manufacturing Technology, 48*(9-12), 1045-1059. doi: 10.1007/s00170-009-2361-8

Kang, X., & Peng, Q. (2010). Data integration from product design to assembly planning in a collaborative environment. *International Journal of Manufacturing Research, 5*(1), 120-137.

Khaled, E. G., Saleh, M., Hindocha, S., Griffin, M., & Khan, W. S. (2011). Tissue engineering for bone production- stem cells, gene therapy and scaffolds. *Open Orthop J, 5 Suppl 2*, 289-295. doi: 10.2174/1874325001105010289
TOORTHJ-5-289 [pii]

Khan, Z. (2010). Getting a handle on effective design for assembly. *Assembly, 53(9)*, 1-4.

Kim, G. H. (2008). Electrospun PCL nanofibers with anisotropic mechanical properties as a biomedical scaffold. *Biomed Mater, 3*(2), 025010. doi: S1748-6041(08)66609-7 [pii]
10.1088/1748-6041/3/2/025010

Kim, M. S., Jun, I., Shin, Y. M., Jang, W., Kim, S. I., & Shin, H. (2010). The development of genipin-crosslinked poly(caprolactone) (PCL)/gelatin nanofibers for tissue engineering applications. *Macromol Biosci, 10*(1), 91-100. doi: 10.1002/mabi.200900168

Langer, R. (2009). Perspectives and challenges in tissue engineering and regenerative medicine. *Adv Mater, 21*(32-33), 3235-3236. doi: 10.1002/adma.200902589

Langer, R., & Vacanti, J. P. (1993). Tissue engineering. *Science, 260*(5110), 920-926.

Lee, K., Silva, E. A., & Mooney, D. J. (2011). Growth factor delivery-based tissue engineering: general approaches and a review of recent developments. *J R Soc Interface, 8*(55), 153-170. doi: rsif.2010.0223 [pii]
10.1098/rsif.2010.0223

Li, C. Y., Yuan, W., Jiang, H., Li, J. S., Xu, F. J., Yang, W. T., & Ma, J. (2011). PCL film surfaces conjugated with P(DMAEMA)/gelatin complexes for improving cell immobilization and gene transfection. *Bioconjug Chem, 22*(9), 1842-1851. doi: 10.1021/bc200241m

Li, T. (2010). Applying TRIZ and AHP to develop innovative design for automated assembly systems. *International Journal of Advanced Manufacturing Technology, 46*(1-4), 301-313. doi: 10.1007/s00170-009-2061-4

Li, W., Xing, M., & Peng, Q. (2011, August 28 - 31). *Bioreactor Improvement Based on Design for Assembly in Virtual Environments.* Paper presented at the ASME 2011 International Design Engineering Technical Conferences & Computers and Information in Engineering Conference, Washington, DC.

Liang, M. S., & Andreadis, S. T. (2011). Engineering fibrin-binding TGF-beta1 for sustained signaling and contractile function of MSC based vascular constructs. *Biomaterials, 32*(33), 8684-8693. doi: S0142-9612(11)00876-3 [pii]
10.1016/j.biomaterials.2011.07.079

Liu, F., Lu, N., & Kuang, B. (2011). A Variant Design Method of Assembly. In L. C. Z. C. L. S. T. L. Zhang (Ed.), *Manufacturing Engineering and Automation I, Pts 1-3* (Vol. 139-141, pp. 1126-1130).

Liu, H., Shen, B., & Fan, Q. (2010). *Digital virtual assembly process design and assembly process simulation technology*. Paper presented at the International Conference on Computer Design and Applications (ICCDA).

Liu, X., Smith, L. A., Hu, J., & Ma, P. X. (2009). Biomimetic nanofibrous gelatin/apatite composite scaffolds for bone tissue engineering. *Biomaterials, 30*(12), 2252-2258. doi: S0142-9612(08)01067-3 [pii]
10.1016/j.biomaterials.2008.12.068

Liu, Y., Zhang, L., Zhou, G., Li, Q., Liu, W., Yu, Z., . . . Cao, Y. (2010). In vitro engineering of human ear-shaped cartilage assisted with CAD/CAM technology. *Biomaterials, 31*(8), 2176-2183. doi: S0142-9612(09)01324-6 [pii]
10.1016/j.biomaterials.2009.11.080

Lu, D., Cardiel, J., Cao, G., & Shen, A. Q. (2010). Nanoporous scaffold with immobilized enzymes during flow-induced gelation for sensitive H(2)O(2) biosensing. *Adv Mater, 22*(25), 2809-2813. doi: 10.1002/adma.201000189

Lu, J., Wei, J., Yan, Y., Li, H., Jia, J., Wei, S., . . . Liu, C. (2011). Preparation and preliminary cytocompatibility of magnesium doped apatite cement with degradability for bone regeneration. *J Mater Sci Mater Med, 22*(3), 607-615. doi: 10.1007/s10856-011-4228-4

Ma, P. X. (2008). Biomimetic materials for tissue engineering. *Adv Drug Deliv Rev, 60*(2), 184-198. doi: S0169-409X(07)00297-9 [pii]
10.1016/j.addr.2007.08.041

Macchiarini, P., Jungebluth, P., Go, T., Asnaghi, M. A., Rees, L. E., Cogan, T. A., . . . Birchall, M. A. (2008). Clinical transplantation of a tissue-engineered airway. *Lancet, 372*(9655), 2023-2030. doi: S0140-6736(08)61598-6 [pii]
10.1016/S0140-6736(08)61598-6

Markx, G. H. (2008). The use of electric fields in tissue engineering: A review. *Organogenesis, 4*(1), 11-17.

Mathew, A., & Rao, C. S. P. (2010). A CAD system for extraction of mating features in an assembly. *Assembly Automation, 30*(2), 142-146. doi: 10.1108/01445151011029772

Murphy, W. L., Peters, M. C., Kohn, D. H., & Mooney, D. J. (2000). Sustained release of vascular endothelial growth factor from mineralized poly(lactide-co-glycolide) scaffolds for tissue engineering. *Biomaterials, 21*(24), 2521-2527. doi: S0142961200001204 [pii]

Nikolov, S., Petrov, M., Lymperakis, L., Friak, M., Sachs, C., Fabritius, H. O., . . . Neugebauer, J. (2010). Revealing the design principles of high-performance biological composites using ab initio and multiscale simulations: the example of lobster cuticle. *Adv Mater, 22*(4), 519-526. doi: 10.1002/adma.200902019

Nowak, A. P., Breedveld, V., Pakstis, L., Ozbas, B., Pine, D. J., Pochan, D., & Deming, T. J. (2002). Rapidly recovering hydrogel scaffolds from self-assembling diblock copolypeptide amphiphiles. *Nature, 417*(6887), 424-428. doi: 10.1038/417424a
417424a [pii]

Ott, L. M., Weatherly, R. A., & Detamore, M. S. (2011). Overview of tracheal tissue engineering: clinical need drives the laboratory approach. *Ann Biomed Eng, 39*(8), 2091-2113. doi: 10.1007/s10439-011-0318-1

Park, H. K., Nam, K. O., Kim, D. J., Ahn, H. J., Lee, J. H., Im, K., & Shaw, R. (2010). A conceptual design of assembly strategy and dedicated tools for assembly of 40 degrees sector. *Fusion Engineering and Design, 85*(10-12), 1981-1985. doi: 10.1016/j.fusengdes.2010.07.009

Phipps, M. C., Clem, W. C., Grunda, J. M., Clines, G. A., & Bellis, S. L. (2012). Increasing the pore sizes of bone-mimetic electrospun scaffolds comprised of

polycaprolactone, collagen I and hydroxyapatite to enhance cell infiltration. *Biomaterials, 33*(2), 524-534. doi: S0142-9612(11)01172-0 [pii]
10.1016/j.biomaterials.2011.09.080

Place, E. S., Evans, N. D., & Stevens, M. M. (2009). Complexity in biomaterials for tissue engineering. *Nat Mater, 8*(6), 457-470. doi: nmat2441 [pii]
10.1038/nmat2441

Ploeger, L. S., Dullens, H. F., Huisman, A., & van Diest, P. J. (2008). Fluorescent stains for quantification of DNA by confocal laser scanning microscopy in 3-D. *Biotech Histochem, 83*(2), 63-69. doi: 793255696 [pii]
10.1080/10520290802127586

Poppa, K. R., Stone, R. B., & Asme. (2010). *SORTING RESULTS OF AUTOMATED CONCEPT GENERATORS BASED ON DESIGN FOR MANUFACTURE AND ASSEMBLY.*

Qian, Y. F., Zhang, K. H., Chen, F., Ke, Q. F., & Mo, X. M. (2011). Cross-linking of gelatin and chitosan complex nanofibers for tissue-engineering scaffolds. *J Biomater Sci Polym Ed, 22*(8), 1099-1113. doi: jbs3154 [pii]
10.1163/092050610X499447

Ren, L., Tsuru, K., Hayakawa, S., & Osaka, A. (2002). Novel approach to fabricate porous gelatin-siloxane hybrids for bone tissue engineering. *Biomaterials, 23*(24), 4765-4773. doi: S0142961202002260 [pii]

Santin, M., Huang, S. J., Iannace, S., Ambrosio, L., Nicolais, L., & Peluso, G. (1996). Synthesis and characterization of a new interpenetrated poly(2-hydroxyethylmethacrylate)-gelatin composite polymer. *Biomaterials, 17*(15), 1459-1467. doi: 0142961296897699 [pii]

Schofer, M. D., Roessler, P. P., Schaefer, J., Theisen, C., Schlimme, S., Heverhagen, J. T., . . . Paletta, J. R. (2011). Electrospun PLLA nanofiber scaffolds and their use in combination with BMP-2 for reconstruction of bone defects. *PLoS One, 6*(9), e25462. doi: 10.1371/journal.pone.0025462
PONE-D-11-05046 [pii]

Services, U. D. o. H. a. H. (2006). 2020: A New Vision —A Future for Regenerative Medicine, 2011, from http://www.hhs.gov/reference/newfuture.shtml

Seth, A., Vance, J. M., & Oliver, J. H. (2011). Virtual reality for assembly methods prototyping: a review. *Virtual Reality, 15*(1), 5-20. doi: 10.1007/s10055-009-0153-y

Song, J. H., Kim, H. E., & Kim, H. W. (2008). Production of electrospun gelatin nanofiber by water-based co-solvent approach. *J Mater Sci Mater Med, 19*(1), 95-102. doi: 10.1007/s10856-007-3169-4

Su, Q., Liu, L., & Whitney, D. E. (2010). A Systematic Study of the Prediction Model for Operator-Induced Assembly Defects Based on Assembly Complexity Factors. *Ieee Transactions on Systems Man and Cybernetics Part a-Systems and Humans, 40*(1), 107-120. doi: 10.1109/tsmca.2009.2033030

Subbiah, T., Bhat, G. S., Tock, R. W., Parameswaran, S., & Ramkumar, S. S. (2005). Electrospinning of nanofibers. *Journal of Applied Polymer Science, 96*(2), 557-569. doi: 10.1002/app.21481

Suutarla, S., Rautio, J., Ritvanen, A., Ala-Mello, S., Jero, J., & Klockars, T. (2007). Microtia in Finland: comparison of characteristics in different populations. *Int J Pediatr Otorhinolaryngol, 71*(8), 1211-1217. doi: S0165-5876(07)00160-7 [pii]
10.1016/j.ijporl.2007.04.020

Szpalski, C., Wetterau, M., Barr, J., & Warren, S. M. (2011). Bone Tissue Engineering: Current Strategies and Techniques Part I-Scaffolds. *Tissue Eng Part B Rev*. doi: 10.1089/ten.TEB.2011.0427

Tanner, K. E. (2010). Bioactive composites for bone tissue engineering. *Proc Inst Mech Eng H, 224*(12), 1359-1372.

Tavares, S. M. O., & de Castro, P. M. S. T. (2011). Impact of Integral Structures in the Design for Manufacture and Assembly of Airframes. In D. Z. Z. Q. B. Z. S. F. Su (Ed.), *Advanced Design and Manufacture Iii* (Vol. 450, pp. 279-282).

Thomas, A., Legoy, J.-M., & Amann, M. (2010). Improved design quality [pump assembly]. *Sulzer Technical Review, 1*(6-9).

Van Vlierberghe, S., Dubruel, P., & Schacht, E. (2011). Biopolymer-based hydrogels as scaffolds for tissue engineering applications: a review. *Biomacromolecules, 12*(5), 1387-1408. doi: 10.1021/bm200083n

Viola, J., Lal, B., & Grad, O. (2003). The Emergence of Tissue Engineering as a Research Field, 2011, from http://www.nsf.gov/pubs/2004/nsf0450/start.htm

Wang, C., Yu, H., & Zhang, W. (2010). Object-oriented models for aero-engine assembly. *International Journal of Internet Manufacturing and Services, 2*(3-4), 354-364.

Wei, K., Li, Y., Mugishima, H., Teramoto, A., & Abe, K. (2011). Fabrication of core-sheath structured fibers for model drug release and tissue engineering by emulsion electrospinning. *Biotechnol J*. doi: 10.1002/biot.201000473

Wong, V. W., Rustad, K. C., Longaker, M. T., & Gurtner, G. C. (2010). Tissue engineering in plastic surgery: a review. *Plast Reconstr Surg, 126*(3), 858-868. doi: 10.1097/PRS.0b013e3181e3b3a3
00006534-201009000-00016 [pii]

Wu, L., Jing, D., & Ding, J. (2006). A "room-temperature" injection molding/particulate leaching approach for fabrication of biodegradable three-dimensional porous scaffolds. *Biomaterials, 27*(2), 185-191. doi: S0142-9612(05)00494-1 [pii]
10.1016/j.biomaterials.2005.05.105

Xiang, P., Li, M., Zhang, C. Y., Chen, D. L., & Zhou, Z. H. (2011). Cytocompatibility of electrospun nano fi ber tubular scaffolds for small diameter tissue engineering blood vessels. *Int J Biol Macromol, 49*(3), 281-288. doi: 10.1016/j.ijbiomac.2011.05.004

Xu, X., & Li, D. (2010). *Variant design process programming of assembly based on dimension constraint complexity*. Paper presented at the The 8th World Congress on Intelligent Control and Automation (WCICA).

Yip-Hoi, D. (2010). *CAD instruction techniques for advanced assembly modeling and mechanisms design*. Paper presented at the Annual Conference and Exposition, Conference Proceedings.

Zhang, P., Wu, H., Lu, Z., Deng, C., Hong, Z., Jing, X., & Chen, X. (2011). RGD-conjugated copolymer incorporated into composite of poly(lactide-co-glycotide)

and poly(L-lactide)-grafted nanohydroxyapatite for bone tissue engineering. *Biomacromolecules, 12*(7), 2667-2680. doi: 10.1021/bm2004725

Zhang, Y., Fan, W., Nothdurft, L., Wu, C., Zhou, Y., Crawford, R., & Xiao, Y. (2011). In vitro and in vivo evaluation of adenovirus combined silk fibroin scaffolds for bone morphogenetic protein-7 gene delivery. *Tissue Eng Part C Methods, 17*(8), 789-797. doi: 10.1089/ten.tec.2010.0453

Zhang, Y., Ouyang, H., Lim, C. T., Ramakrishna, S., & Huang, Z. M. (2005). Electrospinning of gelatin fibers and gelatin/PCL composite fibrous scaffolds. *J Biomed Mater Res B Appl Biomater, 72*(1), 156-165. doi: 10.1002/jbm.b.30128

Zhao, J., Han, W., Chen, H., Tu, M., Huan, S., Miao, G., . . . Zhou, C. (2011). Fabrication and in vivo osteogenesis of biomimetic poly(propylene carbonate) scaffold with nanofibrous chitosan network in macropores for bone tissue engineering. *J Mater Sci Mater Med*. doi: 10.1007/s10856-011-4468-3

Zhou, L., Pomerantseva, I., Bassett, E. K., Bowley, C. M., Zhao, X., Bichara, D. A., . . . Sundback, C. A. (2011). Engineering ear constructs with a composite scaffold to maintain dimensions. *Tissue Eng Part A, 17*(11-12), 1573-1581. doi: 10.1089/ten.TEA.2010.0627

Zimmermann, G., Wagner, C., Schmeckenbecher, K., Wentzensen, A., & Moghaddam, A. (2009). Treatment of tibial shaft non-unions: bone morphogenetic proteins versus autologous bone graft. *Injury, 40 Suppl 3*, S50-53. doi: S0020-1383(09)70012-9 [pii]

10.1016/S0020-1383(09)70012-9

Zou, D., Zhang, Z., He, J., Zhu, S., Wang, S., Zhang, W., . . . Jiang, X. (2011). Repairing critical-sized calvarial defects with BMSCs modified by a constitutively active form of hypoxia-inducible factor-1alpha and a phosphate cement scaffold. *Biomaterials, 32*(36), 9707-9718. doi: S0142-9612(11)01045-3 [pii]

10.1016/j.biomaterials.2011.09.005

Appendix A:

SEM images of vapour crosslinked gelatin/PCL composite scaffolds.

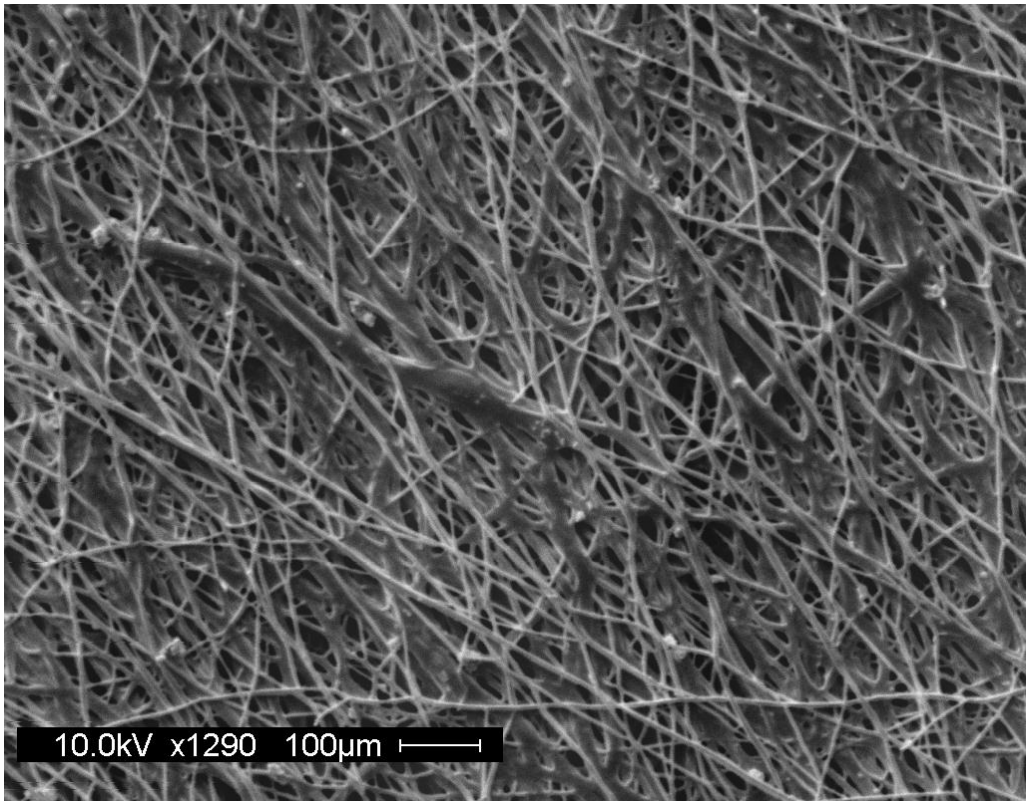

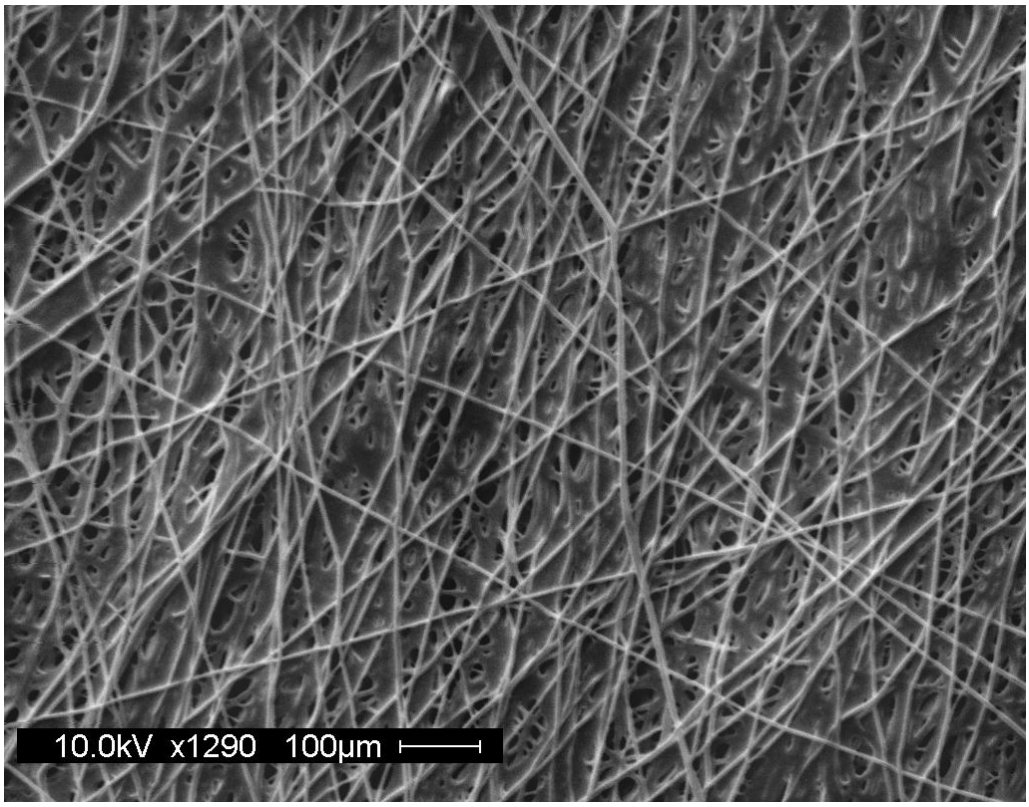
10.0kV x1290 100µm

Appendix B:

SEM images of SBF deposited gelatin/PCL composite scaffolds.

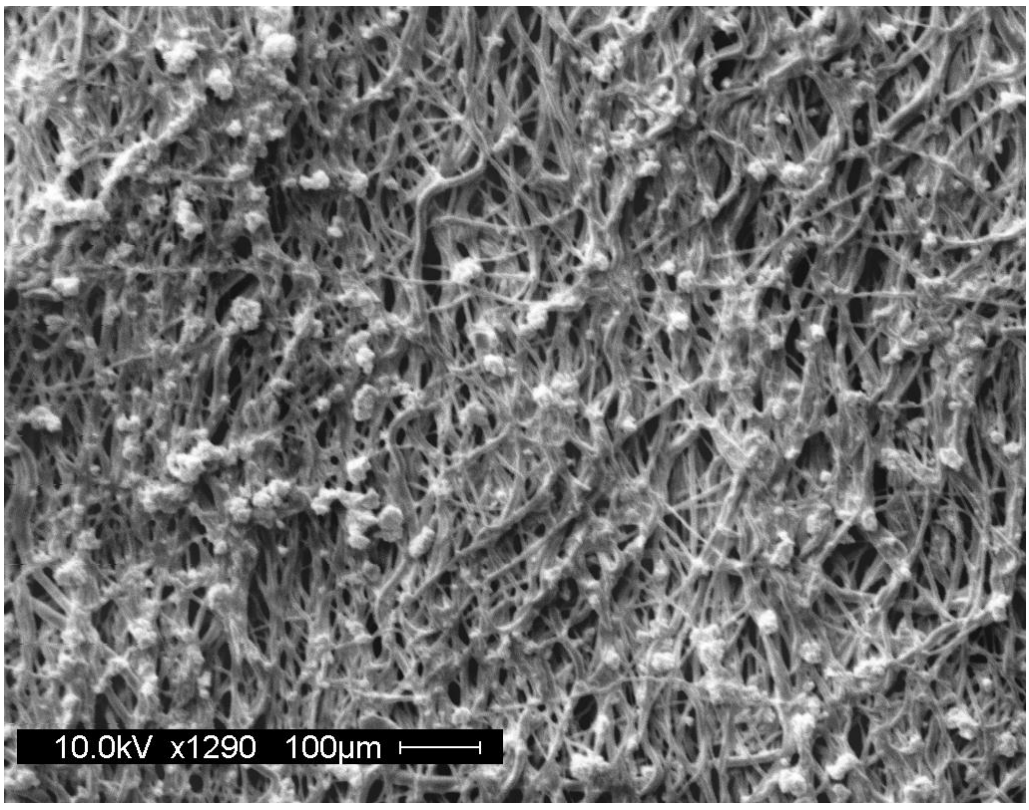

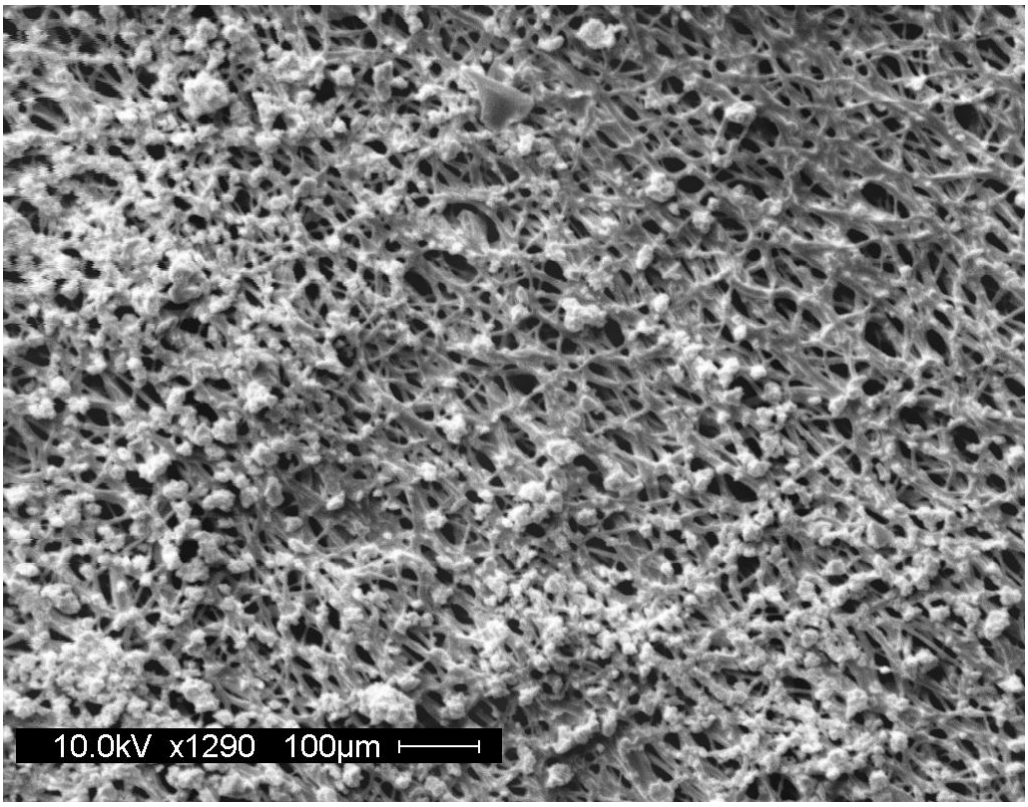
10.0kV x1290 100µm

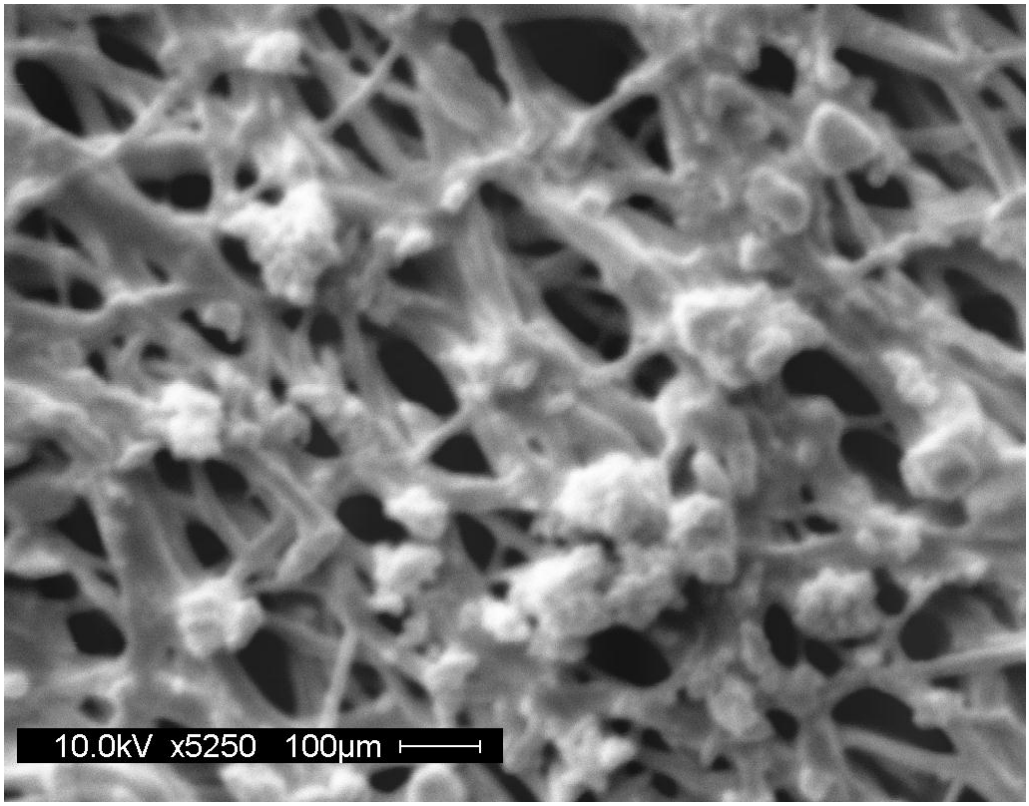
10.0kV x5250 100µm

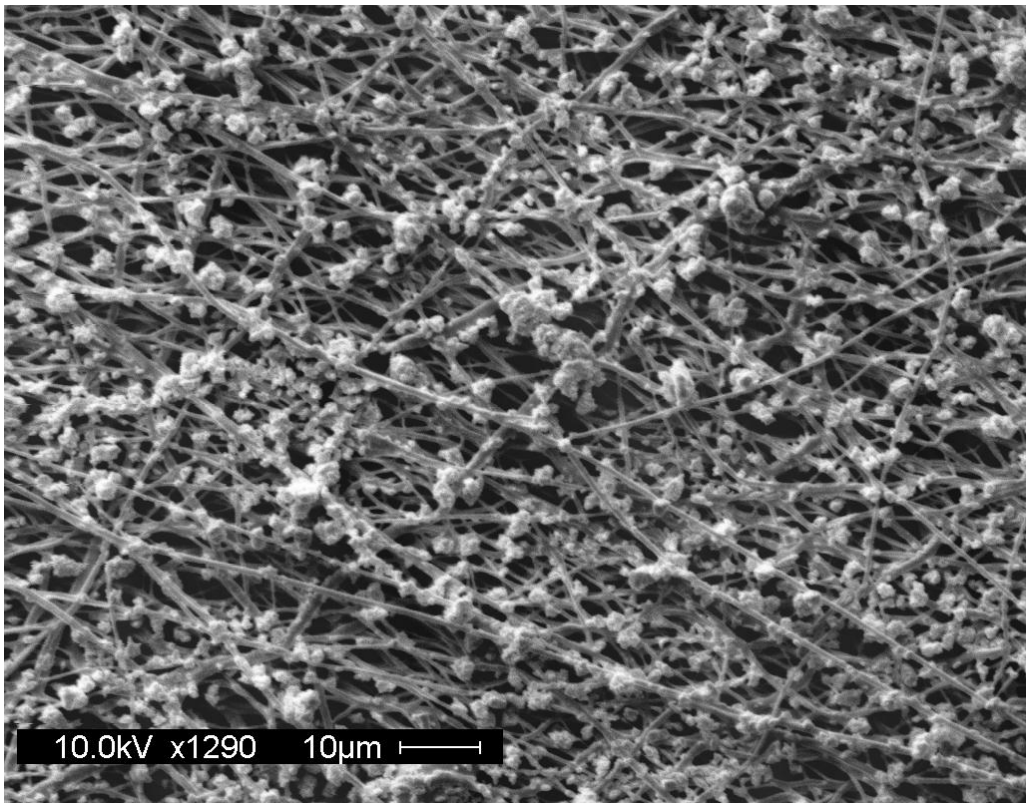
10.0kV x1290 10µm


10.0kV x1290 100µm

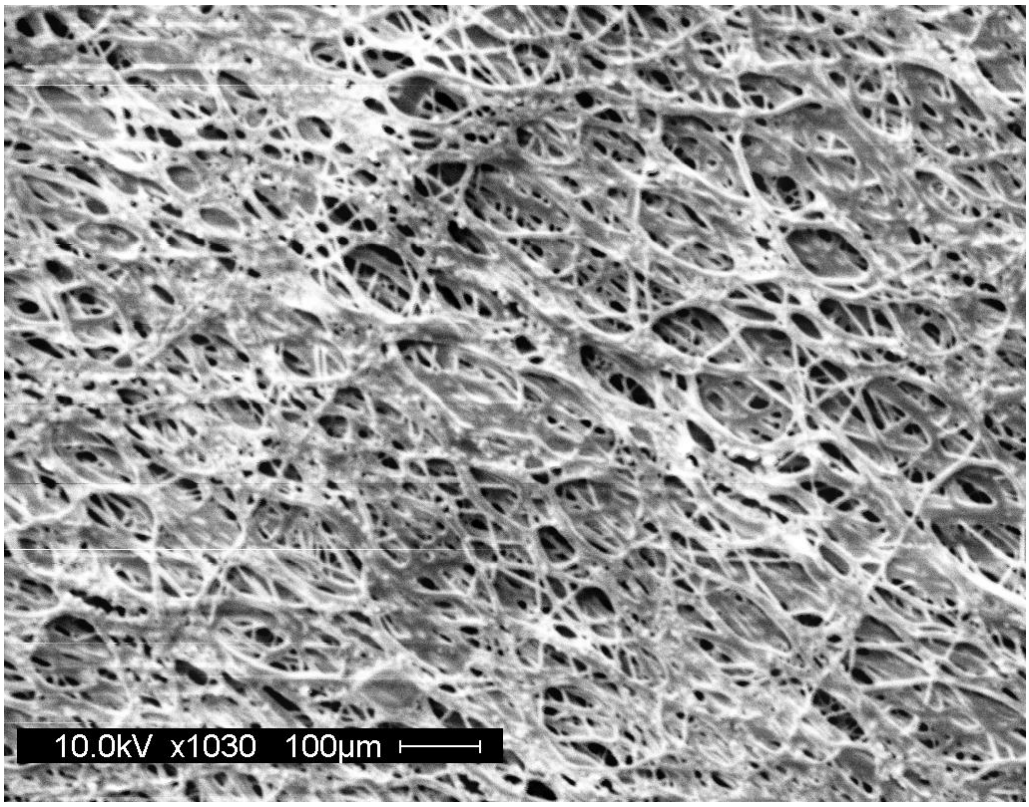
10.0kV x1030 100µm

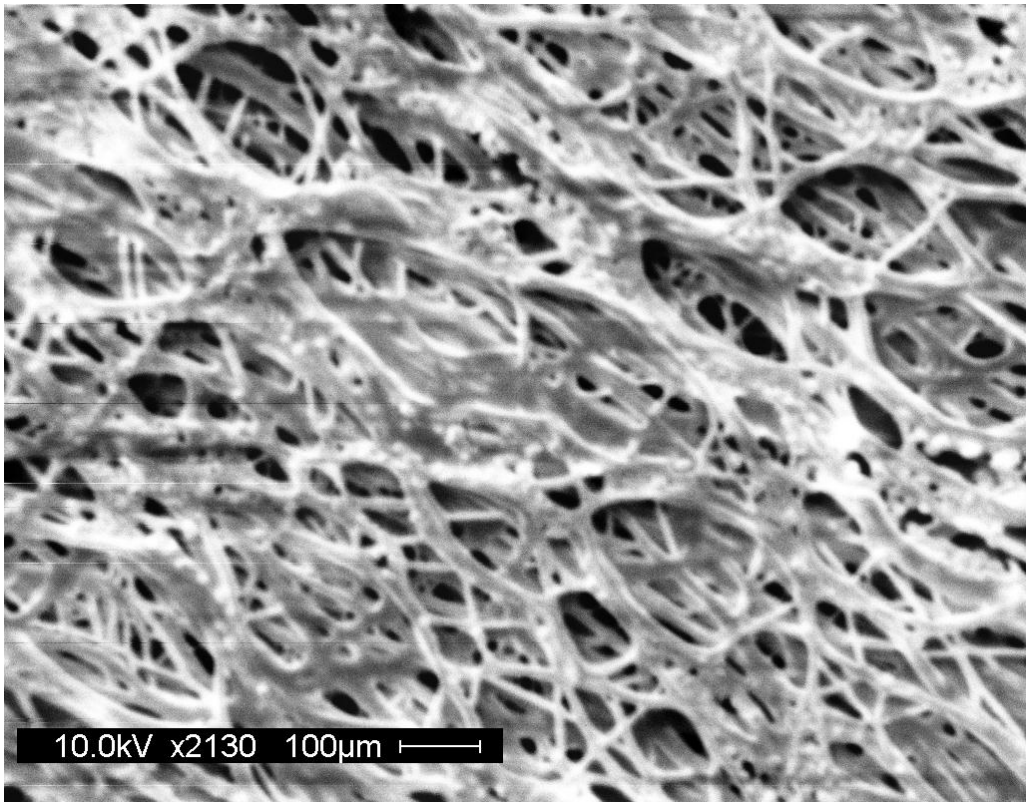
10.0kV x2130 100µm

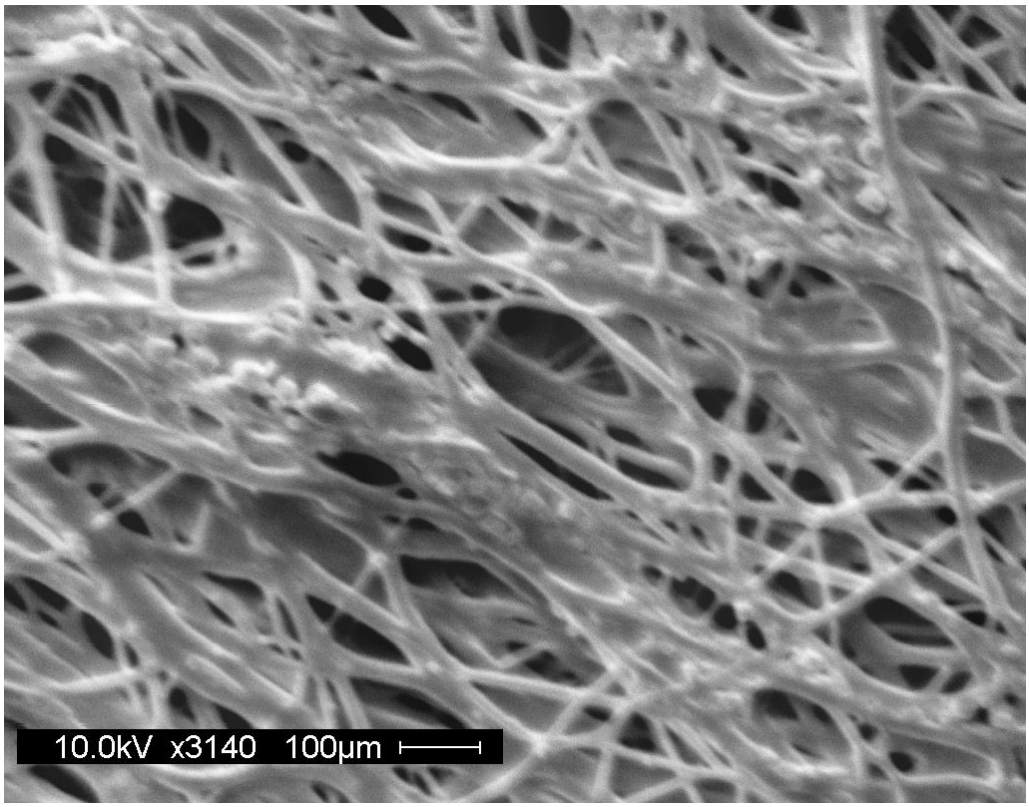
10.0kV x3140 100µm

Appendix C:

Confocal microscopy images of traditional composite scaffolds.

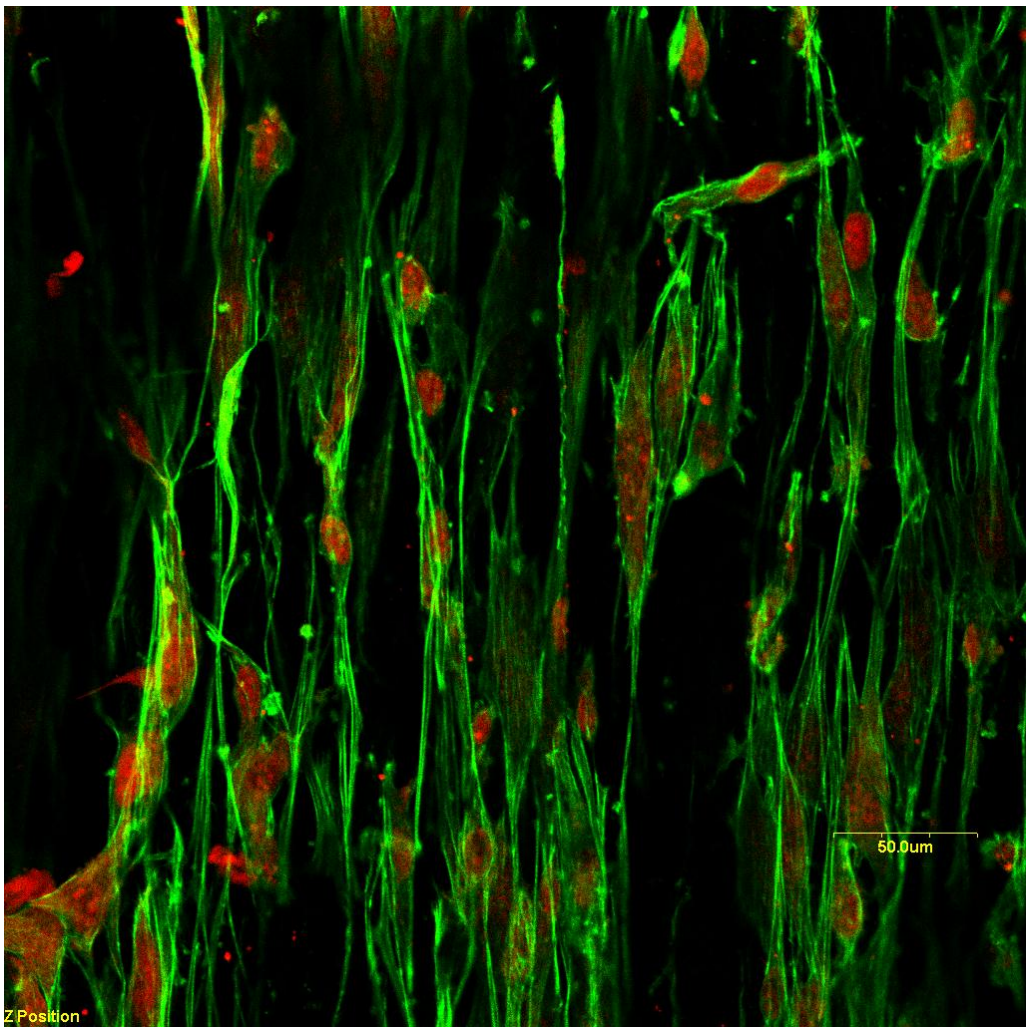

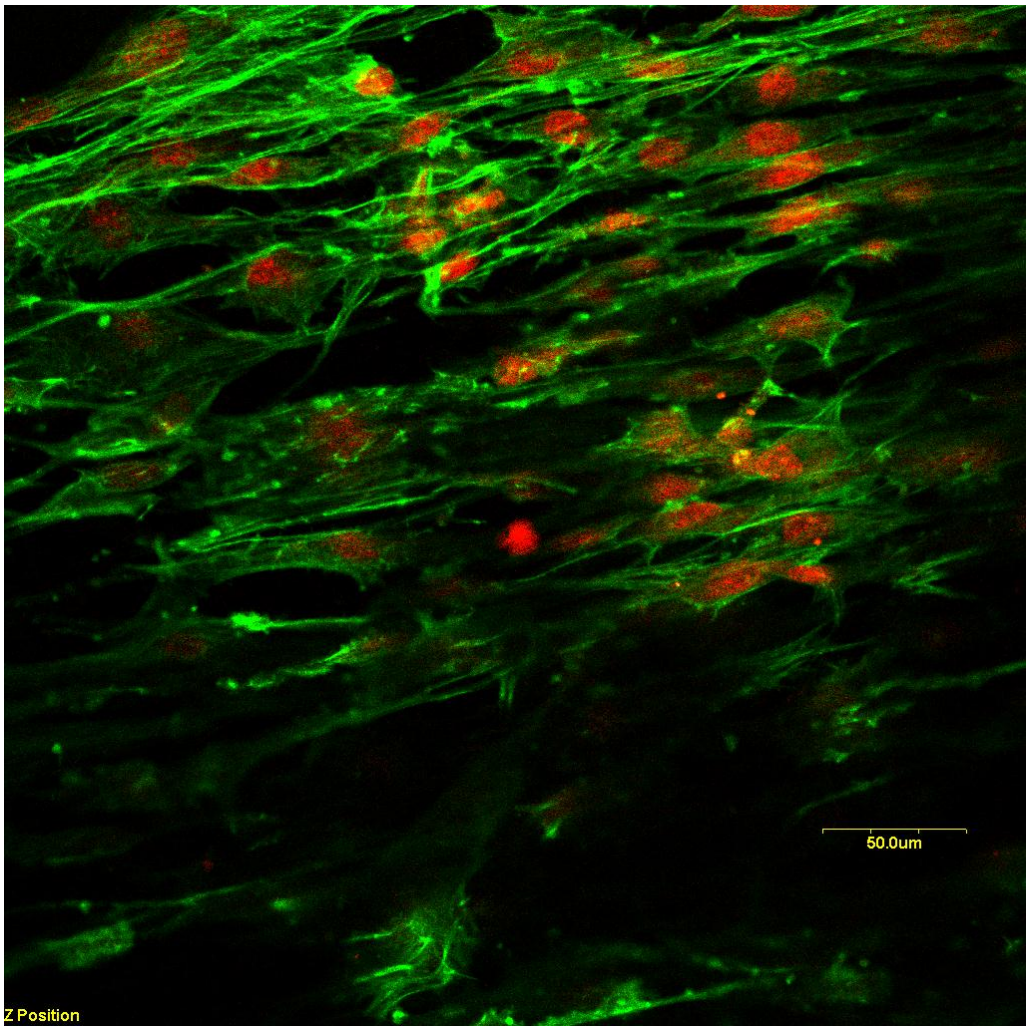
50.0um
Z Position

Appendix D:

Confocal microscopy images of new composite scaffolds.

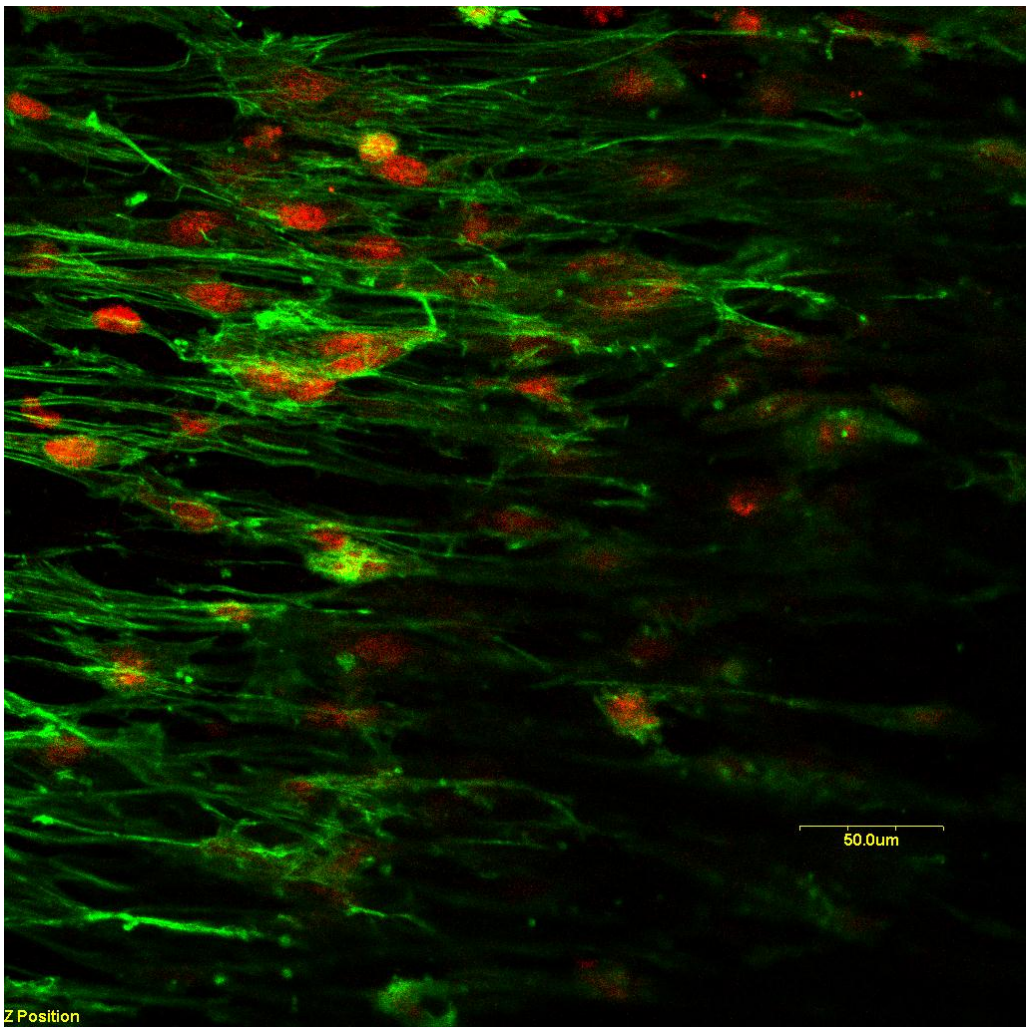

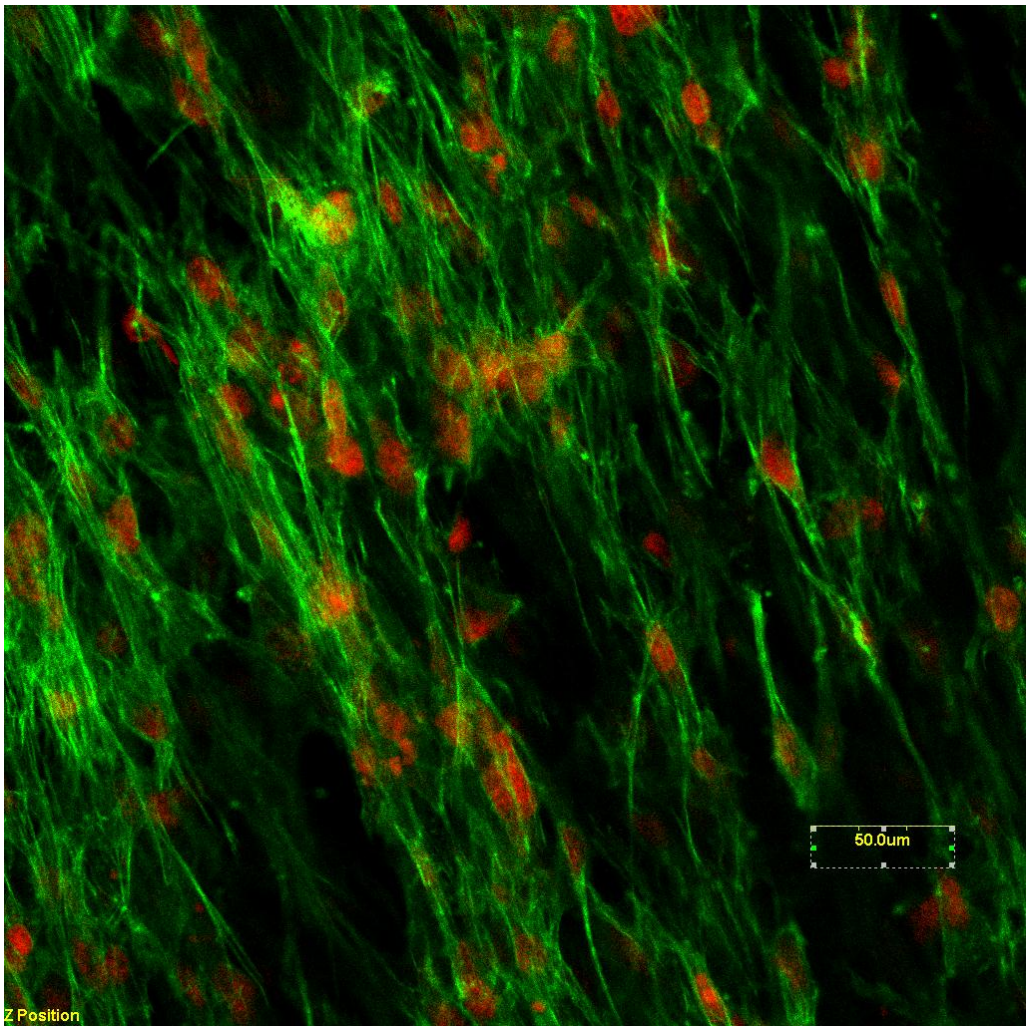
50.0um
Z Position

Appendix E:

Stress-strain curves of tensile tests.

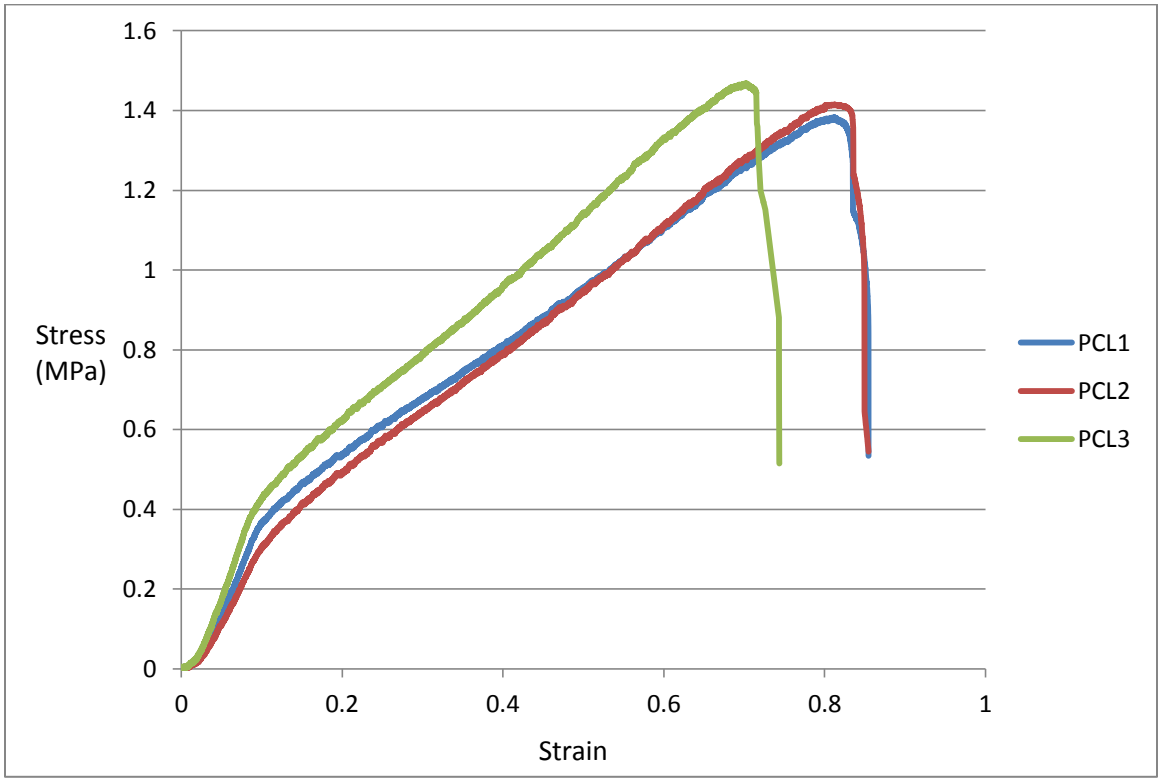

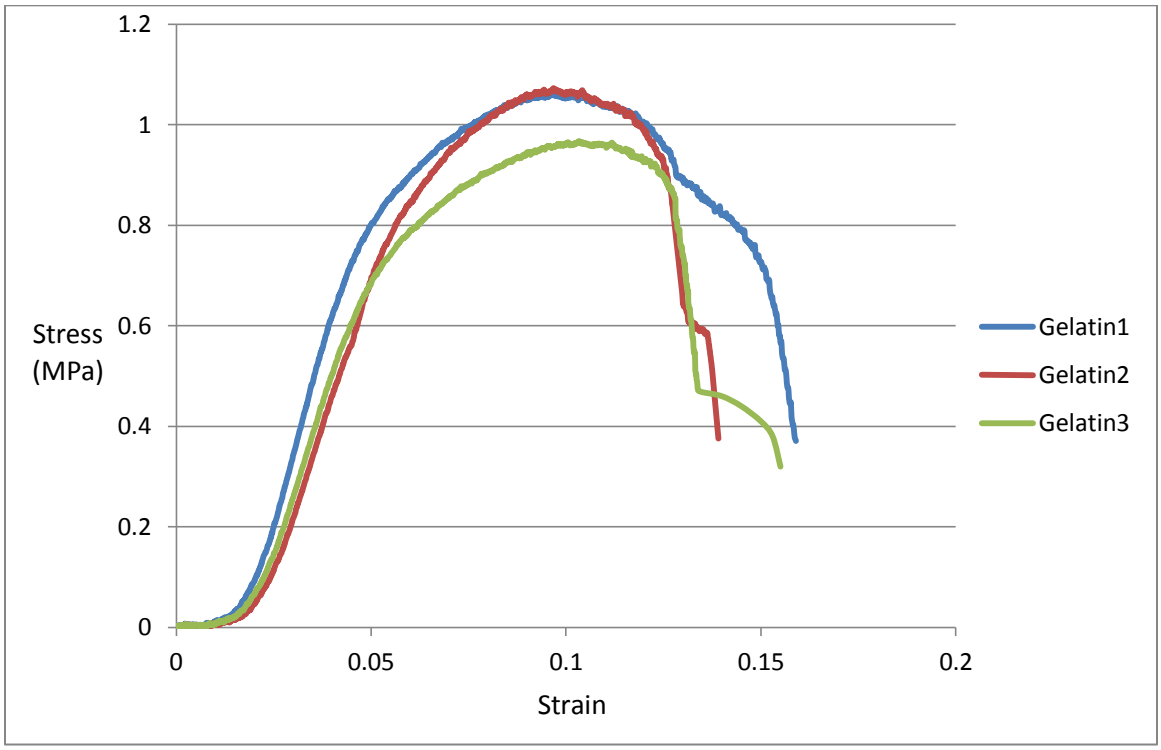
1.2
1
0.8
0.6
0.4
0.2
0
Stress (MPa)
0
0.05
0.1
0.15
0.2
Strain
Gelatin1
Gelatin2
Gelatin3

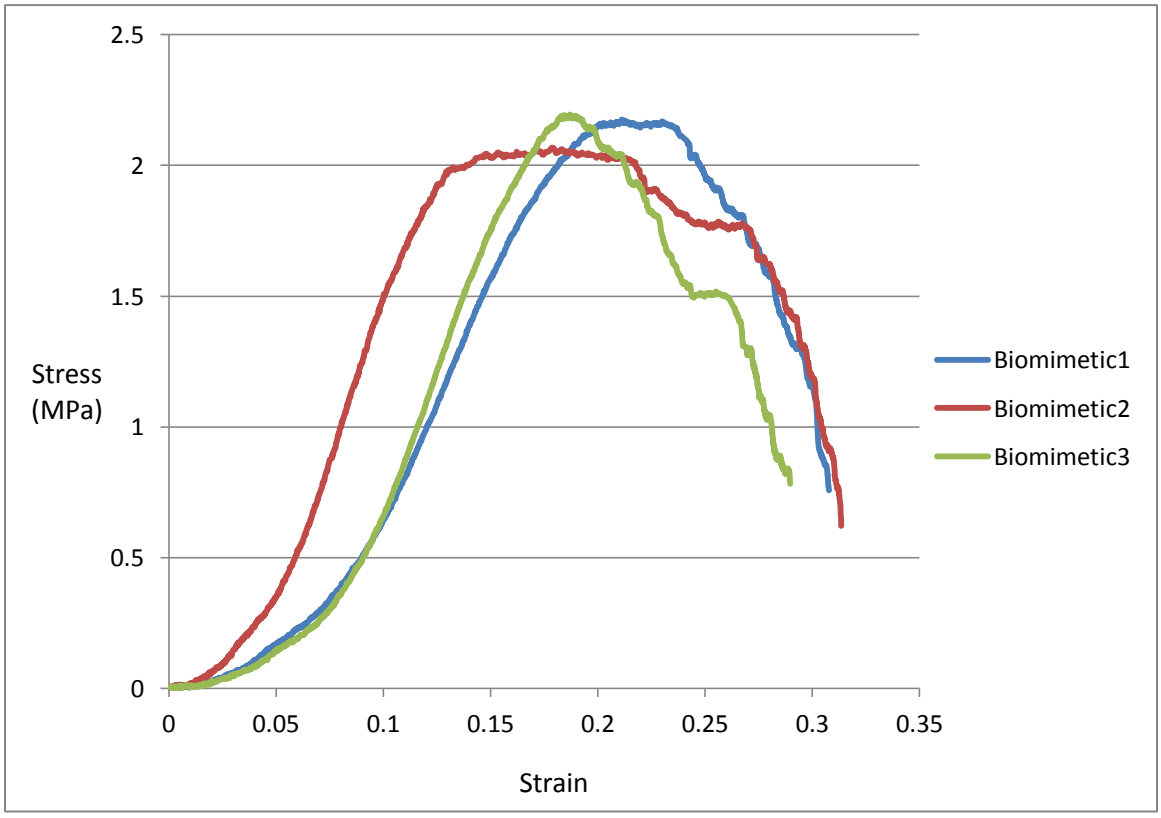
2.5
2
1.5
1
0.5
0
Stress (MPa)
0
0.05
0.1
0.15
0.2
0.25
0.3
0.35
Strain
Biomimetic1
Biomimetic2
Biomimetic3